Protein-RNA Domain-Domain Interactions in a tRNA Synthetase System
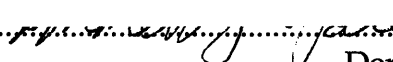
by

Andrew J. Gale

B.A., Bethel College, Kansas
(1988)

Submitted to the Department of Biology
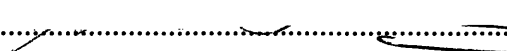in Partial Fulfillment of the Requirements for the Degree of

Doctor of Philosophy

at the
Massachusetts Institute of Technology
September, 1995

Signature of Author..
Department of Biology
August 28, 1995

Certified by...
Paul R. Schimmel
John D. and Catherine T. MacArthur Professor
of Biochemistry and Biophysics
Thesis Supervisor

Accepted by..
Frank Solomon
Chairman, Biology Department Graduate Committee

To My Parents

Protein-RNA Domain-Domain Interactions in a tRNA Synthetase System

by

Andrew J. Gale

ABSTRACT

The aminoacyl-tRNA synthetases are a family of proteins that provide the enzymatic basis for the genetic code by catalyzing the transfer of an amino acid to its cognate tRNA. The synthetases are divided into two classes on the basis of conserved sequence motifs that correspond to two specific active site architectures. The focus of this work is the class I methionyl-tRNA synthetase (MetRS).

All tRNAs adopt a similar L-shaped tertiary structure. This structure has two domains. One consists of the acceptor stem and the TΨC stem and loop and the other consists of the dihydrouridine stem and loop and the anticodon stem and loop. Aminoacyl tRNA synthetases in both classes contain non-conserved domains in addition to the conserved active site domains. These non-conserved domains may have been aquired through the course of evolution in order to increase specificity and efficiency of aminoacylation. In the case of MetRS, the non-conserved C-terminal domain is predominantly α-helical and contains residues that interact directly with the anticodon of the initiator methionine tRNA (tRNA^{fMet}).

The interactions of critical portions of each of the two major domains of tRNA^{fMet} with MetRS and with one of its domains were studied in this work. Sub-pieces of the protein and tRNA were constructed for this purpose. The anticodon binding domain of *E. coli* methionyl-tRNA synthetase was fused to maltose binding protein. This fusion protein and the released, isolated domain are stable and have native-like structural characteristics as shown by circular dichroism and thermal denaturation studies. The fusion protein and the isolated domain bind specifically to a small RNA hairpin oligonucleotide that recapitulates the anticodon stem-loop of tRNA^{fMet}, as shown by the technique of affinity coelectrophoresis. The binding specificity and affinity of the fusion protein and the C-terminal domain duplicate that of the interaction between native methionyl tRNA synthetase and the anticodon stem-loop oligonucleotide. Thus, the anticodon binding domain is

functionally independent of the class defining catalytic core and can be joined to another protein with little change in RNA binding characteristics.

The binding of a mutant MetRS variant to the individual domains of tRNA^{fMet} was studied with RNA hairpin substrates that recapitulate the acceptor stem (microhelix). The dissociation constants of MetRS for wild-type and mutant microhelix^{fMet}, as well as a noncognate microhelix, were determined. The combination of kinetic data for the aminoacylation of these microhelices and binding affinities for these microhelices established that specificity determinants in the acceptor stem of tRNA^{fMet} affect discrimination primarily during the transition state of catalysis.

The structures of transfer RNAs appear to be strained when bound to synthetases. Through our analysis of microhelix binding and anticodon stem-loop binding, as well as the binding of full length tRNA^{fMet}, we were able estimate the free energy of strain for the binding of tRNA^{fMet} to MetRS.

Acceptor helix interactions occur primarily with the N-terminal catalytic domain. However, substitution of Arg533 to Ala in the C-terminal domain affected acceptor stem binding with little effect on anticodon stem-loop binding. This mutation is located in a C-terminal peptide appendix that extends from the C-terminal domain of MetRS to fold back near the active site in the N-terminal domain. These experiments provide a direct demonstration of how acceptor helix interactions provide a functional connection between the two domains of the enzyme.

Thesis Supervisor: Professor Paul Schimmel
Title: John D. and Catherine T. MacArthur Professor
      of Biochemistry and Biophysics

TABLE OF CONTENTS

List Of Figures

11

12

Acknowledgements

I would like to thank Paul Schimmel first and foremost for his guidance and support during my years in his laboratory. In particular, he always was able to find the positive in any work that I was doing and continually gave me encouragement. He also brought together a great group of people in his lab and provided an excellent work environment.

I have enjoyed greatly working and socializing with many members of the Schimmel lab (past and present). The postdoctoral fellows in the lab have been an invaluable resource for me, in large part because of their diverse backgrounds. All of them have been willing to provide advice and expertise. In particular I would like to acknowledge Jonathan Burbaum for his mentorship during my first year in the lab and also his continued friendship and interest in my work. I would also like to acknowledge Jim Landro for his excellent advice and help. Finally I would like to thank Susan Martinis for her support and continued encouragement over the years and most of all for her friendship. I would also like to thank Anne Garcia for her talent for keeping the lab running smoothly and her friendship.

I would like to acknowledge Arthur Lander for introducing me to the technique of affinity coelectrophoresis which has been so critical for my entire thesis.

Most of all I would like to thank all of my family members for contributing so much to who I am today. Of course I thank my parents for their unconditional love and support, for instilling in me a love of learning, and for their faith in me. I would also like to thank all of my siblings (Eric & Nancy, Laurie, Steve, Tim & Carol) for being a great family.

Chapter 1

Introduction

.

Aminoacyl-tRNA Synthetases and the Genetic Code

The aminoacyl-tRNA synthetases are enzymes that catalyze the transfer of an amino acid to its cognate tRNA (Berg, 1961; Kisselev and Favorova, 1974; Schimmel and Söll, 1979). Specific recognition of the cognate tRNA and amino acid provides the enzymatic basis for the genetic code by virtue of associating an amino acid with the anticodon trinucleotide of its cognate tRNA. The specificity of these enzymes for the correct amino acid and for the cognate tRNAs is critical for the fidelity of information transfer according to the amino acid/trinucleotide algorithm of the code. The enzymes were probably among the earliest proteins to appear, possibly in the early stages of the transition from the RNA world to the theatre of proteins (Schimmel *et al.*, 1993).

In the aminoacylaton reaction, the amino acid is attached to the 3' end of its cognate tRNA through an ester linkage at either the 2'-OH or the 3'-OH of the terminal adenosine. The overall reaction catalyzed is:

$$\text{ATP + amino acid (AA) + tRNA} \rightleftharpoons \text{AA-tRNA + AMP + PP}_i$$

This reaction takes place in two steps. In the first step the aminoacyl adenylate, an enzyme bound intermediate, is formed. Aminoacyl adenylate synthesis yields an anhydride linkage between the carboxyl group of the amino acid and the 5'-α-phosphate of the ATP[1], with the release of pyrophosphate:

$$\text{E + ATP + AA} \rightleftharpoons \text{E} \cdot \text{AA-AMP + PP}_i$$

---
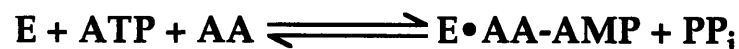
[1] see abbreviations in Appendix B

15

In the second step the activated aminoacyl group is transferred to either the free 2'-OH or 3'-OH of the terminal adenosine of the tRNA:

$$\text{tRNA} + \text{E} \bullet \text{AA-AMP} \rightleftharpoons \text{E} + \text{AA-tRNA} + \text{AMP}$$
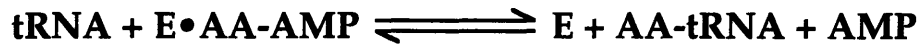
The aminoacyl ester linkage is higher in energy than the peptide bond, thereby making peptide synthesis (from aminoacyl tRNAs) thermodynamically favorable.

The transfer RNA substrates all have essentially the same overall structure (Rich and RajBhandary, 1976). Transfer RNAs contain between 75 and 93 nucleotides that fold into a globular L-shaped two-domain structure (Figure 1-1) (Kim et al., 1974; Robertus et al., 1974; Rich and RajBhandary, 1976). This structure is formed from four helical stems. The acceptor stem ends in the amino acid attachment site. It contains seven base pairs which stack coaxially with the 5 bp of the TΨC stem. The acceptor-TΨC stem thus forms one 12 bp domain of the tRNA structure. This domain is believed to be the historical, or earliest part of the tRNA structure (Weiner and Maizels, 1987; Maizels and Weiner, 1993; Noller, 1993; Schimmel et al., 1993). The second domain is formed from the five bp anticodon stem and the four bp dihydrouridine (DHU) stem which stack coaxially upon each other. The DHU loop and the TΨC loop interact at the corner of the L-shaped tRNA to stabilize the structure. With this organization, the anticodon and the 3'-acceptor end of the tRNA are separated from each other by about 75 Å (Rich and Kim, 1978).

Identity elements for specific aminoacylation take the form of positive determinants that interact specifically with the cognate synthetase for that tRNA or negative determinants that prevent interactions with noncognate

synthetases. Typically identity elements are located in the acceptor stem and the anticodon (Giegé *et al.*, 1993; Saks *et al.*, 1994; Martinis and Schimmel, 1995; McClain, 1995).

Classes of tRNA Synthetases

In spite of their common function, the synthetases vary greatly in subunit structure, polypeptide size and amino acid sequence. In *E. coli*, quarternary structures include α, α_2, α_4 and $\alpha_2\beta_2$, and reported polypeptide sizes range from 334 amino acids (tryptophanyl-tRNA synthetase) to 951 amino acids (valyl-tRNA synthetase) (Burbaum and Schimmel, 1991b; Schimmel, 1991). Though the sequence similarities amongst the synthetases are limited, the enzymes have been divided into two distinct classes based on the alignment of short sequence motifs (Table 1-1) (Eriani *et al.*, 1990; Schimmel, 1991). These sequence motifs correspond to two distinct architectures for the catalytic domains, with both of these architectures centering around an ATP binding motif (Moras, 1992).

The class division also corresponds reasonably well to several other properties of the synthetases. The class I enzymes are mostly monomers while the class II enzymes are usually α_2 dimers (Burbaum and Schimmel, 1991b). All class I synthetases initially aminoacylate the 2'-OH whereas class II synthetases initially aminoacylate the 3'-OH, with the single exception of PheRS, which is a class II enzyme that appears to aminoacylate the 2'-OH of tRNA[Phe] (Table 1-1) (Eriani *et al.*, 1990; Moras, 1992).

Sequence alignments of the synthetases fail to show any evidence of a common ancestor for the two classes of synthetases. Furthermore, there is no evidence of a synthetase switching its class type in evolution (Schimmel,

1991; Buechter and Schimmel, 1993a). Thus, it appears that the two classes arose independently of each other (Nagel and Doolittle, 1991) or that division into two classes occurred very early. The fundamental difference in the catalytic domain architectures for the two classes of synthetases also supports this supposition (Burbaum and Schimmel, 1991b; Moras, 1992).

Structures of tRNA Synthetases

The crystal structures of five class I synthetases have now been solved. These include TyrRS (Brick *et al.*, 1988) and TrpRS (Doublié *et al.*, 1995) from *Bacillus stearothermophilus*, MetRS (Brunie *et al.*, 1990) and GlnRS (Rould *et al.*, 1989) from *Escherichia coli*, and GluRS (Nureki *et al.*, 1995) from *Thermus thermophilus*. All of these structures contain the active site within an N-terminal domain built around a topologically conserved Rossman nucleotide-binding fold (Rossmann *et al.*, 1974). This fold is a six-stranded parallel ß-sheet with alternating α-helices between the ß-strands (in a ß$_3$α$_2$ arrangement for each half of the fold) (Figure 1-2). In these structures, there is a second major domain that comprises the C-terminal portion of the enzyme. This domain is nonconserved and is involved in binding to distal regions of the tRNA, which in many cases is the anticodon. These two domains, therefore, parallel the two domains of the tRNA, in that the N-terminal domain interacts with the acceptor-TΨC domain and the C-terminal domain interacts with the DHU-anticodon domain (Buechter and Schimmel, 1993a).

The two class-defining sequence motifs are within the conserved N-terminal domain. The first motif is an eleven amino acid signature sequence that ends in the HIGH tetrapeptide (Webster *et al.*, 1984). This motif is located in a loop that follows the first ß-strand of the nucleotide-binding fold (Burbaum and Schimmel, 1991b; Buechter and Schimmel, 1993a). Residues

18

in this motif are involved in ATP binding. The second consensus sequence is a KMSKS pentapeptide (Hountondji *et al.*, 1986) in the second half of the nucleotide binding fold, in a loop following the fifth ß-strand of the Rossman fold (Burbaum and Schimmel, 1991b; Buechter and Schimmel, 1993a). The second lysine in this motif has been proposed to be involved in transition state stabilization for the incipient aminoacyl adenylate intermediate, through binding to the pyrophosphate moiety of ATP (Fersht, 1987; Rould *et al.*, 1989; Mechulam *et al.*, 1991).

Within the framework of the nucleotide-binding fold, the class I synthetases contain idiosyncratic insertions of widely varying sizes. All of the class I enzymes contain an insertion between the two $ß_3\alpha_2$ halves of the nucleotide binding fold designated as consensus polypeptide 1 (CP1). This insertion is positioned to interact with the acceptor stem of a bound tRNA substrate (Rould *et al.*, 1989; Perona *et al.*, 1991). A second insertion designated as CP2 is also present in many of the class I enzymes (Figure 1-2) (Starzyk *et al.*, 1987; Burbaum and Schimmel, 1991b).

Based on sequence similarities and the detailed topology of the catalytic domain, the class I synthetases can be subdivided into three subclasses. Class Ia contains all of the hydrophobic and sulfur-containing amino acids,--MetRS, CysRS, ValRS, IleRS, LeuRS--and possibly ArgRS (Nagel and Doolittle, 1991; Landès *et al.*, 1995). Class Ib contains TyrRS and TrpRS. Class Ic consists of GlnRS and GluRS (Burbaum and Schimmel, 1991b; Moras, 1992).

Within the class I synthetases, the C-terminal domain is not conserved across the class. Most notably, in MetRS the C-terminal domain is predominantly α-helical (Brunie *et al.*, 1990), while in GlnRS it is a ß-barrel structure (Rould *et al.*, 1989; Rould *et al.*, 1991). However, sequence alignments suggest that the class Ia enzymes are related in their C-terminal

19

domains (Eriani *et al.*, 1991; Hou *et al.*, 1991; Shiba and Schimmel, 1992a). In both GlnRS and MetRS, the C-terminal domains are involved in specific recognition of the anticodons of the cognate tRNAs (Rould *et al.*, 1989; Ghosh *et al.*, 1990; Ghosh *et al.*, 1991; Rould *et al.*, 1991). Therefore, one of the idiosyncratic insertions (CP1) and the C-terminal domains are involved in specific tRNA binding (Moras, 1992; Schimmel *et al.*, 1993).

The class II synthetases are defined by the presence of three degenerate sequence motifs (Eriani *et al.*, 1990). Crystal structures of class II synthetases show that their active site architecture is distinct from that seen in the class I synthetases (Cusack *et al.*, 1990; Ruff *et al.*, 1991). The catalytic domain of class II synthetases is built around a seven-stranded antiparallel ß-sheet flanked by three α-helices (Figure 1-3). Crystal structures have now been solved for six class II synthetases. (In all cases the active site architecture is conserved.) These enzymes are AspRS (Ruff *et al.*, 1991), SerRS (Cusack *et al.*, 1990), LysRS (Onesti *et al.*, 1995), PheRS (Mosyak *et al.*, 1995), GlyRS (Logan *et al.*, 1995), and HisRS (Arnez *et al.*, 1995).

The three shared sequence motifs are all within the conserved active site domain. Motif 1 consists of an α-helix followed by the first ß-strand of the active site ß-sheet. This motif is involved in the formation of a dimer interface. Motif 2 encompasses the second and third ß-strands of the ß-sheet. Motif 3 contributes the seventh ß-strand and an α-helix. Substrate binding and catalysis take place on the surface of the ß-sheet (Cavarelli *et al.*, 1994), with residues in motifs 2 and 3 making contacts with bound ATP (Cusack *et al.*, 1993; Belrhali *et al.*, 1994).

Class II synthetases have nonconserved polypeptide insertions within the catalytic domain as well as entire nonconserved domains analogous to those found in the class I synthetases. These additional domains may be

20

either on the N-terminal or C-terminal side of the conserved domain (Buechter and Schimmel, 1993a). Two examples with the nonconserved domain on the N-terminal side are AspRS and SerRS. AspRS has a ß-barrel domain fused to the conserved active site domain (Ruff *et al.*, 1991), whereas SerRS has an extended antiparallel coiled-coil domain protruding out from the active site domain (Cusack *et al.*, 1990). In both cases these additional domains are involved in binding to their respective cognate tRNAs at sites distal to the acceptor stem (Ruff *et al.*, 1991; Cavarelli *et al.*, 1993; Cusack *et al.*, 1993; Biou *et al.*, 1994).

For both class I and class II synthetases, the catalytic and additional nonconserved domains together form a two domain structure that can be generalized to all of the synthetases (Buechter and Schimmel, 1993a; Schimmel *et al.*, 1993). In this model, the nonconserved domain that is unique to each synthetase is involved in binding to sites on the tRNA distal to the acceptor stem, while within the conserved catalytic domain, nonconserved inserted polypeptides perform enzyme-specific roles such as acceptor stem recognition (Buechter and Schimmel, 1993a). As mentioned earlier, tRNAs also have a two domain structure. Therefore, in the synthetase-tRNA complex, each discrete domain of the synthetase interacts with a separate domain of the tRNA (Buechter and Schimmel, 1993a).

Co-crystals of Synthetase-tRNA Complex

Three crystal structures of synthetases have been solved in complex with their cognate tRNAs. They are the class I *E. coli* GlnRS (Rould *et al.*, 1989), and the class II *S. cerevisiae* AspRS (Ruff *et al.*, 1991) and *T. thermophilus* SerRS (Biou *et al.*, 1994). In the GlnRS/tRNA^{Gln} co-crystal, the synthetase binds to the minor groove side of the acceptor stem causing the 3'-acceptor

strand of the L-shaped tRNA to make a sharp turn towards the anticodon rather than to continue in a helical conformation. A critical feature of this conformational distortion is that an antiparallel ß-loop of protein inserts into the end of the acceptor helix and disrupts the U1·A72 bp. This antiparallel ß-loop structure is part of the CP1 insertion (Rould et al., 1989).

The C-terminal half of GlnRS forms two antiparallel ß-barrel-like domains that interact with the anticodon of tRNA^{Gln}. The anticodon of the complexed tRNA differs greatly in conformation from the anticodon structure of free tRNA^{Phe} (Robertus et al., 1974). In free tRNA^{Phe}, the three anticodon bases are stacked upon one another. These anticodon bases of bound tRNA^{Gln} are splayed out in different directions, thus enabling them to interact with separate recognition pockets in the anticodon binding domain of GlnRS (Rould et al., 1991).

The co-crystal structure of the class II AspRS shows that AspRS binds to tRNA in a manner different than GlnRS (Ruff et al., 1991). AspRS binds to the major groove side of the acceptor stem and interacts primarily with the discriminator base G73 and the U1·A72 bp. The CCA end of the tRNA remains coaxially stacked on the acceptor helix, so that the conformation is relatively unchanged relative to free tRNA^{Asp} (Moras et al., 1980). The anticodon stem and loop of tRNA^{Asp} in the complex undergoes a significant conformational change upon binding. The entire anticodon stem is bent toward the enzyme and the anticodon loop is unraveled such that five bases (including the three anticodon bases) protrude outward. As in the GlnRS structure, this arrangement maximizes the contacts of anticodon bases with the protein (Ruff et al., 1991; Cavarelli et al., 1993).

The class II SerRS has a unique N-terminal domain that consists of a long antiparallel coiled-coil α-helix extending out from the catalytic domain

of the synthetase. This structure is present in both *E. coli* and *T. thermophilus* SerRS (Cusack *et al.*, 1990; Biou *et al.*, 1994). In the co-crystal structure, this coiled-coil domain interacts with the long variable arm of tRNA^{Ser}. This additional domain is analogous to the nonconserved anticodon binding domains of GlnRS and AspRS. However, SerRS does not interact with the anticodon of tRNA^{Ser}, which is not surprising given the six-fold degeneracy of serine codons which must be decoded by five different serine tRNA isoacceptors which are all charged by the same enzyme. In the co-crystal structure, the end of the acceptor stem of tRNA^{Ser} is not visible in the electron density map. However, the orientation of the tRNA is consistent with acceptor stem binding similar to that of tRNA^{Asp}, with little distortion of the acceptor stem and with protein interactions on the major groove side (Biou *et al.*, 1994).

As mentioned, these co-crystal structures have demonstrated critical differences between class I and class II synthetases in acceptor stem binding and orientation of the terminal adenosine, which is the site of amino acid attachment (Moras, 1992). These differences may explain why the site of initial attachment of the amino acid is class specific (Moras, 1992; Schimmel and Ribas de Pouplana, 1995).

Microhelix Aminoacylation and an Operational RNA Code for Amino Acids

In ten synthetase systems that have been tested, oligonucleotide substrates based on acceptor or acceptor-TΨC stems (Figure 1-1) are specifically aminoacylated by their cognate tRNA synthetase (Frugier *et al.*, 1994; Hamann and Hou, 1995; Martinis and Schimmel, 1995). These include the class I CysRS (Hamann and Hou, 1995), IleRS (Nureki *et al.*, 1993), MetRS (Martinis and Schimmel, 1992; Martinis and Schimmel, 1993) , TyrRS (Quinn *et al.*,

1995), and ValRS (Frugier *et al.*, 1992), as well as class II AlaRS (Francklyn and Schimmel, 1989), AspRS (Frugier *et al.*, 1994), GlyRS (Francklyn *et al.*, 1992) , HisRS (Francklyn and Schimmel, 1990; Rudinger *et al.*, 1992) , and SerRS (Sampson and Saks, 1993). In several of these systems, the synthetase is known to interact strongly with the anticodon of its cognate tRNA, and yet microhelix aminoacylation is anticodon-independent.

The determinants for specificity of microhelix aminoacylation in each tRNA define an operational RNA code that relates nucleotides and structures in an acceptor stem to the attachment of a specific amino acid. These acceptor stem interactions were proposed by de Duve (1988) to be a "second genetic code" (see also Möller and Janssen, 1990).

Identity elements for microhelix aminoacylation are commonly found in the first 4 base pairs of the acceptor stem (positions 1·72, 2·71, 3·70, and 4·69) and the N73 'discriminator base'. The discriminator base N73 (A, U, C, G) was correlated in early work by Crothers *et al.* (1972) with the specificity of tRNA aminoacylation. In subsequent work, N73 has proven to contribute to the identity of virtually every tRNA species (McClain, 1993; Martinis and Schimmel, 1995; McClain, 1995).

At the molecular level, the operational RNA code consists of a spatial distribution of atoms in three dimensions, quite unlike the simple 'one dimensional' feature of the genetic code. Major elements of the operational RNA code for alanine are the $2\text{-}NH_2$ group of G3 which projects into the minor groove (Musier-Forsyth *et al.*, 1992), and the 2'-hydroxyl groups of G4, U70, and C71 which line the edges of the minor groove (Musier-Forsyth and Schimmel, 1992).

For aminoacylation of microhelices with methionine, the A73 discriminator base and G2·C71, C3·G70 and 4·69 bp's are important (Martinis

and Schimmel, 1992; Martinis and Schimmel, 1993). The specific atomic groups needed for recognition have not been worked out. Interestingly, the 4·69 bp is not conserved between the two tRNA^{Met} isoacceptors (G·C in tRNA^{fMet} and U·A in tRNA^{Met}). However, the 4·69 bp is the only one that is different between the first four bp's of tRNA^{Met} and the tRNA^{Ile} (LAU) isoacceptor, which has a C4·G69 bp. As it turns out, the C4·G69 bp is a negative determinant for tRNA^{Met} aminoacylation as well as a positive determinant for tRNA^{Ile} aminoacylation (Martinis and Schimmel, 1993; Nureki et al., 1993).

Activities of Discrete Domains and Truncated Synthetases

Given the nature of the discrete structural domains of synthetases and of tRNAs, one question is whether a catalytic domain by itself is sufficient for microhelix charging. Related to this question is the idea that the catalytic domains of synthetases may be the modern remnants of the primordial synthetases.

Among the synthetases there are several experimental examples of the isolation of discrete domains that retain function. In the class II AlaRS, the functions of the enzyme are arranged in modular fashion along the primary sequence (Jasin et al., 1983). E. coli AlaRS is a homotetramer of 875 amino acid subunits (Putney et al., 1981a; Putney et al., 1981b). C-terminal deletions were made within the gene to code for truncated versions of the synthetase. Fragments shorter than 699 amino acids were monomeric. A 461 amino acid N-terminal fragment is capable of adenylate synthesis and aminoacylation, albeit with reduced charging activity with tRNA^{Ala} as a substrate. An N-terminal fragment of 368 amino acids is virtually incapable of tRNA binding and aminoacylation but retains full adenylate synthesis activity (Jasin et al.,

1983; Regan *et al.*, 1987). Therefore, the 461 amino acid N-terminal fragment delineates the catalytic domain of AlaRS. Significantly, this $AlaRS_{1-461}$ fragment aminoacylates microhelix^{Ala} at the same rate as does native AlaRS (Buechter and Schimmel, 1993b).

The class II SerRS has an N-terminal domain that consists of a coiled-coil of two antiparallel α-helices which extend for 60 Å (Cusack *et al.*, 1990). This domain interacts with the long variable loop of tRNA^{Ser} (Biou *et al.*, 1994). Deletion of this coiled-coil domain does not affect adenylate synthesis but reduces the efficiency of aminoacylation by more than 4 orders of magnitude. Furthermore, tRNA^{Ser} binding was not detectable with the deletion protein (Borel *et al.*, 1994). Thus, like AlaRS, adenylate synthesis activity of SerRS is independent of major determinants for tRNA binding.

Khoda *et al.* (1987) split the class I MetRS from *Thermus thermophilus* into four stable domains by proteolysis. The first two domains at the N-terminal end seem to correspond to the catalytic and anticodon binding domains of *E. coli* MetRS. A protein comprised of just these two *T. thermophilus* MetRS domains is fully active for aminoacylation. Of these two domains, the N-terminal one contains the conserved class defining motifs, is fully active for adenylate synthesis, and even aminoacylates *E. coli* tRNA^{fMet} (at a reduced efficiency). The latter result implies that the catalytic domain by itself can charge tRNA^{fMet} without having anticodon interactions.

In *E. coli* MetRS, Trp461 in the nonconserved anticodon binding domain is critical for anticodon recognition (Ghosh *et al.*, 1990). Kim and Schimmel (Kim and Schimmel, 1992) created deletion mutants of MetRS that removed from four to eleven amino acids surrounding Trp461. These mutant proteins were stable and retained adenylate synthesis activity. One deletion mutant protein aminoacylated a microhelix based on the acceptor

stem of tRNA^{fMet} at the same rate as did wildtype metRS. Thus, adenylate synthesis activity and acceptor stem aminoacylation were shown to be functionally independent of anticodon binding.

Thus, the results with AlaRS, MetRS, and SerRS demonstrate that adenylate synthesis activity can be decoupled from the protein needed for much of the tRNA binding activity. Moreover, the studies with the class II AlaRS and class I MetRS explicitly show that acceptor helix interactions and microhelix charging are intimately associated with the part of the protein needed for adenylate synthesis.

Noncovalent Assembly of Synthetases

Burbaum and Schimmel (1991a) split *E. coli* MetRS between the two major domains, by inserting a stop codon and a new start codon at an internal position of the coding sequence of the gene for the synthetase. The two polypeptides were then expressed together and the complex of the two polypeptides was able to complement a strain of *E. coli* which encoded a MetRS with a high K_m for methionine. The assembled polypeptides also retained significant aminoacylation activity *in vitro*. This result demonstrated that high activity is independent of a covalent connection between the two domains of the enzyme.

In similar work with the class I *E. coli* IleRS, Shiba and Schimmel (Shiba and Schimmel, 1992a) split the gene for IleRS in 18 widely disparate locations so that the complete IleRS protein was expressed as two polypeptides from separate plasmids. Eleven of these fragment pairs were able to reconstitute IleRS activity sufficient to complement an *E. coli ileS* null strain. None of the individual fragments separately complemented the null

strain. It was also possible to split IleRS into 3 protein fragments that reconstituted full length, functional IleRS (Shiba and Schimmel, 1992b).

These biochemical results give, within both classes of synthetases, examples of the discrete natures of the functional domains of the synthetases.

Assembly of a Synthetase-tRNA Complex in Evolution

The conserved catalytic domain of tRNA synthetases probably represents the core primordial synthetase and is responsible for the operational RNA code (Figure 1-4). One speculation is that these primordial synthetases were capable of aminoacylating small RNA oligonucleotides or larger RNA structures that contained acceptor helix-like motifs (Buechter and Schimmel, 1993a; Schimmel *et al.*, 1993; Schimmel and Ribas de Pouplana, 1995). As template-directed protein synthesis developed, the anticodon domain was added to the primordial RNAs and at this point additional domains were added to the synthetases to facilitate interactions with distal regions of the emerging tRNA (Figure 1-4). As is suggested by the results with split MetRS and IleRS, additional synthetase domains may have originally been associated with the catalytic domain in a noncovalent complex, with the genes for the domains fusing later to produce modern synthetases (Buechter and Schimmel, 1993a; Schimmel *et al.*, 1993).

Two other groups have independently noted the possibility of acceptor stem-like RNA motifs in a primordial RNA world (Weiner and Maizels, 1987; Maizels and Weiner, 1993; Noller, 1993). Because several RNA viruses contain acceptor stem-like motifs at the 3' ends of their genomic RNA, including plant viruses which have RNA genomes that are specifically aminoacylated, Maizels and Weiner (Weiner and Maizels, 1987; Maizels and Weiner, 1993) proposed that tRNAs originated as motifs that tagged genomic

RNAs for replication in an RNA world. Because contacts of the acceptor stem and anticodon are segregated clearly between 23S and 16S rRNA, respectively, Noller proposed that the two major domains of tRNAs had independent origins (Noller, 1993).

MetRS as an Example of a Class I Enzyme

The work presented here focuses on *E. coli* methionyl-tRNA synthetase. *E. coli* methionyl-tRNA synthetase is a homodimer of 676 amino acid subunits (Dardel *et al.*, 1984). Mild trypsinolysis produces a stable monomeric polypeptide that is 551 amino acids in length (Cassio and Waller, 1971). This form of the enzyme has nearly wild-type activity. The crystal structure of the truncated enzyme has been solved at 2.5 Å resolution (Zelwer *et al.*, 1982; Brunie *et al.*, 1990) (Figure 1-5). Deletions of coding sequences of *metG* were used to fine-map the trypsin cleavage site of MetRS (Mellot *et al.*, 1989). In these studies, the MetRS polypeptide was reduced to 547 amino acids without significant loss of activity or stability. Progressive shortening of the C-teminus beyond this point caused a significant loss in thermostability and activity (Mellot *et al.*, 1989).

A variety of approaches have been used to determine the residues within MetRS that are involved in tRNA binding, as well as the nucleotides in tRNA[Met] that define its identity. Crosslinking with tRNA derivatives carrying lysine-reactive moieties was responsible for the first identification of regions involved in RNA binding (Hountondji and Blanquet, 1985; Valenzuela and Schulman, 1986; Leon and Schulman, 1987b; Leon and Schulman, 1987a). Subsequent mutagenesis targeted to these regions identified specific residues that interact with tRNA[Met] (Ghosh *et al.*, 1990; Ghosh *et al.*, 1991; Kim *et al.*, 1993a).

29

Within the C-terminal domain is a region that contains several residues needed for anticodon binding. Trp461 is among the most important of those involved in anticodon binding (Ghosh *et al.*, 1990) (Figure 1-5). (Some evidence suggests that Trp461 interacts directly with C34 of the anticodon (Ghosh *et al.*, 1990).) A Trp461Phe substitution increases K_m for tRNA^{fMet} by 60-fold. A Trp461Ala substitution decreases the efficiency of aminoacylation by 125-fold beyond that of the Trp461Phe mutant, thereby making the K_m not measurable (Meinnel *et al.*, 1991b). Further mutagenesis and genetic selection protocols have identified Asp391, Arg395 (Ghosh *et al.*, 1991; Kim *et al.*, 1993a), Asp449, Asp456 (Meinnel *et al.*, 1991b; Schmitt *et al.*, 1993), Asn452, Arg453, Pro460 and Lys465 (Kim *et al.*, 1994) as also being involved in anticodon discrimination.

Each subunit of MetRS binds zinc to a Cys$_4$ cluster within the CP1 insert that divides the catalytic domain. This zinc is essential for activity but is proposed to play a structural role rather than a catalytic role (Fourmy *et al.*, 1993a; Fourmy *et al.*, 1993b; Landro and Schimmel, 1993). It is known that the acceptor stem of tRNA^{Met} has nucleotides that are critical for the identity of tRNA^{Met} (Lee *et al.*, 1992; Martinis and Schimmel, 1992; Meinnel *et al.*, 1993). The co-crystal structure of the class I *E. coli* glutaminyl-tRNA synthetase with tRNA^{Gln} shows that residues in the CP1 insertion make contacts with the tRNA^{Gln} acceptor stem (Rould *et al.*, 1989). The peptide F102-T124 in CP1 of GlnRS has some structural similarity to peptide E102-I124 in CP1 of MetRS (Perona *et al.*, 1991). Though it seems likely, it has not been explicitly demonstrated that residues located in CP1 (possibly including the metal binding motif) of MetRS make specific contacts with the acceptor-stem of tRNA^{Met}.

A separate region of MetRS has also been shown to interact specifically with the acceptor stem of tRNA^{Met}. In the crystal structure of the truncated MetRS, an extension of the C-terminal domain--termed a C-terminal peptide appendix--wraps back around the N-terminal domain adjacent to the active site (Figure 1-5) (Brunie *et al.*, 1990). Kim *et al.* (Kim *et al.*, 1993b) determined that Arg533 in this peptide appendix is involved in binding to the acceptor stem of tRNA^{fMet}. Other work (by the author) provided more direct evidence that the peptide appendix made acceptor helix contacts (Kim *et al.*, 1993b). Chapter 5 of this thesis discusses some of this work.

Much is known about the identity elements in tRNA^{Met}. Schulman and coworkers showed through RNA chemical modification and replacement of nucleotides that the anticodon of tRNA^{Met} is a main determinant of identity (Stern and Schulman, 1977; Schulman and Pelka, 1983; Saks *et al.*, 1994). Replacement of any of the three anticodon nucleotides results in significant reduction of the aminoacylation rate by MetRS. Nucleotide C34 at the wobble position is especially critical for recognition, with mutations causing a decrease in aminoacylation rate of $>10^5$ (Schulman and Pelka, 1983; Schulman *et al.*, 1983). Changes in anticodon loop size also have a detrimental effect on aminoacylation (Schulman and Pelka, 1983). Alteration of the anticodon of tRNA^{fMet} can also change the identity of the tRNA. For example, changing the anticodon of tRNA^{Met} (CAU) to that of tRNA^{Val} (UAC) changed the identity of the mutant tRNA^{fMet} to valine. The "reverse" construction--replacing the anticodon of tRNA^{Val} with the CAU anticodon of tRNA^{fMet}--yielded a mutant tRNA^{Val} that was charged with methionine (Schulman and Pelka, 1988).

The success of these anticodon replacements may be due in part to each of the tRNAs having the same acceptor stem discriminator base. (As

discussed earlier, the acceptor stem of tRNA^{fMet} also contains nucleotides important for aminoacylation.) In *S. cerevisiae* tRNA^{Asp}, replacement of the anticodon with the tRNA^{Met} anticodon (CAU) was not sufficient to allow methionylation with yeast MetRS. However, the additional substitution of the discriminator base G73 with an A, was sufficient to promote methionylation. Substitution of U32, G37 and C38 in the anticodon loop, with the corresponding nucleotides from tRNA^{fMet}, also had a positive effect on methionylation efficiency. These results illustrate the role of sequence context and the importance of the acceptor stem discriminator base interactions (Senger *et al.*, 1992).

Rationale for Experiments Presented in Thesis

This thesis focuses on dissecting out the two discrete domains of tRNA^{fMet} and studying their interactions with full length and truncated MetRS and with the isolated C-terminal anticodon binding domain. The work focused also on comparing the stability and activity of the discrete protein domain with that of the native protein. Most of the earlier work on domains of synthetases has used catalytic activity *per se* as the measure of function. I investigated primarily RNA binding which was independent of activity. In particular, I focused on the interaction of the isolated C-terminal domain of MetRS with the anticodon trinucleotide in the context of the whole tRNA and of a small RNA hairpin oligonucleotide. Separately, I studied the interaction of the acceptor helix of tRNA^{fMet} with MetRS. Thus, each of the two major domains of tRNA^{fMet} was investigated.

The binding energies so obtained and kinetic data enabled me to separate the contribution to tRNA recognition of protein interactions in the initial binding step from those in the transition state of catalysis. In addition,

using binding energies for the individual tRNA domains, I was able to estimate the strain induced in the full tRNA when its two domains are joined together and bound simultaneously to MetRS.

In order to measure the relatively weak binding interactions, it was necessary to adapt a special gel binding technique to the protein-RNA system studied here. Chapter 2 discusses the affinity coelectrophoresis technique which was utilized.

Chapters 3 and 4 discuss the production, characterization, and RNA binding affinity of the C-terminal domain of MetRS, in the form of a fusion protein and as a separate, free domain. This work has been presented (in part) in Gale and Schimmel (1995b). Chapter 5 discusses work done in collaboration with Dr. Sunghoon Kim to characterize a mutation in the C-terminal peptide appendix of MetRS that is involved in acceptor stem binding (Kim *et al.*, 1993b). Chapter 6 analyzes the binding of various acceptor stem microhelix RNA substrates to both the full length dimeric and native MetRS (MetRS$_{1-676}$) and the truncated monomer form of MetRS (MetRS$_{1-547}$). These binding interactions are interpreted in the context of the aminoacylation activities of these microhelices.

All of this work focused on isolating interactions between domains of synthetases with domains of the tRNA, and using these data to dissect out specific contributions to tRNA recognition. By showing that it was possible to separate the individual domain-domain interactions within the MetRS-tRNA complex and still retain function, I also obtained support for the feasibility of the assembly of the synthetase-tRNA complex in evolution from individual protein and RNA domains.

Classes of tRNA Synthetases [a]

Class I	Class II
Arg, Cys, Glu, Gln, Ile, Leu, Met, Tyr, Trp, Val	Ala, Asn, Asp, Gly, His, Lys, Phe, Pro, Ser, Thr
Class Defining Motifs	Class Defining Motifs
HIGH KMSKS	Motif 1 Motif 3 Motif 3
Catalyze Aminoacylation at 2'-OH	Catalyze Aminoacylation at 3'-OH
Primarily Monomeric	Multimeric
Catalytic Domain Structure	Catalytic Domain Structure
Rossman nucleotide binding fold 6-stranded parallel ß-sheet	7-stranded antiparallel ß-sheet

[a] Adapted in part from (Eriani *et al.*, 1990)

Table 1-1

34

Legend to Figure 1-1

Schematic of the tRNA cloverleaf secondary structure, its folded L-shaped tertiary structure, and minihelix and microhelix RNAs

A. The secondary structure of tRNA is depicted on the left in the cloverleaf form. The numbering is based on the most common tRNA length of 76 nucleotides. The right structure illustrates the tertiary structure of the tRNA. In the tertiary structure of a tRNA, the acceptor stem stacks coaxially on the TΨC stem-loop to form one arm of the L-shaped tRNA. The dihydrouridine (DHU) stem-loop stacks coaxially on the anticodon stem-loop to form the other arm of the tRNA. Tertiary interactions between the loops at the corner of the molecule are critical for maintaining the tertiary structure of the molecule. B. The left hairpin helix represents a minihelix substrate, which is composed of the acceptor-TΨC stem and the TΨC loop. The right hairpin helix represents a microhelix substrate, which is composed of the acceptor-stem and the TΨC loop. Adapted from (Martinis and Schimmel, 1995)

Figure 1-1

Representation of the conserved active site domain of class I aminoacyl-tRNA synthetases

The class I aminoacyl-tRNA synthetase active site consists of alternating ß-strands and α-helices which form a six-stranded parallel ß-sheet (in a ß$_3$α$_2$ arrangement for each half of the motif). This structure is a Rossman nucleotide binding fold which is found in enzymes that bind adenine nucleotide cofactors (Rossmann *et al.*, 1974). The approximate locations of the 11 amino acid (ending in HIGH) signature sequence and the KMSKS consensus sequence are shown. Alpha-helices are shown as cylinders, and ß-strands are shown as arrows. Adapted from Starzyk *et al.* (1987).
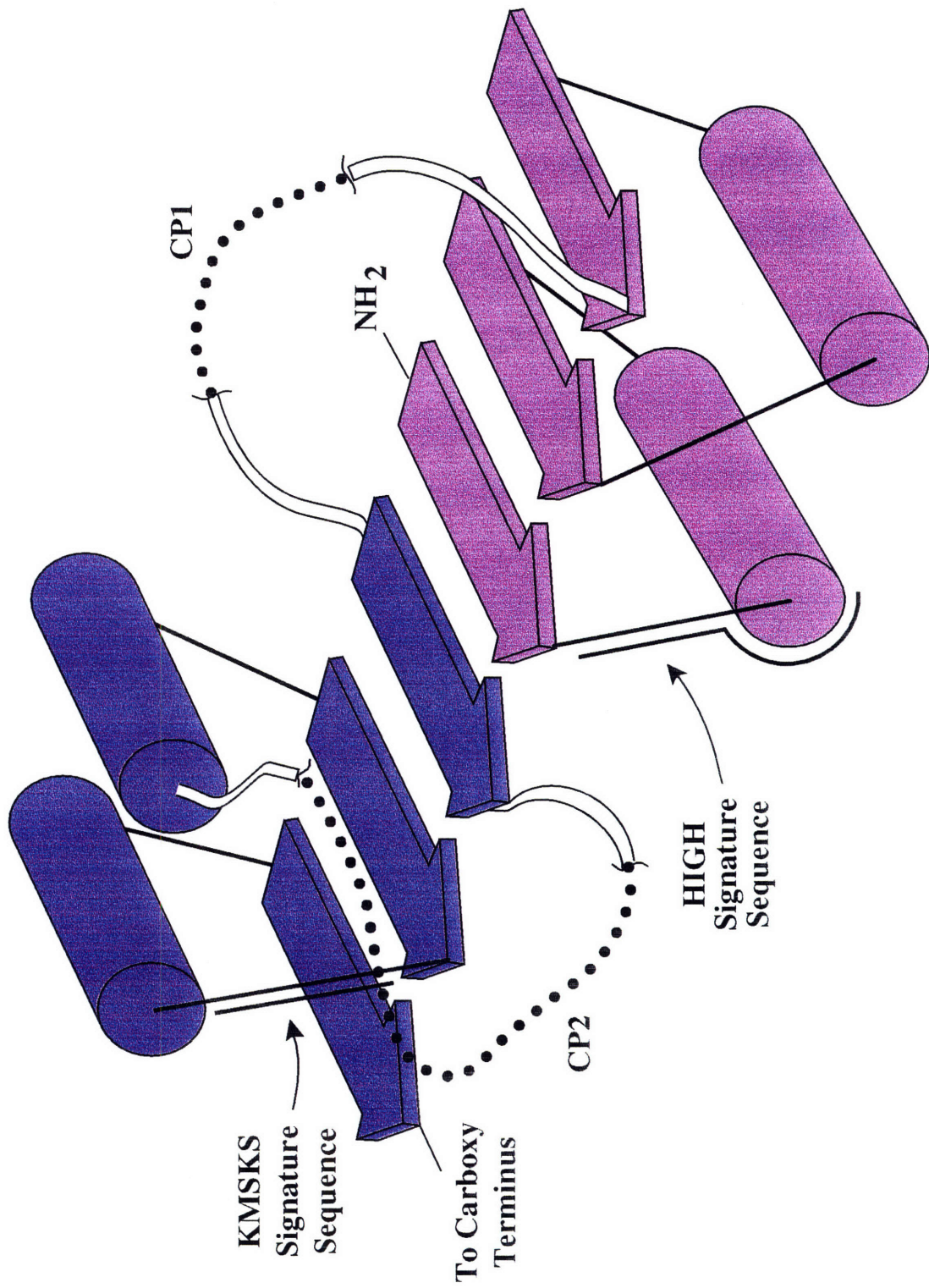
CP1

NH₂

KMSKS
Signature
Sequence

To Carboxy
Terminus

HIGH
Signature
Sequence

CP2

Figure 1-2

Representation of the conserved active site domain of class II aminoacyl-tRNA synthetases

The class II aminoacyl-tRNA synthetase active site consists of a seven-stranded antiparallel ß-sheet. The locations of the three sequence motifs characteristic of the class II synthetases are highlighted. Alpha-helices are shown as cylinders, and ß-strands are shown as arrows.

To Amino Terminus

To Carboxy Terminus

■ Motif 1
■ Motif 2
■ Motif 3
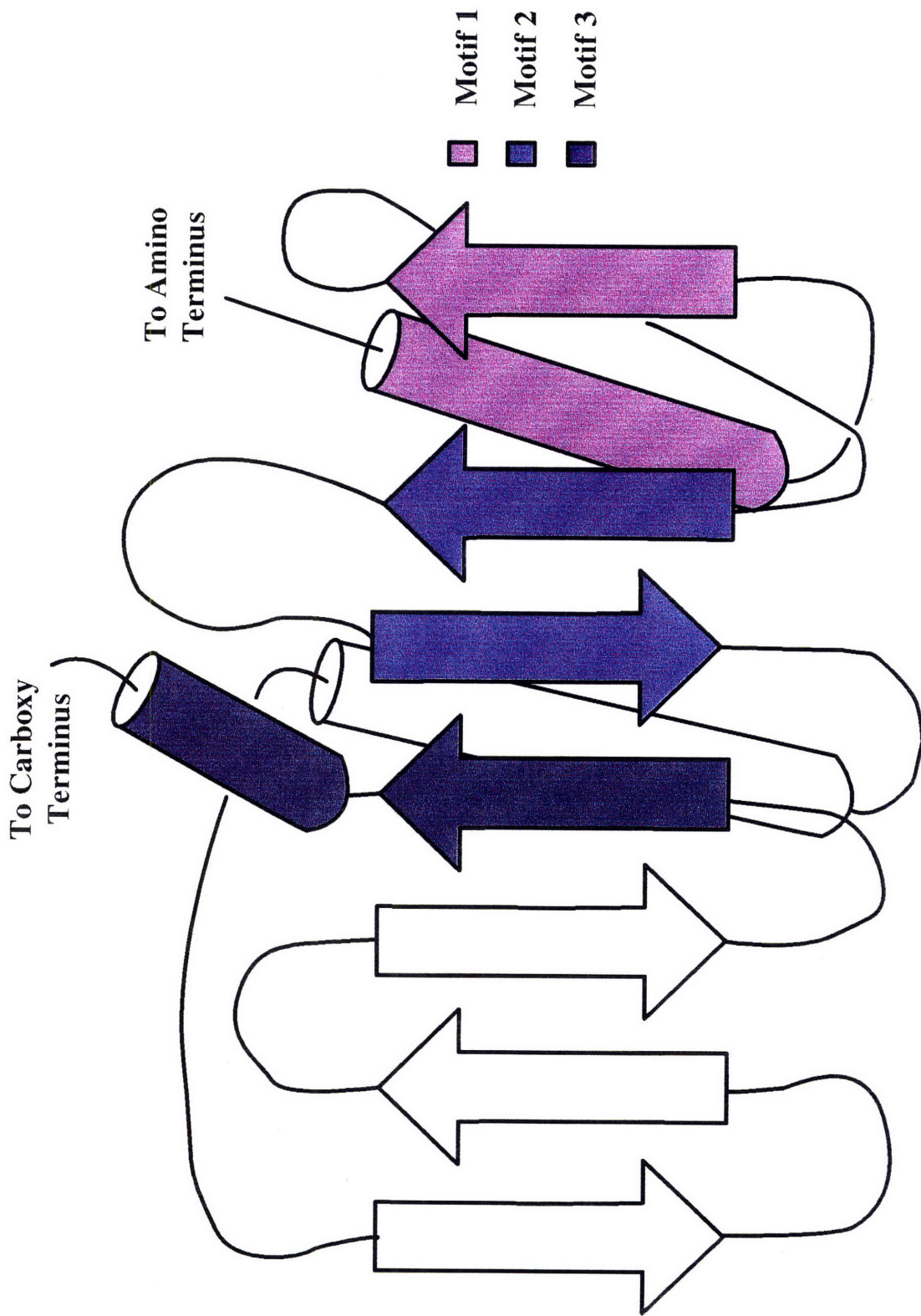
Figure 1-3

Legend to Figure 1-4

Assembly of RNA/protein domains during the evolution of a synthetase-tRNA complex

Transfer RNAs and synthetases may have coevolved from primordial RNAs and primordial synthetases. The conserved synthetase domain was the primordial synthetase that interacted with an RNA acceptor-TΨC-like domain, resulting in an operational RNA code for amino acids that related RNA structure/sequence to specific amino acids. As a template-dependent translation process developed, the anticodon-D-stem-biloop domain was added to the primordial tRNAs and an additional nonconserved domain was added to the synthetases to facilitate interactions with these distal regions of the tRNA, such as the anticodon. In the process, acceptor stems with their amino acids became associated with specific anticodon sequences and the genetic code was established. Adapted from Schimmel *et al.* and Schimmel & Ribas (Schimmel *et al.*, 1993; Schimmel and Ribas de Pouplana, 1995).

41

Acceptor-TΨC Stem Loop Domain

Anticodon-D Stem-Biloop Domain

Conserved Domain

Non-conserved Domain

Conserved Domain

Non-conserved Domain
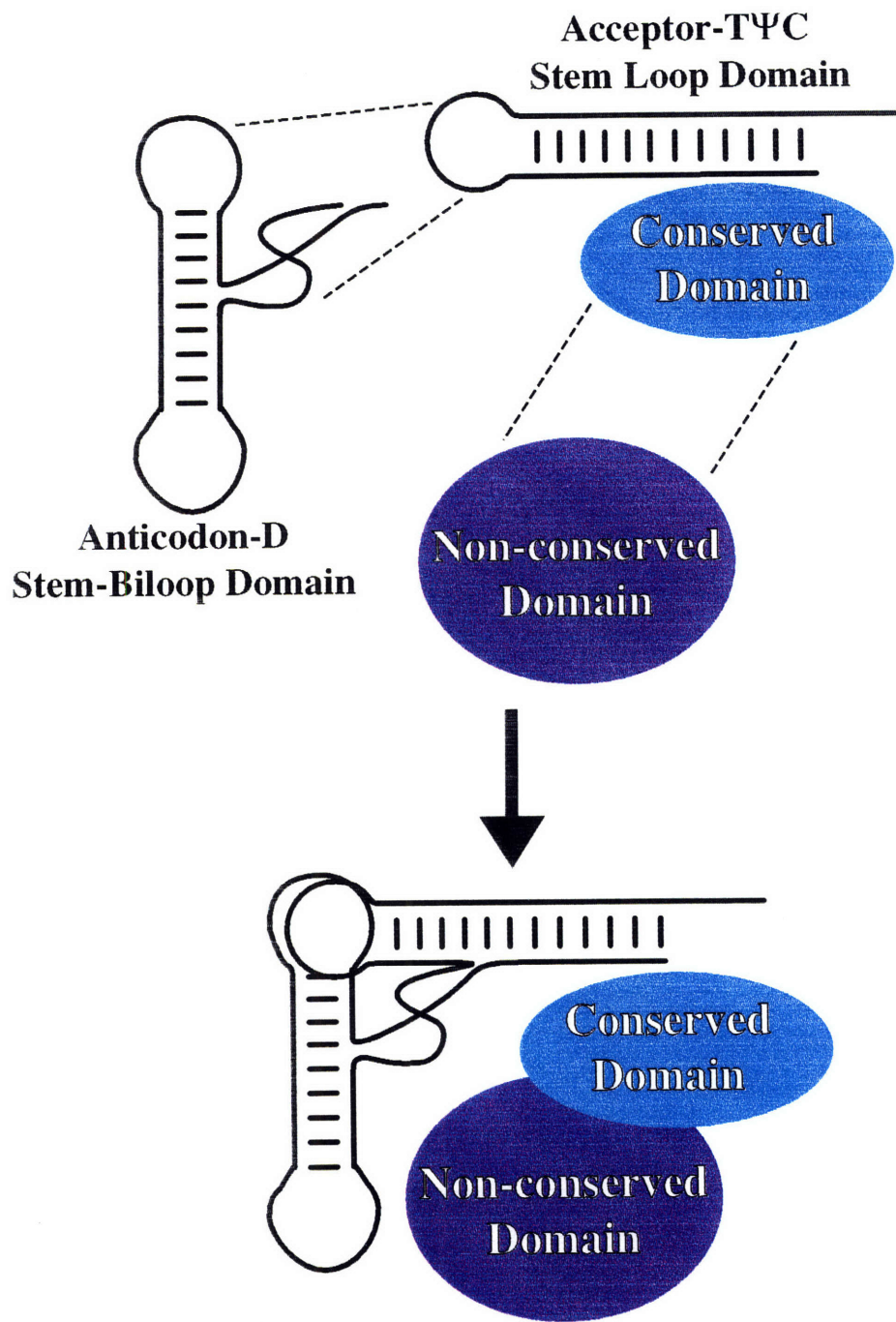
Figure 1-4

Legend to Figure 1-5

Crystal structure of truncated monomeric MetRS

The crystal structure of the truncated monomeric form of MetRS (residues 1-551) has been solved to 2.5 Å resolution (Brunie *et al.*, 1990). Shown (in dark blue) in this depiction of the crystal structure is the N-terminal catalytic domain, including the Rossman nucleotide binding fold. The C-terminal non-conserved, anticodon binding domain is highlighted in light blue. Trp461, which is thought to interact with the anticodon, is highlighted in red. The C-terminal peptide appendix is shown in green.

N-terminal
catalytic
domain

C-terminal
peptide
appendix

C-terminal
anticodon
binding
domain

Trp461
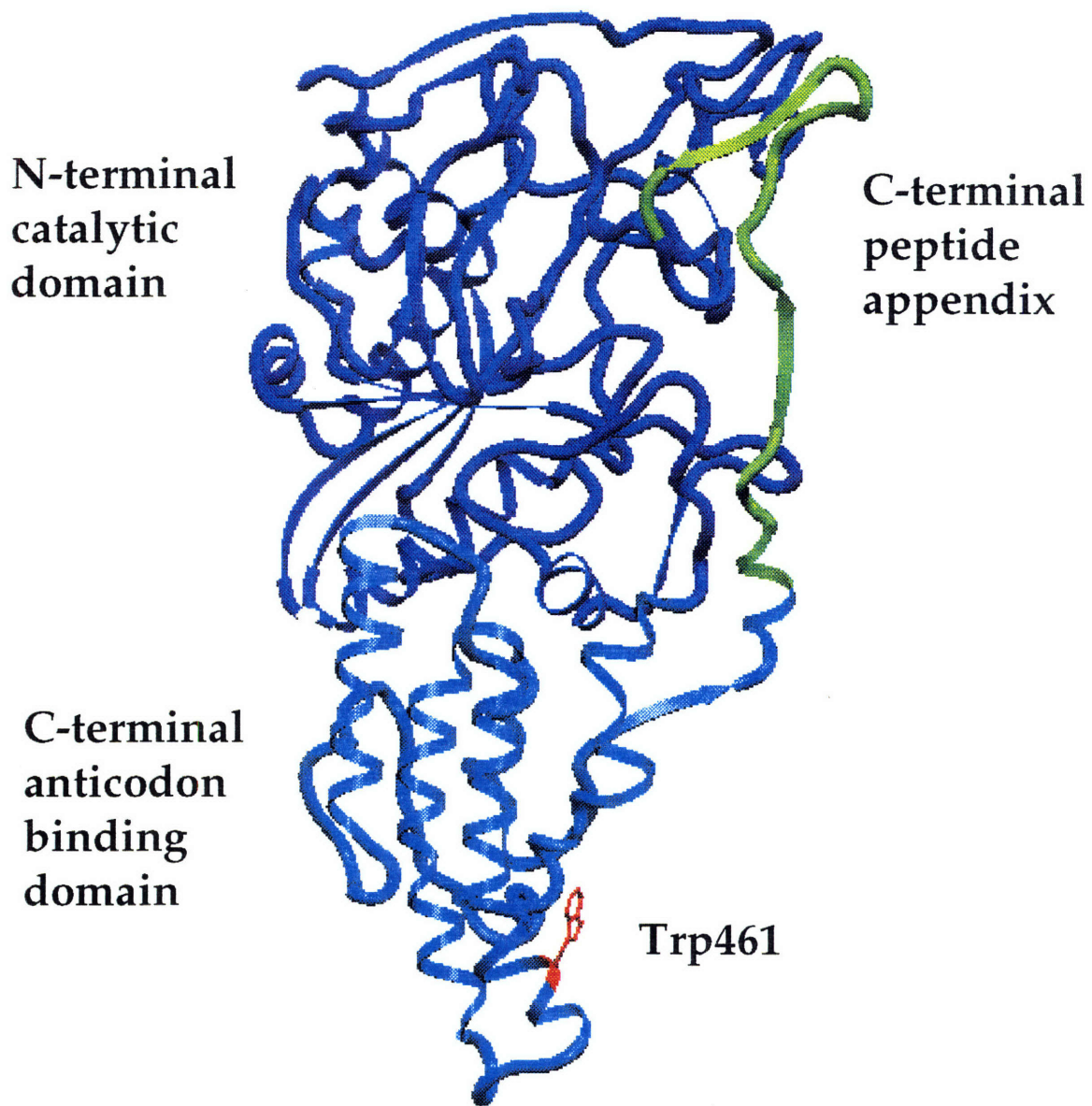
Figure 1-5

Chapter 2

Affinity Coelectrophoresis for Dissecting Protein-RNA Domain-Domain Interactions in a tRNA Synthetase System

INTRODUCTION

Affinity coelectrophoresis (ACE) is a gel retardation method that allows the measurement of binding under equilibrium conditions in a gel (Lee and Lander, 1991; Lim et al., 1991). As described below, it is useful for analyzing the relatively weak interactions between an aminoacyl-tRNA synthetase and its cognate tRNA. Furthermore, it is uniquely ideal for characterizing the interactions between individual synthetase and tRNA domains. Interactions between aminoacyl-tRNA synthetases and isolated domains of their cognate tRNAs can be demonstrated to be kinetically specific (Francklyn and Schimmel, 1989; Buechter and Schimmel, 1993a; Martinis and Schimmel, 1995) but the binding affinity is often so low that it can be difficult to measure by other commonly used techniques for measuring binding affinities. This chapter explains the method and summarizes the application of ACE to the interactions of aminoacyl-tRNA synthetases and their RNA substrates. This chapter is adapted from (Gale and Schimmel, 1995a).

MATERIALS

Synthesis and Radioactive Labeling of RNA Oligonucleotides. RNA oligonucleotides were chemically synthesized on a Gene Assembler Plus synthesizer (Pharmacia LKB Biotechnology Inc., Piscataway, NJ) as previously described (Usman et al., 1987; Scaringe et al., 1990; Musier-Forsyth et al., 1991). The RNA substrate was 5'-[^{32}P]-labelled according to (Silberklang et al., 1977; Park and Schimmel, 1988).

Custom gel electrophoresis equipment for these experiments was made by Owl Scientific (Cambridge, MA). Low melting point agarose (LMP agarose) (BRL, Gaithersburg, MD) (1%) was prepared in 50 mM Hepes (pH 7.5), 0.1 mM EDTA, 4 mM MgCl$_2$, 1 mM ß-ME, and 100 µg/ml BSA.

METHODS AND RESULTS

Affinity coelectrophoresis was used to investigate the binding of the wild-type and mutant enzymes to the RNA substrates. Affinity coelectrophoresis is a technique that was developed by Lee and Lander (1991) to investigate binding of proteins to glycosaminoglycans under equilibrium conditions. It is also generally applicable to protein-nucleic acid binding interactions (Lim et al., 1991) and we found it to be particularly useful for visualizing the relatively weak binding interactions of aminoacyl-tRNA synthetases and their cognate tRNAs (Kim et al., 1993b; Gale and Schimmel, 1995b).

A Teflon comb with 10 parallel bars that have a footprint of 35 X 2 mm and are separated from each other by 5 mm was placed on Gelbond film (FMC Bioproducts, Rockland, ME) in a Plexiglas casting tray. A Teflon comb that made a well measuring 73 X 1 mm was placed 4 mm from one end of the parallel bars (Figures 2-1 and 2-2). The agarose was poured to a depth of about 2 mm. When the combs were removed, 10 parallel 35 X 2 mm wells perpendicular to a 73 X 1 mm slot resulted. The appropriate protein was then prepared in a series of concentrations in buffer at twice the desired final concentrations. These samples were mixed 1:1 with 2% LMP agarose and loaded into the 35 X 2 mm wells. The range of protein concentrations in the gel was from 0.05 μM to 2.5 μM for the experiment with MetRS and tRNA[fMet].

The 5'-[^{32}P]-RNA (10,000 to 150,000 cpm) was mixed 1:1 with 2% LMP agarose at a final concentration of roughly 10 nM and loaded into the 73 X 1 mm slot along with 0.02% bromophenol blue and 0.02% xylene cyanol. Alternatively the 5'-[^{32}P]-RNA was diluted to 70 μl in the buffer described

above along with 0.02% bromophenol blue, 0.02% xylene cyanol, and 3% glycerol and then loaded into the 73 X 1 mm slot. The gel was electrophoresed at 100-150 V for 1.5 to 2 hours in a thermostated circulating gel box (Hoefer Super Sub, model HE100 (Hoefer Scientific, San Francisco, CA)) at 25 °C. The gel running buffer was the gel buffer without ß-ME and BSA. Gels were dried in an open vacuum oven with low heat or under a heat lamp and visualized using a PhosphorImager from Molecular Dynamics (Sunnyvale, CA). The protein moves in the gel as does the RNA, however, this shift is much less than the RNA shift. The movement of the protein due to electrophoresis can be visualized by staining the dried gel with coomassie brilliant blue (0.05%) in 50% MeOH and 10 % acetic acid. The staining for protein (and detection of its movement) is most conveniently done after visualization of the radioactive RNA on a PhosphorImager screen.

The 5'-[^{32}P]-RNA was electrophoresed most of the way through the protein in each lane. The K_d was determined by measuring the vertical shift m of [^{32}P]-RNA in each protein lane, relative to a protein-free lane (Figure 2-2). This shift should be proportional to the fraction of RNA bound to protein at equilibrium in the gel, assuming that the kinetics of association and dissociation are rapid relative to electrophoresis times and that there are only 2 states, bound and free. The shift value m is divided by the maximum possible shift n to give a retardation coefficient R ($R = m/n$, Figure 2-2). Given the retardation coefficient R, if R_∞ is the maximum possible value of R than $R/R_\infty = \theta$, where θ represents the fractional saturation of the RNA with protein.

Because R is proportional to θ, data from ACE can be analyzed using the Scatchard equation. For a first order reaction the model for binding is:

$$P + A \rightleftharpoons PA \qquad K_d = [P][A]/[PA]$$

with

$$\theta = [PA]/([PA] + [A])$$

where P is protein and A is the RNA fragment. Since $\theta = R/R_\infty$, the expression for binding can be written as

$$R = R_\infty/[1 + (K_d/[P])]$$

Because $[P] = [P_{tot}] - [PA]$ and $[PA]$ is very low relative to $[P_{tot}]$ (because the exeperiments are conducted with trace levels of A (RNA)) this equation becomes

$$R = R_\infty/[1 + (K_d/[P_{tot}])].$$

Therefore,

$$R + (R \cdot K_d)/[P_{tot}] = R_\infty$$

which rearranges to

$$R/[P_{tot}] = -R/K_d + R_\infty/K_d.$$

Therefore, a Scatchard plot of R vs. $R/[P_{tot}]$ gives a linear plot whose slope is equal to $-1/K_d$ (Lim et al., 1991).

Affinity coelectrophoresis was first used to investigate the dissociation constant of MetRS for tRNA[fMet] (Figure 2-3). In this ACE gel tRNA[fMet] was electrophoresed through lanes containing MetRS. A dissociation constant was determined from a Scatchard plot as described above. The Scatchard plot gave a value for the dissociation constant of 0.5 µM, at pH 7.5, 25 °C (Figure 2-3). This value compares with a published K_d of 0.06 µM given by Blanquet et al. (1973a) which was determined spectrofluorimetrically under similar conditions. It is not clear why the value determined by affinity coelectrophoresis is weaker than that determined by Blanquet et al.. We determined a K_d of MetRS for tRNA[fMet] by fluorescence quenching using conditions similar to that of Blanquet et al. and obtained a value of 0.3 µM

(data not shown). This determination by fluorescence titration is consistent with the electrophoresis results.

DISCUSSION

In subsequent chapters of this thesis are many examples of affinity coelectrophoresis applied to the interaction of MetRS and various small RNA substrates that recapitulate either the acceptor stem or anticodon stem and loop of a tRNA. Dissociation constants for these small RNA substrates range from 5 μM to 500 μM. Though very weak, many of these binding interactions are sequence specific.

The technique of affinity coelectrophoresis has several advantages that make it attractive for measuring the binding interactions between aminoacyl-tRNA synthetases and small RNA substrates. The synthetase-tRNA dissociation constants are generally on the order of 0.1 to 1 μM at pH 7.5 (Helene et al., 1971; Blanquet et al., 1973a; Lam and Schimmel, 1975; Schimmel and Söll, 1979; Meinnel et al., 1991b). Compared to other protein-nucleic acid complexes, these interactions are relatively weak, presumably because of the need for turnover during protein synthesis. Therefore, many standard techniques for measuring dissociation constants do not work well. Filter binding assays have been used for measuring dissociation constants of tRNAs to aminoacyl-tRNA synthetases (Yarus and Berg, 1967; Yarus and Berg, 1970), but generally these assays need to be done at an acidic pH value (pH 5.5 - 6.0) where tRNAs bind more tightly to aminoacyl-tRNA synthetases (Schimmel and Söll, 1979). Even at pH 5.5 small RNA substrates such as acceptor stem microhelices may be bound with an affinity below the sensitivity of the filter binding assay. Fluorescence quenching has also been used to measure

50

synthetase-tRNA interactions (Helene *et al.*, 1971; Blanquet *et al.*, 1973a; Blanquet *et al.*, 1973b; Lam and Schimmel, 1975). This method also does not work well for small RNA substrates because the concentrations of optically dense RNA necessary to quench the protein fluorescence signal are not practical. (The large size of the RNA substrate makes a technique like equilibrium dialysis also impractical.) Affinity coelectrophoresis, in contrast, is capable of measuring dissociation constants up to values above 100 μM.

Affinity coelectrophoresis does have limitations. Measuring weak binding constants requires large amounts of protein. For experiments in which the binding constants for the acceptor stem microhelix to $MetRS_{1-547}$ were measured (see chapters 5 and 6), the protein concentration range was from 10 μM to 350 μM in a total volume of 160 μL for each of 8 lanes. Thus, about 11.5 mg of $MetRS_{1-547}$ (MW= 62,400 daltons) were required for one experiment. Therefore, good expression systems and purification protocols are necessary to obtain the quantities of protein needed for this technique.

However, for measuring binding constants to full length tRNAs much less protein is needed. A concentration range of about 1/5 of the expected K_d to 5 times the expected K_d is appropriate to measure the K_d. In the case of $MetRS_{1-676}$ with $tRNA^{fMet}$ shown here (Figure 2-3) the range was from 0.05 to 2.5 μM $MetRS_{1-676}$. Therefore, this experiment used a total of 86 μg of $MetRS_{1-676}$ (subunit MW = 76,000 daltons).

It is clear, then, that the technique of affinity coelectrophoresis is uniquely qualified to measure the weak binding interactions between synthetases and small RNA substrates that recapitulate segments of the tRNA. Furthermore, it has the additional advantage of being a straightforward technique for measuring the interaction between synthetases and full length tRNAs at physiologic pH and buffer conditions.

51

A.　　　　　　　　　　　　　**B.**
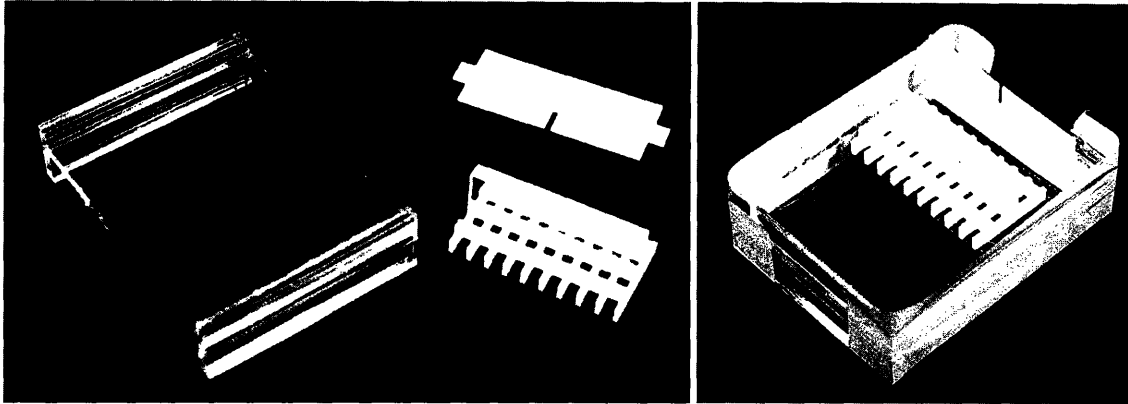
Figure 2-1

Affinity coelectrophoresis gel casting apparatus

A. The components of the ACE gel casting apparatus. Plexiglass casting tray (left), slot-forming comb (upper right) and the lane-forming comb (lower right). B. The assembled gel casting apparatus. The Plexiglass casting tray is assembled with tape along the edges to seal the tray and hold up the slot-forming comb. The lane-forming comb is placed on the tray with the lanes perpendicular to the slot-forming comb.

Legend to Figure 2-2

Schematic representation of an affinity coelectrophoresis gel before and after electrophoresis

A. Prior to electrophoresis, protein is cast in agarose in parallel rectangular lanes in increasing concentrations from right to left. Labeled RNA is aliquoted into the slot at the top of the gel. B. Following electrophoresis the RNA has moved through the rectangular zones of protein but is slowed by binding to the protein. The amount of retardation is indicated by the value m and a retardation coefficient R $= m/n$ is proportional to the fractional saturation of RNA with protein. This figure is similar to that of Figure 1 of Lee and Lander (1991).

Figure 2-2

54
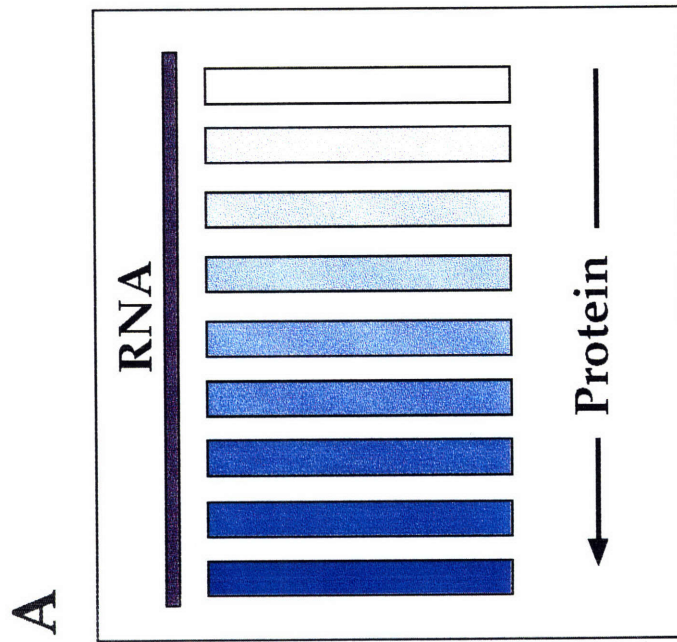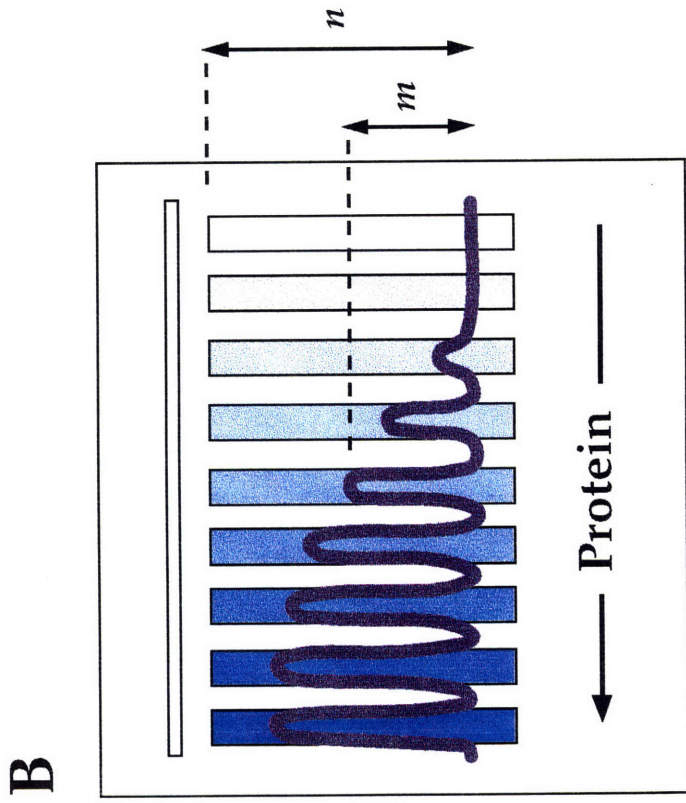
Legend to Figure 2-3

Affinity coelectrophoresis (ACE) to determine the binding constant of MetRS for tRNA^fMet

A. Gel electrophoresis of MetRS in lanes of increasing concentration from right to left with [^{32}P]-end labeled tRNA^fMet electrophoresed through the protein lanes at pH 7.5, 25 °C. B. Scatchard plot of the measured R values versus R/[MetRS]. The slope of the line is equal to $-1/K_d$.

A.

2.5 ◼◣ 0.05 μM
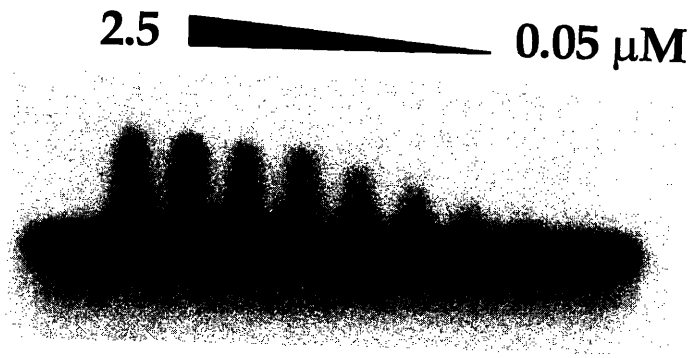
B.
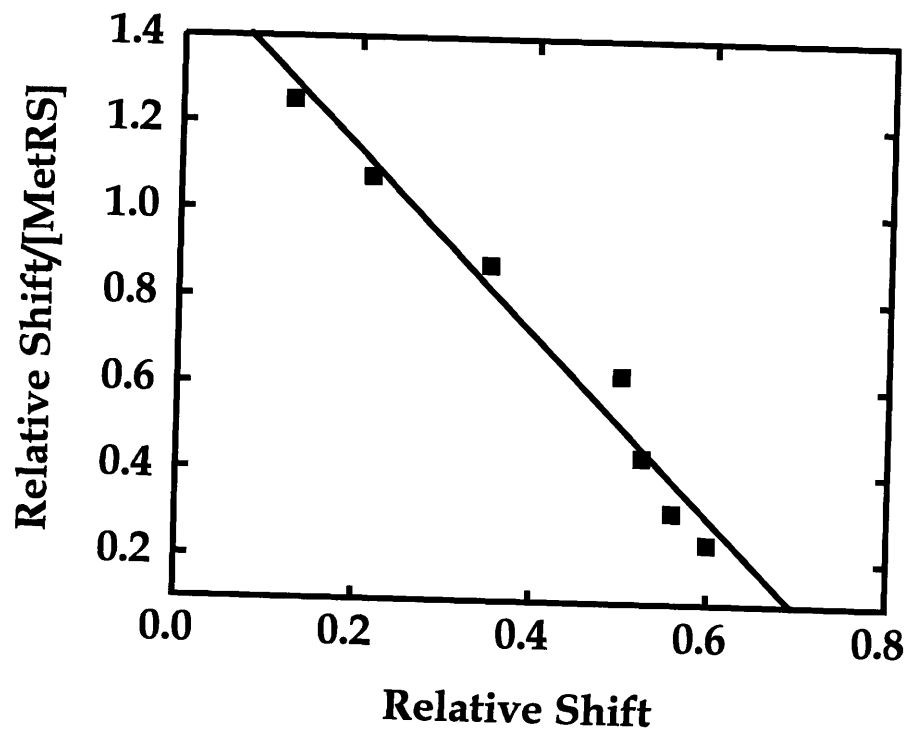
Figure 2-3

Chapter 3.

Construction, Purification and Physical Properties of Fused and Unfused C-terminal Domain Proteins

INTRODUCTION

MetRS, like other tRNA synthetases, is composed of two major domains. The class-defining catalytic domain is within the N-terminal half of the structure, while the C-terminal domain is predominantly α-helical and is known to contain residues that interact directly with the anticodon of tRNA^{Met} (Valenzuela and Schulman, 1986; Ghosh et al., 1990; Ghosh et al., 1991; Meinnel et al., 1991b; Kim et al., 1993a; Auld and Schimmel, 1995) (Figure 3-1). Previous work demonstrated that MetRS could be split so that the two domains of the synthetase were expressed as separate polypeptides. A non-covalent complex of these two domains maintained high levels of activity (Burbaum and Schimmel, 1991a). This finding showed that the function of the combined domains is independent of a covalent connection between them.

Based on this previous work, and considering the pathways for the evolution of the two-domain structure of tRNA synthetases, we considered whether the anticodon binding domain could function as a discrete unit when joined to an arbitrary protein. In particular, a peptide "appendix" at the end of the anticodon-binding domain curls back to the active site of the N-terminal domain of MetRS, thereby linking together the two structures (Brunie et al., 1990; Kim et al., 1993b) (Figure 3-1). We thought that this linkage, as well as the packing interaction of the domain interface, might be necessary to achieve a conformation for RNA binding by the C-terminal domain.

We decided to produce this C-terminal domain as a fusion protein in order to facilitate solubility and purification. We chose to define the start of the C-terminal domain as residue I367 based upon the work of Burbaum et al. (1991a) in which MetRS was split into two co-expressed polypeptides that

were able to reconstitute active MetRS. In this work Burbaum *et al.*

engineered a split in the protein at six different locations from residue 355 to

374. Three of the six constructs produced active MetRS, including one that

started the C-terminal polypeptide at I367 (preceded by a methionine start

codon).

In this work we fused amino acids 367 to 547 of the anticodon binding

domain of *E. coli* MetRS with maltose binding protein (MBP-C$_{367-547}$) (Guan *et*

al., 1987; Maina *et al.*, 1988). We also made one variation of this fusion

protein that contained a Trp461 Ala substitution in the C-terminal domain

(MBP-C$_{367-547}$(W461A)).

These fusion proteins contained a linker between the gene for MBP

and the C-terminal domains which encoded ten amino acids that included a

Factor Xa protease cleavage site (Figure 3-2). This linker allowed for the

separation of the C-terminal domains from MBP so that they could also be

characterized as isolated proteins. The first stage of the analysis of these

fusion proteins and C-terminal domain fragments was to physically

characterize them to determine whether or not the C-terminal domains in

these proteins maintained native-like structure. The results of the

characterization of MBP-C$_{367-547}$ and C$_{367-547}$ have been reported (Gale and

Schimmel, 1995b) and the text that follows is adapted with permission from

that report (Copyright 1995, American Chemical Society).

MATERIALS AND METHODS

Construction of Fusion Proteins. Phagemid pJB104 encodes the

monomeric form of *Eschcerichia coli* methionyl tRNA synthetase (residues 1 to

547) (Kim and Schimmel, 1992). (All work in this chapter was done with the

547 amino acid N-terminal fragment of MetRS which hereafter will simply be

referred to as "MetRS$_{1-547}$".) Site-directed mutagenesis with the Sculptor *in vitro* mutagenesis system (Amersham, Arlington Heights, IL) was used to insert a *Bam* HI site in the MetRS$_{1-547}$ gene of phagemid pJB104 directly before the codon for I367. The mutagenic primer, 5'-CGATATCATCAATGGATCCAGAGAGTTTCGC-3', was used for this purpose. All oligonucleotides were synthesized by the MIT Biopolymers Laboratory. This construct (phagemid pAG117) was cleaved with *Bam* HI to produce a 759 bp fragment that was inserted into the *Bam* HI site of plasmid pMal-c2 (New England Biolabs, Inc., Beverly, MA) (Guan *et al.*, 1987; Maina *et al.*, 1988) to produce a gene fusion between *MalE* and codons 367 to 547 of MetRS including a linker between the two genes that encodes for 10 amino acids, including a Factor Xa cleavage site. The resulting plasmid is designated as pAG120 (Figure 3-2).

Site directed mutagenesis was used to change the codon for W461 (TGG) in the gene for MetRS$_{1-547}$ in the phagemid pJB104 to an alanine codon (GCG) (phagemid pAG123). The mutagenic primer 5'-TGTTTCGCCACCACCGCCGGAGCCTGTTCATC-3' was used for this purpose. This mutation was then "marker-transferred" into pAG120 by cleaving both pAG123 and pAG120 with *Cla* I to remove a 492 bp fragment. The mutant fragment from pAG123 was then inserted into pAG120 to produce a plasmid that encodes for a fusion between maltose binding protein and residues 367 to 547 of MetRS with a W461A mutation (protein MBP-C$_{367-547}$(W461A), plasmid pAG124).

The sequence of all plasmid constructs and mutants were verified by DNA sequencing. Sequencing was done using Sequenase (United States Biochemical, Cleveland OH) according to the manufacturer's instructions.

Purification of Fusion Proteins. Plasmids pAG120 and pAG124 were transformed into *E. coli* strain TG1 (*K12, SupE hsdΔ5 thi Δ(lac-proAB) F'[traD36 proAB+ lacI^q lacZΔM15]*). Expression of the fusion proteins was induced with 0.5 mM IPTG and the cells were harvested at late log phase. Cells were resuspended in buffer containing 20 mM Tris-HCl (pH 7.5), 200 mM NaCl, 1 mM EDTA, 10 mM ß-ME, and 0.5 mM PMSF, and lysed in a French press at 15,000 lbs/in.^{2}. The lysate was centrifuged at 27,000 X g for 15 minutes and the resulting supernatant was precipitated with 0.2 % polyethyleneimine (PEI) and then centrifuged at 12,000 X g for 10 minutes. The supernatant was then dialyzed into 25 mM Tris-HCl (pH 7.5), 1 mM ß-ME (Buffer A). The fusion proteins in this solution were purified using an FPLC system with a Mono Q HR 10/10 column (Pharmacia LKB Biotechnology, Uppsala, Sweden) with a linear NaCl gradient from 0 to 400 mM. Fractions containing fusion protein were identified by SDS-PAGE, concentrated to about 20 mg/mL protein, and then purified using an FPLC Superose 12 column (Pharmacia LKB Biotechnology, Uppsala, Sweden) in 25 mM Tris-HCl (pH 7.5), 200 mM NaCl, and 1 mM ß-ME.

Alternatively, for large scale preparations, a 500 mL DEAE-TSK column (Pharmacia LKB Biotechnology, Uppsala, Sweden) was substituted for the MonoQ column. After the protein sample was loaded the column was washed with 600 mL of Buffer A, and then the fusion protein was eluted with a linear NaCl gradient from 0 to 400 mM in 1600 mL. Fractions containing fusion protein were identified by SDS-PAGE, concentrated to about 5-10 mg/mL, and then purified over a 100 cm X 2.4 cm Sephacryl 100HR column (Pharmacia LKB Biotechnology, Uppsala, Sweden) in 25 mM Tris-HCl (pH 7.5), 200 mM NaCl, and 1 mM ß-ME. Protein concentration was determined by absorbance at 280 nm (Edelhoch, 1967; Cassio and Waller, 1971).

MetRS$_{1-547}$ was produced from a high-expression construct made by inserting the MetRS gene from phagemid pJB104 into the plasmid pKK223-3 expression vector with its *tac* promoter (Pharmacia Biotech, Inc., Piscataway, NJ). Phagemid pJB104 was cleaved with *Eco* RI and *Sal* I, and plasmid pKK223-3 was cleaved with *Eco* RI and both were digested with mung bean nuclease to remove single stranded ends (Sambrook *et al.*, 1989). The MetRS$_{1-547}$ gene was blunt-end-ligated (Sambrook *et al.*, 1989) into plasmid pKK223-3 to produce plasmid pAG112. MetRS$_{1-547}$ was purified as described earlier for the fusion protein except that after PEI precipitation the supernatant was fractionated with ammonium sulfate, and proteins precipitated at 30-55% ammonium sulfate were resuspended in 25 mM Tris-HCl (pH 7.5) and 1 mM ß-ME. This solution was then dialyzed into the same buffer to remove ammonium sulfate and purified by FPLC as described earlier for MBP-C$_{367-547}$.

Cleavage of Fusion proteins. The fusion proteins were cleaved using Factor Xa (New England Biolabs, Inc., Beverly, MA) in 50 mM Tris-HCl (pH 7.5), 100 mM Nacl, 2 mM CaCl$_2$. MBP-C$_{367-547}$ at a concentration of 1 mg/mL was incubated with Factor Xa at a concentration of 5 µg/mL (200:1, w:w) for 12 hours at room temperature. This reaction was then dialyzed into 25 mM Tris-HCl (pH 7.5), 1 mM ß-ME and the C-terminal domain (C$_{367-547}$, see Figure 3-2) was separated from maltose-binding protein by anion exchange using a Mono Q HR 10/10 column (Pharmacia LKB Biotechnology, Uppsala, Sweden) as described earlier.

Circular Dichroism Spectroscopy. CD experiments were performed on an AVIV model 62DS CD spectrometer with an AVIV model W5TE-159-S thermoelectric temperature-controlled cuvette holder (AVIV Associates, Inc., Lakewood, NJ). All experiments were done in 20 mM sodium phosphate (pH

7.3), 100 mM NaCl and 1 mM ß-ME. Spectra were recorded from 260 to 200 nm in 1 nm wavelength increments with a signal acquired for 5 seconds at each wavelength with a 1.5 nm bandwidth. The signal was recorded in units of mean residue ellipticity ([θ] deg cm^2 dmol^{-1}). Thermal denaturation was monitored by the change in [θ] at 222 nm. Temperature was incremented in 1 °C steps from 25 to 80 °C. The samples were equilibrated for 1 minute at each temperature and the signal was recorded for 5 seconds. The pH of the buffer in this temperature range changed by less than 0.2 pH unit. The melting temperature was determined as the minimum of the first derivative of [θ] at 222 nm versus 1/temperature (Cantor and Schimmel, 1980b). All spectra and thermal denaturation experiments were done at both 50 μg/mL protein and 1 mg/mL protein with a 5 mm pathlength and 0.5 mm pathlength, respectively.

RESULTS

Production and Cleavage of MBP-C$_{367-547}$. We chose the maltose binding protein (MBP) to fuse to the anticodon binding domain of MetRS. This protein has a molecular weight of 42,500 daltons and its interaction with amylose can be used as a basis to purify a fusion protein. In addition, the use of a linker with a Factor Xa cleavage site enables the release of the polypeptide joined to MBP (Figure 3-2). The fusion protein MBP-C$_{367-547}$ was expressed at high levels in *E. coli* strain TG1, typically yielding 40 mg/L of culture. The expressed fusion protein was soluble and stable and therefore amenable to purification (data not shown). We attempted to purify this protein with an amylose resin column (Maina *et al.*, 1988) but, although this column bound MBP with high affinity, MBP-C$_{367-547}$ did not bind well to the amylose resin. Instead, we used ion exchange chromatography on a Mono Q HR 10/10

63

column followed by gel filtration on Superose 12 which yielded MBP-C$_{367-547}$ of about 90% purity (Figure 3-3). Both MBP-C$_{367-547}$(W461A) and MBP-C$_{367-676}$ behaved essentially identically to MBP-C$_{367-547}$ in the purification protocol and gave similar yields.

Factor Xa at a 1:200 (wt:wt) ratio cleaved 100% of the fusion protein, and domain C$_{367-547}$ was then separated from MBP by ion exchange chromatography on a Mono Q HR 10/10 column (Figure 3-3). Edman degradation of the released cleavage product (carried out by the MIT Biopolymers Laboratory) verified that the N-terminus had the sequence ISEFGSIDDI, as expected (Figure 3-2). Although purified domain C$_{367-547}$ was analyzed by circular dichroism, amounts of cleaved domain C$_{367-547}$ sufficient to analyze for RNA binding by affinity coelectrophoresis (>5 mg) were limited. This limitation is primarily due to the relatively high levels of expensive Factor Xa needed to cleave the fusion protein. Therefore, most of the affinity coelectrophoresis analyses were done with the intact fusion protein MBP-C$_{367-547}$ (see Chapter 4). C$_{367-547}$(W461A) was cleaved from MBP and purified with the same protocol as C$_{367-547}$.

Circular Dichroism. According to the X-ray crystal structure of MetRS$_{1-547}$ (Brunie *et al.*, 1990), the secondary structure of domain C$_{367-547}$ is primarily α-helical. Domain C$_{367-547}$ has a CD spectrum similar to that of MetRS$_{1-547}$ with minima at 209 and 222 nm (Figure 3-4A). These minima are characteristic of α-helix secondary structure (Cantor and Schimmel, 1980a). The similarities of the CD spectra of the two proteins suggest that domain C$_{367-547}$ has a native structure like that of the same domain contained in the intact protein. The contribution of the N-terminal domain of MetRS to the CD spectrum decreases the negative peaks at 209 and 222 nm because that domain has short elements of ß-strand, α-helix, and irregular structures

which *in toto* should reduce the overall signal when expressed in units of mean residue ellipticity (Cantor and Schimmel, 1980a).

We also compared the CD spectrum of domain $C_{367-547}$ to spectra of MBP-$C_{367-547}$ and MBP alone (data not shown). Both domains are primarily α-helical and show characteristic minima at 209 and 222 nm. However, the CD spectrum of MBP alone has an overall minimum at 222 nm, whereas domain $C_{367-547}$ has a global minimum at 209 nm. Domain $C_{367-547}$ also has a deeper minimum with a value of -16,500 deg cm^2 $dmol^{-1}$ at 209 nm whereas MBP has a value of -11,000 deg cm^2 $dmol^{-1}$ at 222 nm. The spectrum for MBP-$C_{367-547}$ falls between these two spectra and qualitatively appears to be an average of the combined spectra (data not shown). The spectra for $MetRS_{1-547}$, $C_{367-547}$ and MBP-$C_{367-547}$ all show some dependence on concentration with all three showing somewhat less α-helical character at 50 μg/mL than at 1 mg/mL. The CD spectrum of MBP, however, was concentration-independent over the range of 50 μg/mL to 1 mg/mL. Collectively, these results suggest that there is little difference between the overall structure of domain $C_{367-547}$ in the fusion protein or as an "isolated protein".

The W461A mutant fusion protein and isolated C-terminal domain had CD spectra that were essentially identical to their wildtype counterparts. The CD spectrum of $C_{367-547}$(W461A) has a global minimum at 209 nm with a value of -17,100 deg cm^2 $dmol^{-1}$ at a concentration of 1 mg/mL (Figure 3-5A). Both the spectra for $C_{367-547}$(W461A) and MBP-$C_{367-547}$(W461A) show some dependence on concentration with somewhat less α-helical character at 50 μg/mL than at 1 mg/mL, as seen with the wildtype proteins. These results confirm that mutation of W461 to alanine does not cause any major structural perturbations in the C-terminal domain.

65

Thermal Melting Curves. Thermal melting curves of domain $C_{367-547}$ were performed to evaluate the thermal stability of this domain relative to intact $MetRS_{1-547}$ and to fusion protein $MBP-C_{367-547}$ (Figure 3-4B). Thermal denaturation was monitored at the 222 nm local minimum characteristic of α-helix structure. Experiments were done at both 50 μg/mL and 1 mg/mL for all proteins. $MetRS_{1-547}$ and $MBP-C_{367-547}$ had similar denaturation profiles at 1 mg/mL, where $MetRS_{1-547}$ had an apparent T_m of 61.5 °C and $MBP-C_{367-547}$ had an apparent T_m of 63 °C (Figure 3-4B).

In both cases denaturation was not reversible, probably because of the aggregation of denatured protein. Denaturation of the fusion protein was somewhat concentration-dependent with an apparent T_m of 56 °C at 50 μg/mL. It was not possible to measure the apparent T_m of $MetRS_{1-547}$ at 50 μg/mL because the denatured protein appeared to precipitate out of solution and settle to the bottom of the cuvette. However, the denaturation transition of $MetRS_{1-547}$ at 50 μg/mL appeared to start at the same temperature as $MetRS_{1-547}$ at 1 mg/mL.

The thermal denaturation curve of domain $C_{367-547}$ consistently showed a sharp cooperative transition, but the measured apparent T_m's varied significantly from preparation to preparation (Figure 3-4B). This variation was probably due to differences in the trace amounts of undigested $MBP-C_{367-547}$ and smaller fragments of $C_{367-547}$ present in purified preparations of $C_{367-547}$. In all cases the denaturation was largely nonreversible and aggregation was observed after denaturation. In four experiments with four independent preparations of $C_{367-547}$, apparent T_m's ranged from 62 to 68 °C at 1 mg/mL protein and from 60 to 67.5 °C at 50 μg/mL. The denaturation curve shown in Figure 3-4B has an apparent T_m of 66 °C.

Although some aggregation during the thermal denaturation of these proteins was evident, the cooperativity of the transitions (Figure 3-4B) suggests a native-like structure for the C-terminal domain both independently and as part of the fusion protein MBP-C$_{367\text{-}547}$. Protein C$_{367\text{-}547}$ appears to be as stable as, or more stable than, MetRS$_{1\text{-}547}$ or MBP-C$_{367\text{-}547}$.

Thermal denaturation of MBP-C$_{367\text{-}547}$(W461A) and C$_{367\text{-}547}$(W461A) showed a significant difference between these proteins and their wildtype counterparts in thermal stability. At 1 mg/mL, MBP-C$_{367\text{-}547}$(W461A) has an apparent T_m of 57.5 °C, which is 5.5 °C lower than that for wildtype MBP-C$_{367\text{-}547}$. Protein C$_{367\text{-}547}$(W461A) has an apparent T_m at 1 mg/mL of 58.5 °C, which is 3.5-9.5 °C lower than that of the wildtype C$_{367\text{-}547}$ (Figure 3-5B). Therefore, mutation of W461 to alanine has a significant effect on the thermal stability of the C-terminal domain, both in the fusion protein and in the isolated C-terminal domain.

As was the case for the wildtype proteins, the thermal denaturation of the mutant proteins was not reversible. However, in contrast to MBP-C$_{367\text{-}547}$, MBP-C$_{367\text{-}547}$(W461A) shows very little concentration-dependence. The apparent T_m of MBP-C$_{367\text{-}547}$(W461A) at 50 μg/mL was 55.5 °C, a decrease of only 2 °C. Wildtype MBP-C$_{367\text{-}547}$ shows a difference in apparent T_m of 7 °C in this concentration range. Protein C$_{367\text{-}547}$(W461A) also shows very little concentration-dependence with a decrease of 1 °C to 57.5 °C in its apparent T_m. But this small difference is similar to that observed with wildtype C$_{367\text{-}547}$, though at both concentrations the apparent T_m of the mutant domain is significantly decreased relative to that of the wildtype domain.

In spite of the effect on T_m of the mutation of W461 to alanine, both mutant proteins still have a cooperative melting transition characteristic of a native-like structure. Thus, the W461A mutation has not caused a large

67

structural perturbation of the C-terminal domain, but to some extent it has weakened the stability of the C-terminal domain.

DISCUSSION

Methionyl tRNA synthetase from *Thermus thermophilus* has been analyzed structurally by limited proteolysis. *T. thermophilus* MetRS was cleaved into four stable domains designated T1 through T4, in order of their location from the N-terminal to the C-terminal end of the protein (Kohda *et al.*, 1987). T1, but not T2, is active in aminoacylation, whereas both T1 and T2 could be crosslinked to tRNA^{Met}. These two domains appear to correspond to the N-terminal catalytic domain and the C-terminal anticodon binding domain of *E. coli* MetRS, respectively. Therefore, in *T. thermophilus* MetRS it appears that the two primary domains of the synthetase, the catalytic domain and the anticodon binding domain are stable and functional in an isolated form. Our data indicate that the anticodon binding domain from *E. coli* MetRS is also stable and native-like in structure as an isolated polypeptide.

The C-terminal end of MetRS is an appendix that extends back to the catalytic site (Brunie *et al.*, 1990) (Figure 3-1), where it contributes to binding of the acceptor stem of tRNA^{Met} (Kim *et al.*, 1993b). We thought that this contact might influence the conformation of the anticodon binding domain and that it might also be needed for its stability. However, the stability of domain C$_{367-547}$ in isolation is greater than that of MetRS (Figure 3-4B). The higher thermal stability of domain C$_{367-547}$ compared to MetRS (Figure 3-4B) shows that interactions of the C-terminal peptide appendix with the catalytic site are not required for the stable, native structure formed by domain C$_{367-547}$.

Though the Trp461 Ala substitution did not cause any major perturbations of the structure of MBP-C$_{367-547}$ or of C$_{367-547}$, it did cause a

decrease in thermal stability (Figure 3-5). It is possible that this decrease in thermal stability has some effect on the functionality of this protein. However, in view of the close similarities in the properties of the fused and unfused C-terminal domain, it is likely that any contribution of stability to the function of a W461A mutant MetRS would be similar to the contribution of stability to the function of the isolated W461A mutant domain.

Legend to Figure 3-1

Structure of MetRS$_{1-547}$ and the proposed structure of domain C$_{367-547}$

On the left is the structure of MetRS$_{1-547}$ with residues 367 to 547 highlighted in lighter blue. On the right is the proposed structure of the isolated C-terminal domain, C$_{367-547}$, with the peptide appendix labeled.

Peptide
Appendix
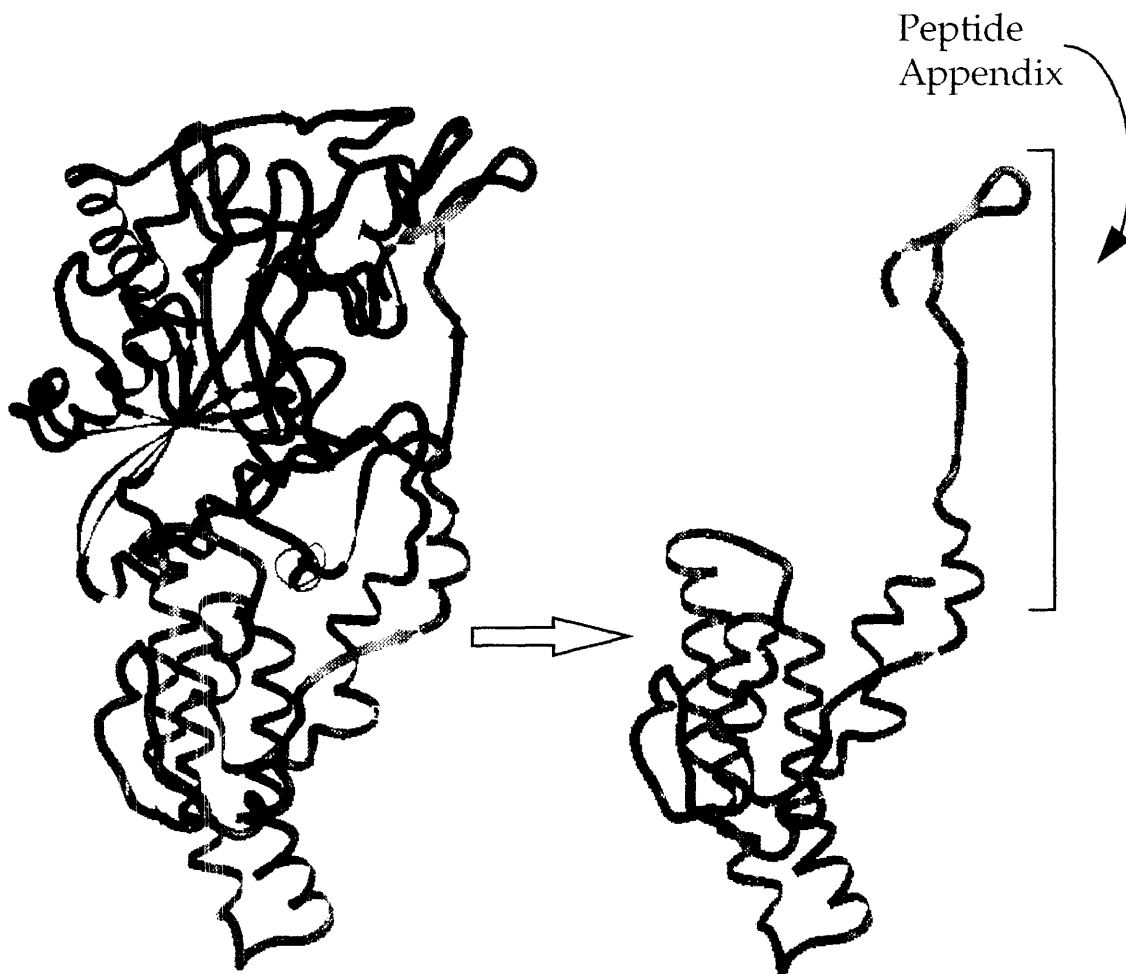
Figure 3-1

Legend to Figure 3-2

Plasmid pAG120 encoding the fusion protein MBP-C$_{367-547}$

The expanded region shows the coding sequence of the junction

between MBP and domain C$_{367-547}$ in the gene for the fusion protein MBP-

C$_{367-547}$. A *Bam* HI site was added to the MetRS$_{1-547}$ gene in phagemid pJB104

directly before the codon for I367. A *Bam* HI fragment was then excised from

plasmid pJB104 and inserted into the *Bam* HI site of plasmid pMal-c2 to give

plasmid pAG120. Adapted with permission from Gale and Schimmel (1995b)

(Copyright 1995, American Chemical Society).

MalE

Eco RI Bam HI

MetRS
367-547

ATG ···· GGG ATCGAGGGAAGGATTTCAGAATTCGGATCCATT ···· AAATAA
Met ···· Gly Ile Glu Gly Arg Ile Ser Glu Phe Gly Ser Ile ···· Lys Stp

Factor Xa
cleavage site

P_{taq}

LacZα

LacI^q

rrnB
terminator

pAG120
7408 bp

Amp^r

pBR322
ori

M13 ori
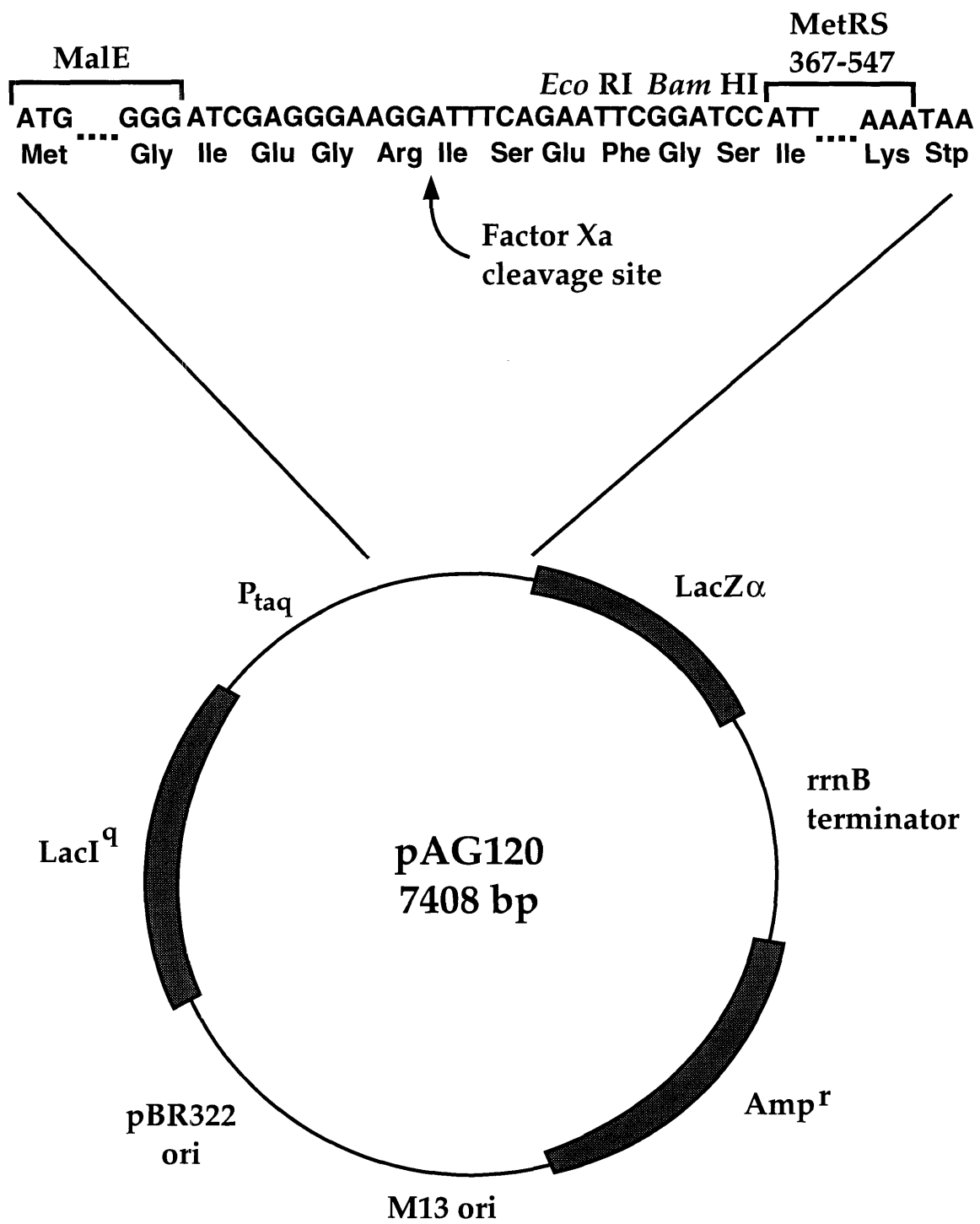
Figure 3-2

Legend to Figure 3-3

SDS-PAGE of extracts of cells expressing MBP-C$_{367-547}$ and the purification and cleavage of MBP-C$_{367-547}$

     This gel shows the stages of the purification of MBP-C$_{367-547}$ and C$_{367-547}$. Left lane, molecular weight standards with molecular weights in kilodaltons given along the left ordinate; A. MetRS$_{1-547}$; B. Protein (7.5 µg) from extracts of uninduced pAG120/TG1 cells; C. Protein (7.5 µg) from extracts of pAG120/TG1 cells induced with 0.5 mM IPTG for 4 hours to express MBP-C$_{367-547}$ at mid-log phase; D. MBP-C$_{367-547}$ (3 µg); E. MBP-C$_{367-547}$ (5 µg) cleaved with Factor Xa; F. MBP (3 µg) cleaved from MBP-C$_{367-547}$ and purified from C$_{367-547}$; G. C$_{367-547}$ (3 µg) cleaved from MBP-C$_{367-547}$ and purified from MBP. Adapted with permission from Gale and Schimmel (1995b) (Copyright 1995, American Chemical Society).

Figure 3-3

75
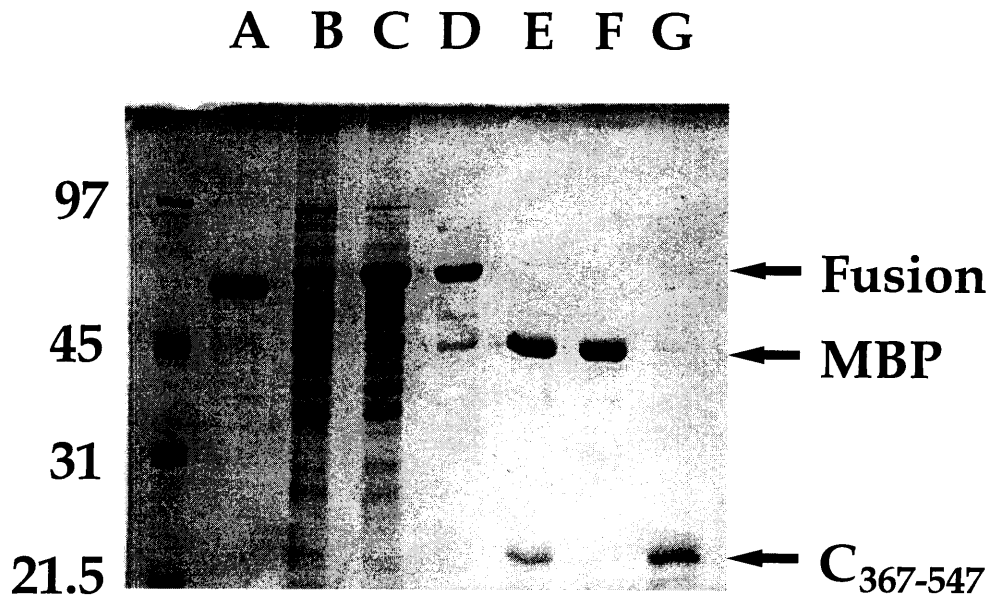
Legend to Figure 3-4

Circular dichroism analysis of domain $C_{367\text{-}547}$

A: CD spectra of $MetRS_{1\text{-}547}$ and $C_{367\text{-}547}$ at 25 °C on an AVIV 62DS CD spectrometer, each at a concentration of 1 mg/mL. B: Thermal denaturation curves of $MetRS_{1\text{-}547}$, $C_{367\text{-}547}$ and $MBP\text{-}C_{367\text{-}547}$, each at a concentration of 1 mg/mL. All CD spectra and thermal denaturation curves were done in 20 mM sodium phosphate (pH 7.3), 100 mM NaCl and 1 mM ß-ME. Adapted with permission from Gale and Schimmel (1995b) (Copyright 1995, American Chemical Society).

A.
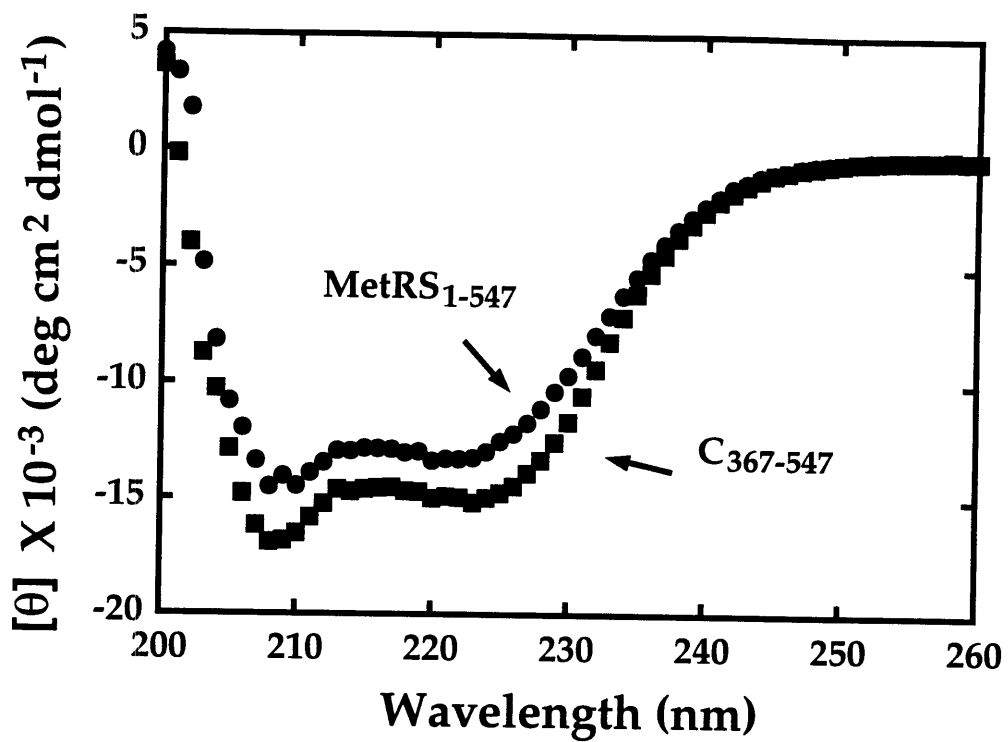
B.
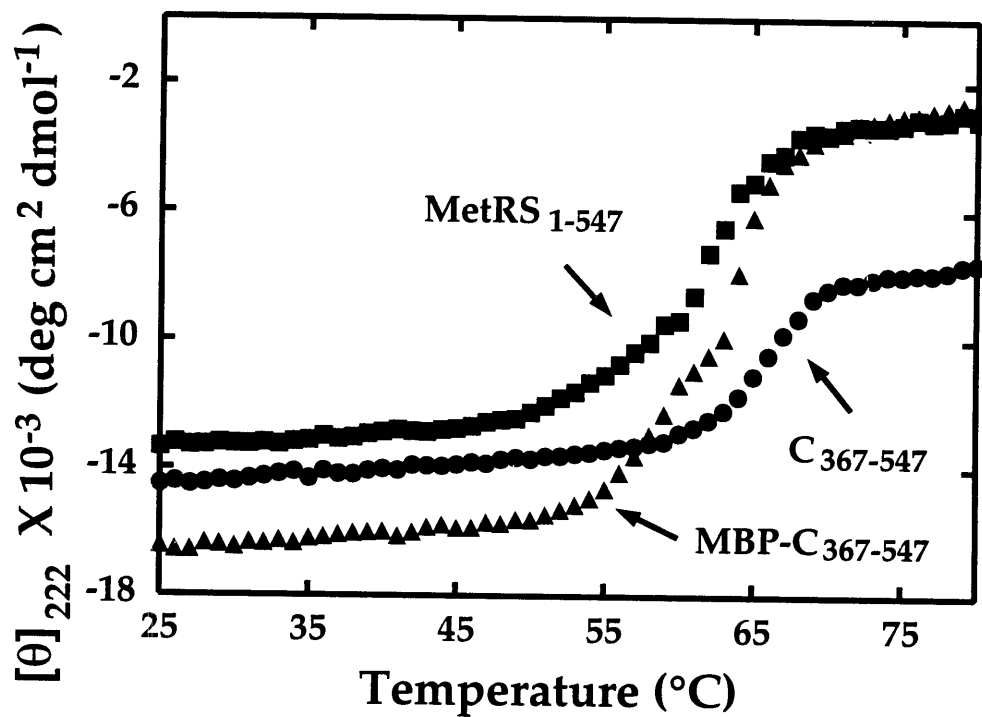
Figure 3-4

Legend to Figure 3-5

Circular dichroism analysis of domain C$_{367-547}$(W461A)

A: CD spectra of MBP-C$_{367-547}$(W461A) and C$_{367-547}$(W461A) at 25 °C on an AVIV 62DS CD spectrometer, each at a concentration of 1 mg/mL. B: Thermal denaturation curves of MBP-C$_{367-547}$(W461A) and C$_{367-547}$(W461A) compared to the denaturation curve of C367-547, each at a concetration of 1 mg/mL. All CD spectra and thermal denaturation curves were done in 20 mM sodium phosphate (pH 7.3), 100 mM NaCl and 1 mM ß-ME.

A.
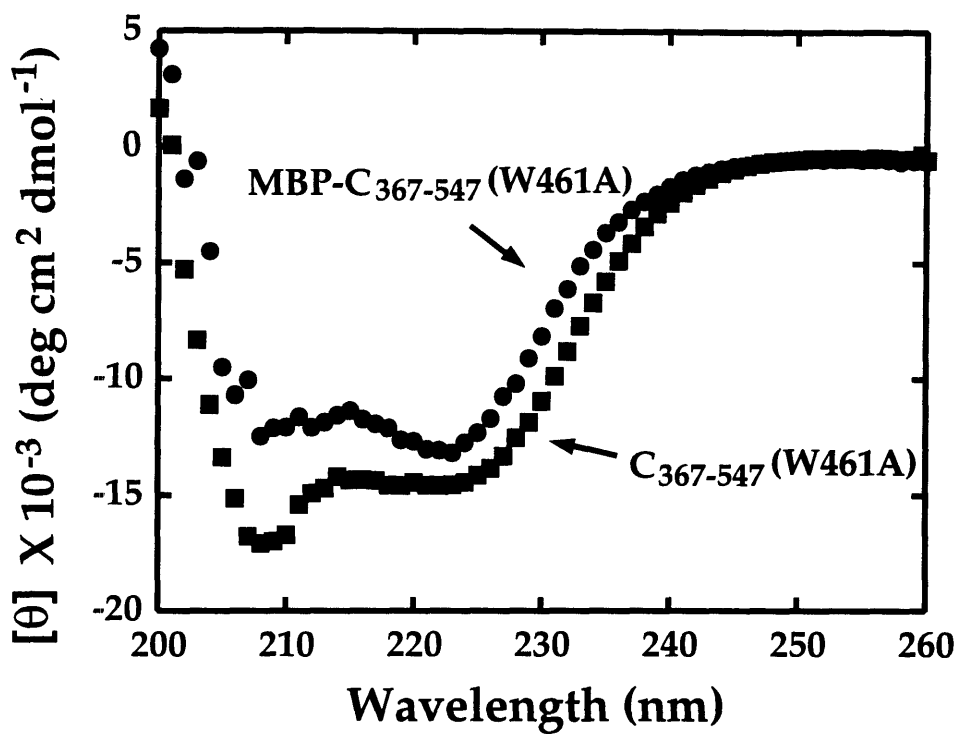
B.
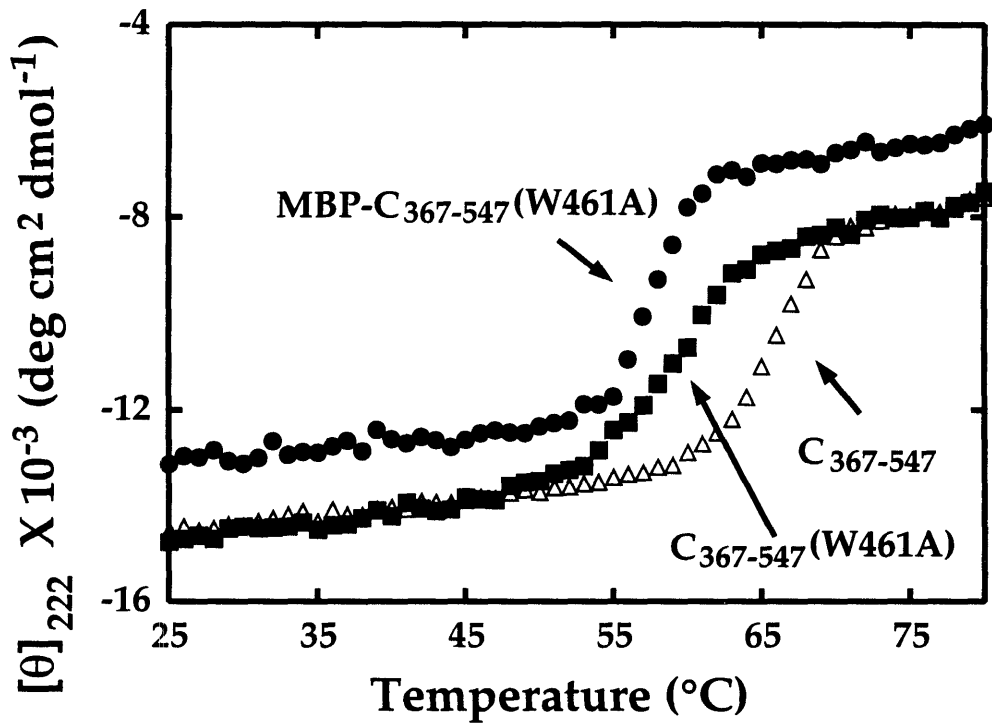
Figure 3-5

Chapter 4

Binding of an Anticodon-Containing RNA Hairpin to an Isolated Domain

INTRODUCTION

In the previous chapter it was demonstrated that a fusion protein of maltose binding protein and the C-terminal, anticodon-binding domain of MetRS (residues 367-547) was stable and soluble and that, as part of this protein, the C-terminal domain had native-like structural and physical properties (see Figure 3-4). It was also demonstrated that the C-terminal domain by itself ($C_{367-547}$) was stable and exhibited native-like structural and physical properties. Finally, a variation of this C-terminal domain construct, containing a mutation of Trp461 to alanine (Figure 3-5) was also found to maintain native-like structural and physical properties.

Considering that these fusion proteins and isolated C-terminal domains appeared to maintain their native structure, the next stage of analysis was to test the functional properties of the C-terminal domain in this context. The C-terminal domain of MetRS has been proposed to have been fused to the core primordial synthetase in order to add the capability for interactions with the second, anticodon-containing domain of tRNA (Schimmel *et al.*, 1993). In the case of MetRS, it is known that the C-terminal domain contains determinants for binding to the anticodon of tRNA^{Met} (Ghosh *et al.*, 1990; Meinnel *et al.*, 1990; Ghosh *et al.*, 1991; Meinnel *et al.*, 1991a; Meinnel *et al.*, 1991b; Kim and Schimmel, 1992; Auld and Schimmel, 1995).

Therefore, the function of this C-terminal domain was analyzed by characterizing its binding properties to the anticodon of tRNA^{fMet}. The RNA substrate used was a small RNA hairpin oligonucleotide that recapitulated the anticodon stem-loop of tRNA^{fMet} (Figure 4-1). The RNA binding function was investigated by the affinity coelectrophoresis (ACE) method (Lee and Lander, 1991) described in chapter 2. This method enabled us to detect directly RNA-protein complexes formed with isolated MetRS fragments and

the RNA hairpin substrate. The results concerning MBP-$C_{367-547}$ and $C_{367-547}$ have been reported (Gale and Schimmel, 1995b) and the text below is adapted with permission from that report (Copyright 1995, American Chemical Society).

MATERIALS & METHODS

Synthesis and Radioactive Labeling of RNA Oligonucleotides. RNA oligonucleotides were chemically synthesized on a Gene Assembler Plus synthesizer (Pharmacia LKB Biotechnology Inc., Piscataway, NJ) as previously described (Usman *et al.*, 1987; Scaringe *et al.*, 1990; Musier-Forsyth *et al.*, 1991). The RNA substrate was 5'-[^{32}P]-labelled according to (Silberklang *et al.*, 1977; Park and Schimmel, 1988).

Affinity Coelectrophoresis. Affinity coelectrophoresis was used to investigate the binding of the proteins to the RNA substrates. Affinity coelectrophoresis was performed as described in Materials and Methods of Chapter 2 (see Figures 2-1 and 2-2).

RESULTS

Affinity Coelectrophoresis. We found that with the ACE assay MetRS$_{1-547}$ binds to tRNA^{fMet} with a K_d of 3.6 ± 1 μM at pH 7.5 and 25 °C (see Chapter 6). Using the same procedure, the dissociation constant for the anticodon stem-loop RNA (Figure 4-1) was 31 ± 5 μM (Figure 4-2A, D and Table 4-1). (By using an anticodon stem-loop structure as a competitive inhibitor of aminoacylation, Meinnel *et al.* (Meinnel *et al.*, 1991a) obtained a K_I = 38 ± 5 μM at pH 7.6 and 25 °C.) The 6- to 7-fold difference between the dissociation constant for tRNA^{fMet} and that for the anticodon stem-loop suggests that much of the binding energy between MetRS$_{1-547}$ and tRNA^{fMet} is derived

from interaction with the anticodon stem-loop domain. This result is consistent with the anticodon of tRNA^{Met} being a major specificity determinant for MetRS (Saks *et al.*, 1994). For example, change of the UAC anticodon of tRNA^{Val} to the CAU anticodon of tRNA^{Met} switches the specificity of aminoacylation of tRNA^{Val} from valine to methionine (Schulman and Pelka, 1988).

Considering that the C-terminal domain had native-like characteristics, we wanted to determine whether it could interact with tRNA^{Met}, and, if so, whether that interaction was recapitulated with the anticodon stem-loop hairpin alone. The fusion protein MBP-C$_{367-547}$ bound to the anticodon stem-loop structure with a dissociation constant of 39 ± 5 μM. This affinity is similar to that of MetRS$_{1-547}$ for the anticodon stem-loop hairpin (Figure 4-2A, B, D and Table 4-1).

In addition, we obtained enough of the free domain C$_{367-547}$ to show that its complex with the anticodon stem-loop structure was essentially the same (K_d = 31 ± 2 μM) as that of the MBP-C$_{367-547}$ fusion protein (Figure 4-3A and Table 4-1). Furthermore, the free domain, C$_{367-547}$, bound to intact tRNA^{fMet} with a K_d of 53 ± 5 μM (Figure 4-3B). While this K_d is somewhat weaker than that for C$_{367-547}$ bound to the anticodon stem-loop, it is close enough to suggest that there is little or no difference in the determinants for binding of the C-terminal domain to the anticodon stem-loop hairpin compared to intact tRNA^{fMet}. By the criterion of RNA binding, therefore, domain C$_{367-547}$ recapitulates the interaction of MetRS$_{1-547}$ for the anticodon stem-loop of tRNA^{fMet}. The binding site for the anticodon stem-loop of tRNA^{fMet} is contained entirely within the C-terminal domain. Furthermore, the C-terminal domain does not appear to interact with any part of the tRNA outside of the anticodon stem-loop domain.

To determine whether the interaction observed in these gels was specific to the anticodon trinucleotide, we investigated the hairpin stem-loop structure with a GAU instead of a CAU anticodon trinucleotide sequence. $MetRS_{1-547}$ binding was weak and $MBP-C_{367-547}$ binding was not detectable to the mutant anticodon stem-loop that contains the anticodon GAU instead of the wildtype anticodon CAU (Figure 4-2C and Table 4-1). The isolated domain $C_{367-547}$ also had no detectable binding to the mutant anticodon stem-loop substrate (Table 4-1). These experiments established that domain $C_{367-547}$ maintains the same specificity as $MetRS_{1-547}$ for interaction with the RNA substrates. Because this specificity duplicates the specificity of interaction seen between MetRS and tRNA^{Met} (Schulman and Pelka, 1983), we believe that $MBP-C_{367-547}$ and $C_{367-547}$ are binding to the RNA substrates in a native orientation.

It is known that a region of the MetRS C-terminal domain from about Ala 451 to Glu 467 is primarily responsible for the discrimination of the tRNA^{Met} anticodon (Meinnel et al., 1991b; Kim et al., 1993c; Kim et al., 1994) along with a region from Asp 387 to Arg 395 (Ghosh et al., 1991; Kim et al., 1993a). In particular, mutation of Trp 461 to Phe or Ala causes a strong reduction in aminoacylation rate that can be attributed primarily to a loss of affinity towards any tRNA with a CAU anticodon (Ghosh et al., 1990; Meinnel et al., 1991a; Meinnel et al., 1991b). Ghosh et al. (Ghosh et al., 1990) showed that substitution of W461 with Phe increased K_m greater than 60-fold with a less than 2-fold increase in k_{cat}. Meinnel et al. (Meinnel et al., 1991b) showed further that substitution of W461 with Ala decreased k_{cat}/K_m 125-fold further beyond the decrease caused by a Phe mutation at that location. In this case, a K_d or K_m was not measurable.

Based on this knowledge we also tested the affinity for an anticodon stem-loop substrate of a C-terminal domain fusion protein with a W461A mutation (MBP-C$_{367-547}$(W461A)). The W461A mutation should eliminate binding to the anticodon stem-loop substrate. This was, in fact, what was observed (Figure 4-4A). The protein MBP-C$_{367-547}$(W461A) does not bind to the anticodon stem-loop RNA substrate. This protein and the isolated domain C$_{367-547}$(W461A) are somewhat less stable than their wildtype counterparts but the physical characterization suggests that they are nonetheless in a native-like conformation (see Chapter 3 and Figure 3-5). Because this mutation (W461A) has the same effect on the fusion protein that it has on MetRS, we believe that this result further confirms that the C-terminal domain (C$_{367-547}$) has a native-like structure and function, regardless of whether it is a part of a fusion protein or is isolated by itself.

DISCUSSION

Although the catalytic domain is shared by all enzymes in the same class, RNA-binding insertions into that domain and the entire second major domain vary from enzyme to enzyme (Starzyk *et al.*, 1987; Schimmel *et al.*, 1993). For example, the second domain of class I methionyl-tRNA synthetase is comprised of α-helices (Brunie *et al.*, 1990) while the corresponding domain of the related class I glutaminyl-tRNA synthetase is rich in ß-structure (Rould *et al.*, 1989; Rould *et al.*, 1991). Moreover, in comparing sequences of a particular tRNA synthetase through evolution, the class-defining catalytic domain is much more strongly conserved than is the second domain. Thus, the class I *E. coli* and human isoleucyl-tRNA synthetases have a 16-20% similarity of sequence throughout the N-terminal catalytic domain, but the C-

terminal domain shows a similarity of only 0-7%, depending on the region of the domain that is considered (Shiba *et al.*, 1994).

The primordial tRNA synthetases probably lacked these idiosyncratic domains and were most likely comprised of the class-defining catalytic domains which could activate amino acids. When bound to an RNA substrate, these small enzymes may have interacted with no more than a few nucleotides adjacent to the amino acid attachment site. These RNA substrates possibly resembled the acceptor-TΨC minihelix domain of contemporary tRNAs (Schimmel *et al.*, 1993). In the case of the class II alanyl-tRNA synthetase, a fragment comprised of approximately half of the enzyme has been directly demonstrated to aminoacylate the minihelix domain of tRNA^{Ala} (Buechter and Schimmel, 1993b). With *E. coli* methionyl-tRNA synthetase, anticodon interactions are mediated through a helix-loop motif which encompasses W461 of the C-terminal domain (Ghosh *et al.*, 1990; Ghosh *et al.*, 1991; Kim *et al.*, 1993a; Auld and Schimmel, 1995). Deletion of 11 amino acids from this motif eliminates interaction with the anticodon of tRNA^{Met} but has no effect on the activity for amino acid activation or on that for aminoacylation of a microhelix comprised of the seven base pairs of the tRNA^{Met} acceptor stem (Kim and Schimmel, 1992). Thus, the capacity of the core enzyme for amino acid activation or aminoacylation of an acceptor stem substrate is not dependent on the integrity of the second domain.

The present work shows that, conversely, the anticodon binding function of the second domain of at least methionyl-tRNA synthetase acts independently of the catalytic domain. We found no evidence for domain-domain cooperativity, at least with respect to the binding of the anticodon stem-loop structure. Our data do not address the question of whether domain-domain interactions at the subunit interface affect the energy of the

86

transition state for aminoacylation (k_{cat}) through subtle conformational effects at the active site. However, because deletion of the helix-loop motif that binds the anticodon does not affect the activity for microhelix aminoacylation (Kim and Schimmel, 1992), we surmise that any domain-domain communication may require an intact tRNA "bridge" that spans across the two structural units. A similar suggestion was made by Wright *et al.* (1993) (Wright *et al.*, 1993) in their analysis of interactions of *E. coli* GlnRS with the acceptor stem helix and anticodon stem-loop domain of tRNA^{Gln}.

The C-terminal end of MetRS is an appendix that extends back to the catalytic site (Brunie *et al.*, 1990), where it contributes to binding of the acceptor stem of tRNA^{Met} (Kim *et al.*, 1993b) (Figure 2-1). We thought that this contact might influence the conformation of the anticodon binding domain and that it might also be needed for its stability. However, the affinity for the anticodon hairpin stem-loop of the free C-terminal domain and of the C-terminal domain $C_{367-547}$ joined to MBP is comparable to that of $C_{367-547}$ joined to the N-terminal domain of MetRS (Table 4-1). We conclude that interactions of the C-terminal peptide appendix of MetRS with the N-terminal domain do not affect the RNA binding conformation of domain $C_{367-547}$. This result is consistent with those of Kim *et al.* (1993b) who showed that a point mutation in the peptide appendix of MetRS (which disrupted acceptor helix contacts) did not affect anticodon binding (see Chapter 5). In addition, the stability of domain $C_{367-547}$ in isolation is greater than that of MetRS (Figure 3-4B). The higher thermal stability of domain $C_{367-547}$ compared to MetRS (Figure 3-4B) shows that interactions of the C-terminal peptide appendix with the catalytic site are not required for the stable, native structure formed by domain $C_{367-547}$.

Because the anticodon binding domain of methionyl tRNA synthetase functions independently of the protein to which it is joined, such as MBP, we imagine that this functional RNA binding unit could be joined to the catalytic core of other tRNA synthetases and then adapted to the particular anticodon-containing tRNA domain of the cognate tRNA. Consistent with this view, recent experiments of Auld and Schimmel (1995) showed that a variant of the anticodon binding helix-loop peptide motifs of IleRS and MetRS could be swapped between the two enzymes, with anticodon binding being switched by a single amino acid swap. In addition to isoleucyl-tRNA synthetase, the class I cysteinyl-, leucyl-, and valyl- tRNA synthetases are closely related to methionyl-tRNA synthetase, and the structures of these enzymes can be modeled after that of the methionine enzyme (Burbaum et al., 1990; Burbaum and Schimmel, 1991b; Eriani et al., 1991; Hou et al., 1991; Shepard et al., 1992). In spite of the large size variations among these five class I enzymes, and in contrast to the less related class I glutaminyl-tRNA synthetase, sequence comparisons of their C-terminal domains suggest that, while highly diverged in sequence, all are made up of α-helices and probably originated from the same progenitor (Shiba and Schimmel, 1992a). Thus, the properties of the anticodon-binding domain of methionyl tRNA synthetase investigated here may be prototypical of this particular domain in this subclass of tRNA synthetases.

Table 4-1: Dissociation constants of $MetRS_{1-547}$ and C-terminal domain variants for the anticodon stem-loop RNA substrate at pH 7.5 and 25 °C[a]

	Dissociation Constant K_d, μM	
Proteins	CAU (wildtype)	GAU
$MetRS_{1-547}$	$31^b \pm 5$	see footnote e
$MBP\text{-}C_{367-547}$	$39^c \pm 5$	not detectable
$C_{367-547}$	$31^d \pm 2$	not detectable
$MBP\text{-}C_{367-547}(461A)$	not detectable	not tested
MBP	not detectable	not tested

[a]The anticodon stem-loop substrate was chemically synthesized with a sequence according to that of $tRNA^{fMet}$ (Figure 4-1). [b]Average of two determinations given in Kim et al. (1993b), and of a single determination made in this work. [c]Average of five determinations made in this work. [d]Average of two determinations made in this work. The K_d values were determined from a Scatchard plot of the data obtained from affinity coelectrophoresis (see Chapter 2 and Figure 4-2). [e]Weak binding to the GAU anticodon substrate was detected for $MetRS_{1-547}$ but the gel shift was smeared making calculation of the K_d difficult. One possible explanation for a weak interaction that produced a smear in the gel is a nonspecific interaction with the tRNA acceptor stem binding site that is located in the N-terminal domain. Adapted with permission from Gale and Schimmel (1995b) (Copyright 1995, American Chemical Society).

Legend to Figure 4-1

Cloverleaf and L-shaped structure of *E. coli* tRNA$^{\text{fMet}}$ and the anticodon stem-loop RNA hairpin

Sequence and cloverleaf structure of *E. coli* tRNA$^{\text{fMet}}$ (left) (Sprinzl *et al.*, 1989), the L-shaped arrangement of the three-dimensional structure (center), and the sequence and hairpin structure of the anticodon stem-loop RNA substrate (right). The hairpin structure is based on the shaded portion to which a C was added to the 3'-end to pair with the unmatched G. Adapted with permission from Gale and Schimmel (1995b) (Copyright 1995, American Chemical Society).
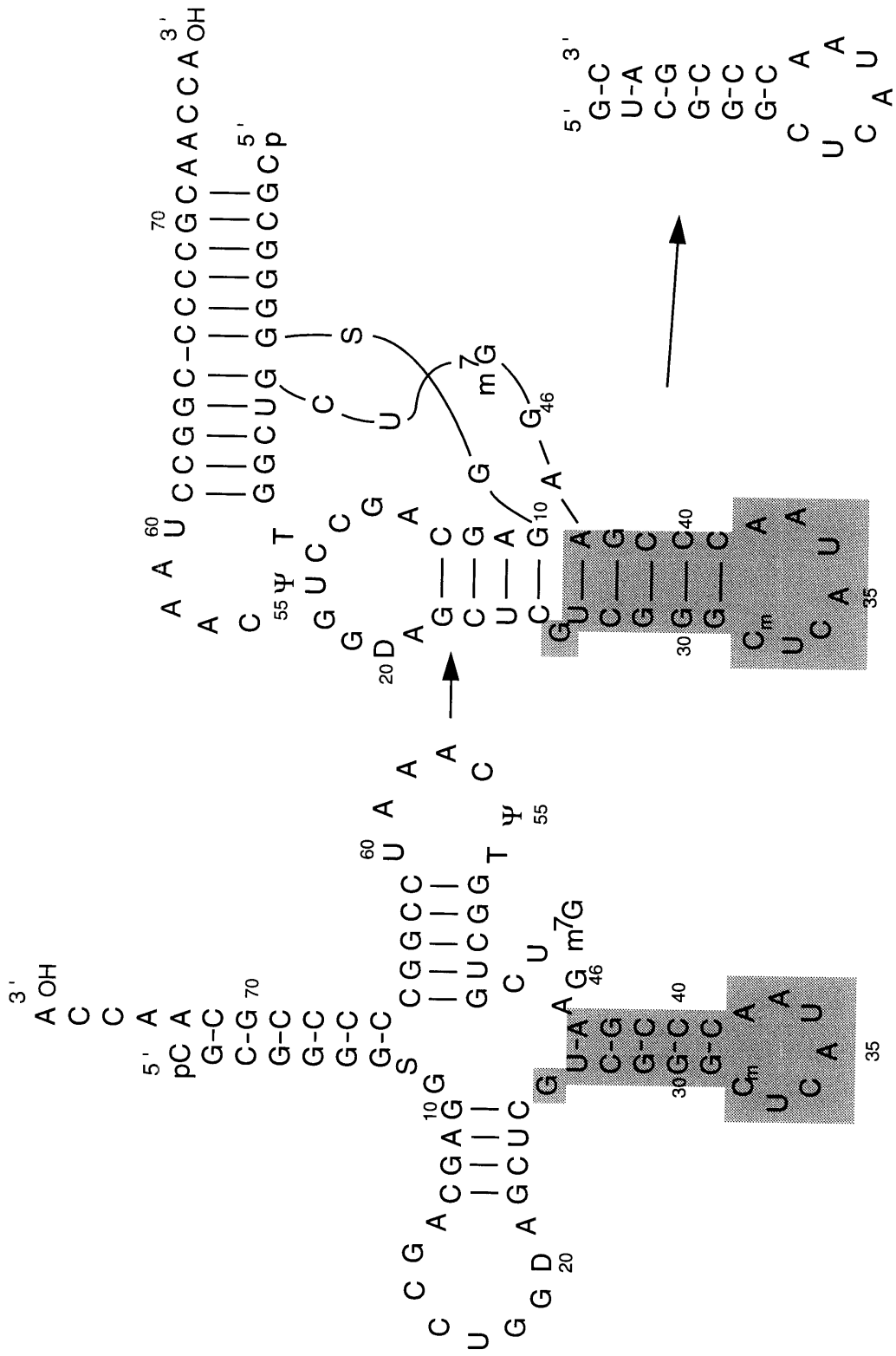
Figure 4-1

Legend to Figure 4-2

ACE gel analysis of the binding of MetRS$_{1-547}$ and MBP-C$_{367-547}$ to the tRNA^{fMet} anticodon stem-loop RNA hairpins

    A. ACE gel of MetRS$_{1-547}$ with the wildtype anticodon stem-loop RNA hairpin (MetRS$_{1-547}$ concentration ranged from 4 to 100 μM). B. ACE gel of MBP-C$_{367-547}$ with the wildtype CAU anticodon stem-loop RNA hairpin (MBP-C$_{367-547}$ concentration range from 4 to 100 μM). C. ACE gels of MetRS$_{1-547}$ (left) and MBP-C$_{367-547}$ (right) with the GAU anticodon mutant of the anticodon stem-loop RNA hairpin (concentration range from 8 to 100 μM for both proteins). D. Scatchard plots of the binding of MetRS$_{1-547}$ and MBP-C$_{367-547}$ to the anticodon stem-loop RNA hairpin. Adapted with permission from Gale and Schimmel (1995b) (Copyright 1995, American Chemical Society).

A. MetRS$_{1\text{-}547}$

100 ◄━━━━━━━━ 4 μM
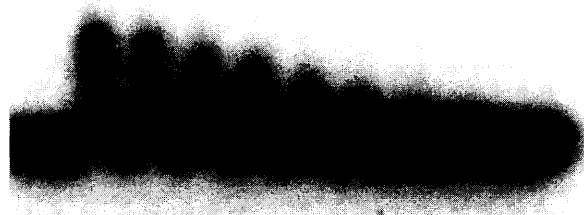
CAU

B. MBP-C$_{367\text{-}547}$

100 ◄━━━━━━━ 4 μM
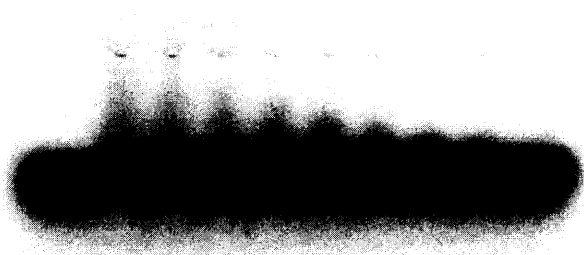
CAU

C. MetRS$_{1\text{-}547}$ MBP-C$_{367\text{-}547}$

100 ◄━━ 8 μM 100 ◄━━ 8 μM
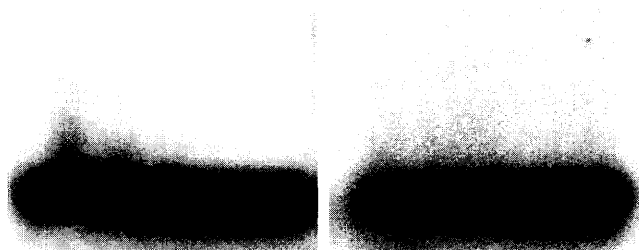
GAU

Figure 4-2

D.
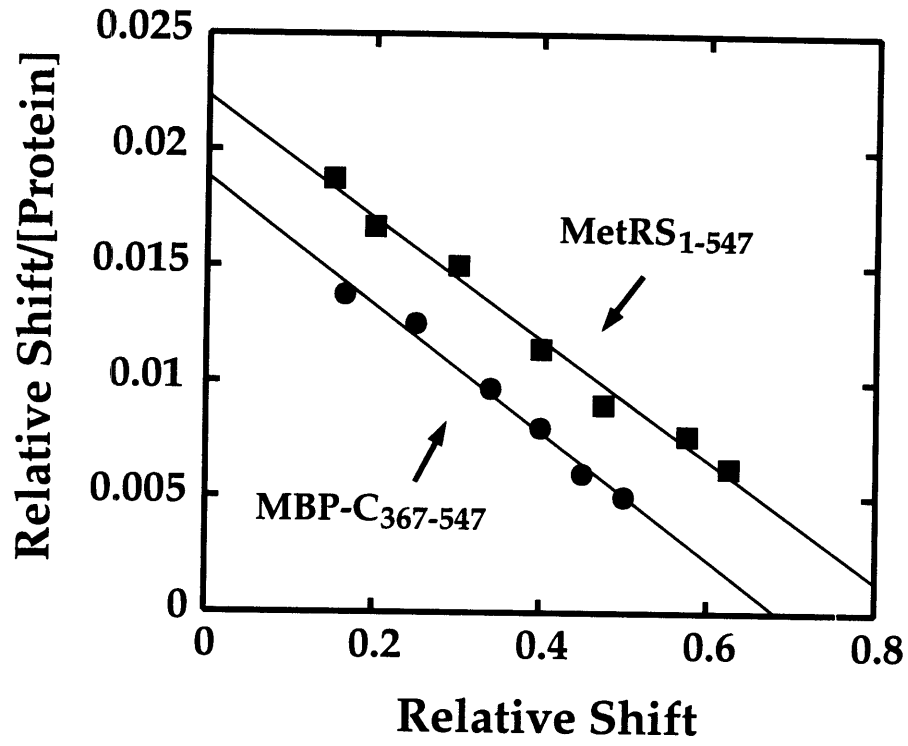
Figure 4-2,D

Legend to Figure 4-3

ACE gel analysis of the binding of domain C$_{367-547}$ to the tRNA^{fMet}

anticodon stem-loop RNA hairpin and to tRNA^{fMet}

    A. ACE gel of C$_{367-547}$ with the wildtype anticodon stem-loop RNA hairpin (C$_{367-547}$ concentration range from 4 to 80 μM). B. ACE gel of C$_{367-547}$ with tRNA^{fMet} (C$_{367-547}$ concentration range from 4 to 80 μM).

A. Anticodon S-L

80 ▰▰▰▰▰▰ 4 µM

B. tRNA^fMet

100 ▰▰▰▰▰ 2 µM
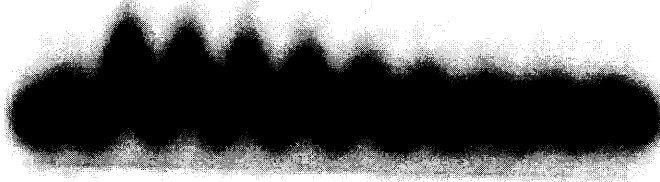
Figure 4-3

MBP-C$_{367-547}$, Anticodon S-L

WT   (W461A)

80 20   100 ━━━━━━━ 4 μM
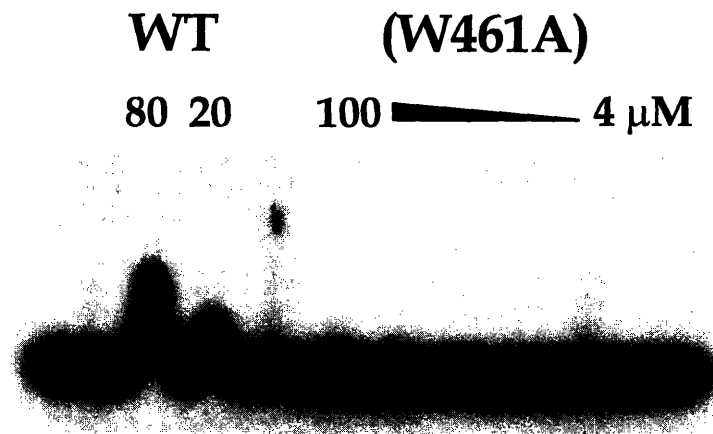
Figure 4-4

ACE gel analysis of the binding of MBP-C$_{367-547}$(W461A) to the tRNA^{fMet}

anticodon stem-loop RNA hairpin

ACE gel of MBP-C$_{367-547}$ (W461A) (right) versus MBP-C$_{367-547}$ (WT)

(left) with the wildtype anticodon stem-loop RNA hairpin (MBP-C$_{367-547}$ (W461A)

concentration range from 4 to 100 μM, MBP-C$_{367-547}$ at 20 and 80 μM).

Chapter 5

Evidence for Interactions of a C-terminal Peptide Appendix with the Acceptor Stem Helix of tRNA^{fMet}

INTRODUCTION

The X-ray crystal structure of the truncated monomeric form of *E. coli* MetRS has been solved to 2.5 Å resolution (Brunie *et al.*, 1990). From this structure it is clear that the synthetase consists primarily of two major domains. The N-terminal domain (1-360) contains the catalytic site built around the Rossman nucleotide-binding fold and the C-terminal domain (361-519) is primarily α-helical. This C-terminal domain is known to have various residues that are involved in binding to the anticodon of tRNA^{Met} (Valenzuela and Schulman, 1986; Ghosh *et al.*, 1990; Ghosh *et al.*, 1991; Meinnel *et al.*, 1991b; Kim *et al.*, 1993a).

In addition to being covalently joined, the two domains are non-covalently linked. Extending from the end of the C-terminal domain is a C-terminal peptide appendix that folds back to interact with the N-terminal domain adjacent to the active site cleft. This peptide has been proposed to guide docking of the tRNA acceptor end to the active site cleft (Mellot *et al.*, 1989). A short motif (Y531-D535) is conserved between methionyl tRNA synthetases from *E. coli, Bacillus stearothermophilus*, and *Saccharomyces cerevisiae* (cytoplasmic) (Kim *et al.*, 1993b).

To investigate the role of this peptide appendix in tRNA binding, point and insertion mutants were made in this conserved motif and the resulting mutants were analyzed for the ability to complement a MetG null strain as well as for *in vitro* activity as measured by aminoacylation assays and binding to small RNA substrates measured by affinity coelectrophoresis (Kim *et al.*, 1993b).

The work that is being reported here is a subset of the data reported in Kim, Landro, Gale and Schimmel (1993b) (adapted with permission, Copyright 1993, American Chemical Society). One mutant in the C-terminal

99

peptide appendix (R533A) had a particularily interesting phenotype so it was investigated further using the technique of affinity coelectrophoresis to characterize its binding affinity to small RNA hairpin substrates that recapitulated the acceptor stem and the anticodon stem-loop of tRNA$^{\text{fMet}}$. Analysis of the other point mutants and the insertion mutants that are discussed in Kim *et al.* (1993b) was done primarily by Dr. Sunghoon Kim and will not be presented here.

MATERIALS & METHODS

Protein Production and Purification. Phagemid pJB104 encoding the monomeric N-terminal active 547-mer of *E.coli* methionyl tRNA synthetase (Kim and Schimmel, 1992) was used to construct (by Dr. S. Kim) the R533A mutant using site-directed mutagenesis (Amersham, Arlington Heights, IL) (Kim *et al.*, 1993b). Wild-type and mutant monomer forms of MetRS were purified as previously described (Burbaum and Schimmel, 1991a; Kim and Schimmel, 1992). Amino acid activation assays and aminoacylation assays are described by Kim *et al.*, 1993 (1993b).

Affinity Coelectrophoresis. Affinity coelectrophoresis was used to investigate the binding of the proteins to the RNA substrates. Affinity coelectrophoresis was done as described in Materials and Methods of Chapter 2 (see Figures 2-1 and 2-2).

RESULTS

To clarify the role of the C-terminal peptide appendix, alanine substitutions at N532, R533, and D535 were made by Kim *et al.* (1993b). Also, two tetrapeptides (GKKG and ALFA) were inserted between I534 and D535. Of these mutant enzymes, the R533A enzyme had the most altered activity.

While amino acid activation activity was only reduced by 35%, aminoacylation activity was reduced by 40-fold (Table 5-1). Kinetic analysis of the aminoacylation of tRNA^{fMet} showed that the K_m for tRNA was increased about 20-fold while the k_{cat} was decreased about 2-fold (Table 5-2) (Kim et al., 1993b). This result suggested that R533 is primarily involved in binding to tRNA.

To isolate further the effect of the R533A mutation on binding to a specific domain of tRNA^{fMet}, dissociation constants of the wild-type and R533A mutant proteins for small RNA substrates based on the anticodon stem-loop and the acceptor stem sequences of tRNA^{fMet} (Figure 5-1) were determined by affinity coelectrophoresis. Wild-type MetRS binds to the acceptor stem microhelix of tRNA^{fMet} with a K_d of 249 μM whereas specific binding of R533A mutant MetRS to the microhelix was not observed (Figure 5-2, Table 5-3). (The smear seen in the protein lanes of the R533A mutant enzyme with acceptor stem microhelix is characteristic of nonspecific binding.) On the other hand, R533A mutant MetRS still binds to the anticodon stem-loop RNA. In fact, the dissociation constant is about 6-fold tighter than that of wild-type MetRS. The wild-type MetRS bound to the anticodon stem-loop with a $K_d = 31 \pm 5$ μM (see Chapter 4, Figure 4-2, and Table 5-3) while R533A mutant MetRS bound with a $K_d = 5.4 \pm 1.0$ μM (Figure 5-3, Table 5-3) (Kim et al., 1993b). This tight binding may indicate a small indirect effect of the R533A mutation on the structure of the anticodon binding region of the enzyme. As a negative control, a MetRS mutant that had 11 amino acids deleted from the anticodon binding motif (Δ11(Y454-A464 $\rightarrow$ S)) (Kim and Schimmel, 1992) was investigated. The deletion mutant protein did not show detectable binding to the anticodon stem-loop RNA (Figure 5-3, Table 5-3) (Kim et al., 1993b).

DISCUSSION

The R533A mutation had a strong effect on aminoacylation of tRNA^{fMet} as well as on aminoacylation of microhelix^{fMet} (Kim *et al.*, 1993b). The effect on aminoacylation of tRNA^{fMet} is primarily an alteration to K_m, suggesting that the mutant does not bind tRNA as well as does the wild-type protein (Table 5-2). The corresponding decrease in microhelix^{fMet} binding suggests that the decrease in tRNA binding is a result of weaker acceptor stem binding interactions. It is not possible to determine kinetic constants for the microhelix substrate because the rate of aminoacylation, even for the wild-type enzyme, is about 10^6 fold lower relative to that of the full length tRNA substrate (see Chapter 6) (Martinis and Schimmel, 1992). Determination of dissociation constants by affinity coelectrophoresis directly established the effect of the mutation on binding by demonstrating that binding of the microhelix substrate by the R533A mutant enzyme is not detectable, whereas the mutant enzyme actually binds the anticodon stem and loop of tRNA^{fMet} somewhat better than does the wild-type enzyme (Kim *et al.*, 1993b).

A general structural organization of both class I and class II synthetases has been proposed (Buechter and Schimmel, 1993a). In this model the synthetases contain two discrete primary domains. The first domain is the active site domain which contains the conserved class defining motifs and interacts with the acceptor stem of the tRNA. The second domain is not conserved among synthetases within the same class. This domain interacts with the more distal regions of the tRNA. One proposal is that synthetases evolved from primitive systems in which core catalytic domains activated amino acids and charged small RNA molecules that subsequently became the acceptor stems of contemporary tRNAs (Schimmel *et al.*, 1993). Additional

102

non-conserved domains were added later, perhaps through a process of gene fusion, to enable interactions with more distal parts of the tRNA structure and thereby increasing efficiency and specificity (Buechter and Schimmel, 1993a).

Methionyl tRNA synthetase is typical of the class I enzymes in that it contains an N-terminal conserved catalytic domain and a C-terminal non-conserved domain. In the case of MetRS, this C-terminal domain is known to interact with the anticodon stem and loop. The C-terminal peptide extension is an exception to this domain organization. Though it extends from the C-terminal domain, it wraps back around the active site in the N-terminal domain.

Although it is known that A73 and the base pairs G2·C71 and C3·G70 in the acceptor stem of tRNA^{Met} are important for the identity of tRNA^{Met} (Martinis and Schimmel, 1992; Meinnel et al., 1993), very little is known about the protein residues within MetRS that make specific contacts with the acceptor stem. The cocrystal structure of the class I E. coli glutaminyl-tRNA synthetase and tRNA^{Gln} shows that residues in the so-called CP1 insertion in the nucleotide binding fold make contacts with the tRNA^{Gln} acceptor stem (Rould et al., 1989). The peptide F102-T124 in CP1 of GlnRS has some structural similarity to peptide E102-I124 in CP1 of MetRS (Perona et al., 1991). However it is not known whether residues located in CP1 of MetRS actually make specific contacts with the acceptor-stem of tRNA^{Met}.

The start of the C-terminal peptide extension is directly adjacent to the junction of the catalytic and anticodon binding domains (Brunie et al., 1990). Therefore it is conceivable that the C-terminal peptide extension was part of the core catalytic domain before insertion of the anticodon binding domain, which was sandwiched between the peptide and the rest of the catalytic

domain. Alternatively, the peptide extension may have been recruited from another genetic source and added to the C-terminal domain. Regardless of the details, the end result is that the two major domains are physically linked by a peptide that is essential for catalytic activity and acceptor stem binding. This linkage may increase the selective pressure to keep the C-terminal domain as part of methionyl tRNA synthetase.

MetRS is part of a subclass of the class I synthetases that includes the cysteinyl-, isoleucyl-, leucyl-, and valyl-tRNA synthetases. The structures of these enzymes can be modeled after that of MetRS and in all cases the C-terminal domain is predicted to be α-helical (Burbaum et al., 1990; Burbaum and Schimmel, 1991b; Eriani et al., 1991; Hou et al., 1991; Shepard et al., 1992). In isoleucyl-tRNA synthetase the 52 C-terminal amino acids of the 939 amino acid synthetase are required for aminoacylation activity (Shiba and Schimmel, 1992a). It is possible that the isoleucyl enzyme has a C-terminal appendix similar to that in MetRS that is part of the active site and makes contacts with the acceptor stem.

Table 5-1: Relative amino acid activation and tRNA^{fMet}

aminoacylation activities of the R533A mutant

Proteins	Amino Acid Activation	Aminoacylation
Wild-Type	100	100
R533A	65	2

Adapted with permission from Kim, Landro, Gale and Schimmel

(1993b) (Copyright 1993, American Chemical Society).

Table 5-2: Kinetic parameters for aminoacylation of tRNA^{fMet} by wild-type and R533A mutant MetRS.

Proteins	K_m, tRNA^{Met} (μM)	k_{cat} (sec^{-1})	Relative k_{cat}/K_m
MetRS$_{1-547}$ WT	2.5	1.7	1
MetRS$_{1-547}$ R533A	50.0	0.8	2.6×10^{-2}

Aminoacylation reactions were carried out in the range of 0.15-100 μM tRNA^{fMet}. Adapted with permission from Kim, Landro, Gale and Schimmel (1993b) (Copyright 1993, American Chemical Society).

Table 5-3: Dissociation Constants of the Wild-Type and Mutant Enzymes for the Anticodon Stem-Loop and Microhelix RNA Substrate at pH 7.5 and 37 °C[a]

proteins	dissociation constant (K_d)	
	anticodon stem-loop (μM)	microhelix (μM)
wild-type	31 ± 5	249
R533A	5.4 ± 1.0	not detectable
Δ11(Y454-A464→S)	not detectable	not determined

[a]The anticodon stem-loop hairpin helix and microhelix were synthesized on the basis of tRNA[fMet] (Figure 5-1). The K_d values were determined from the Scatchard plot of the data obtained from affinity coelectrophoresis. Adapted with permission from Kim, Landro, Gale and Schimmel (1993b) (Copyright 1993, American Chemical Society).

Legend to Figure 5-1

Cloverleaf and L-shaped structures of *E. coli* tRNA^{fMet} and the acceptor stem and anticodon stem-loop RNA hairpins

Sequence and cloverleaf structure of initiator tRNA^{Met} (left), the L-shaped arrangement of the three dimensional structure (center), and sequences and hairpin structures of microhelix^{fMet} (top right) and anticodon stem-loop (lower right) RNA substrates.

Figure 5-1

Legend to Figure 5-2

ACE gel analysis of wildtype MetRS$_{1-547}$ and R533A mutant MetRS$_{1-547}$ with the tRNA^{fMet} acceptor stem RNA hairpin

Affinity coelectrophoresis gels of wildtype MetRS$_{1-547}$ (top) and R533A mutant MetRS$_{1-547}$ (bottom) with acceptor stem microhelix RNA substrate (Figure 5-1). Concentration range for MetRS$_{1-547}$ in both gels was from 10 to 350 μM.

A. MetRS$_{1-547}$

350 ◤▬▬▬▬▬◣ 10 µM

B. MetRS$_{1-547}$ (R533A)

350 ◤▬▬▬▬◣ 10 µM
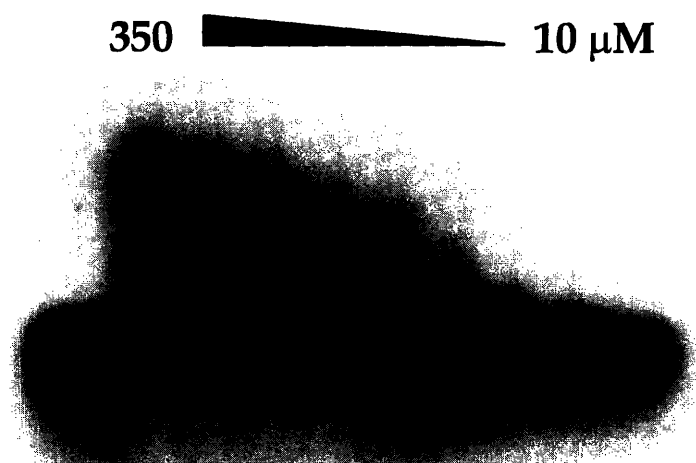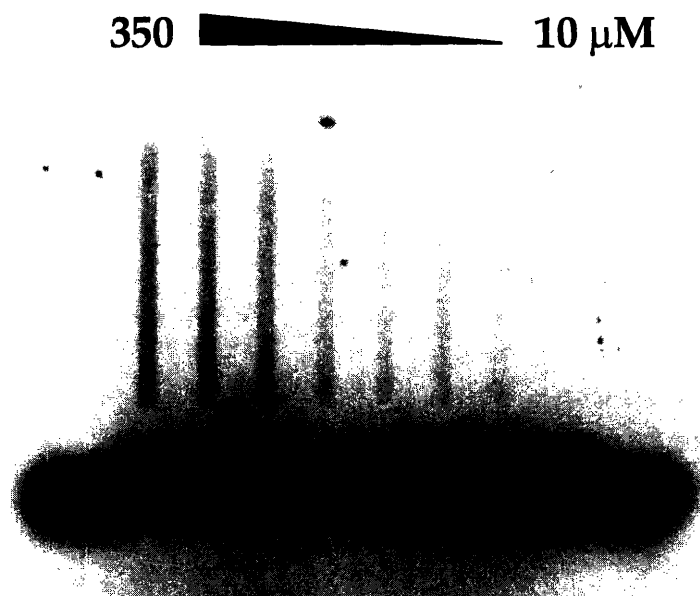
Figure 5-2

Legend to Figure 5-3

ACE gel analysis of MetRS$_{1-547}$ mutant proteins with the tRNA^{fMet} anticodon stem-loop RNA hairpin

A. Affinity coelectrophoresis gel analysis of R533A mutant MetRS$_{1-547}$ and MetRS$_{1-547}$ deletion mutant Δ11(Y454-A464→S) binding to the tRNA^{fMet} anticodon stem-loop RNA substrate. Concentration ranges were from 1 to 40 μM for the R533A protein and from 40 to 125 μM for the Δ11(Y454-A464→S) protein. B. Scatchard analysis of the data for the binding of the R533A MetRS$_{1-547}$ mutant protein to the anticodon stem-loop RNA substrate. Adapted with permission from Kim, Landro, Gale and Schimmel (1993b) (Copyright 1993, American Chemical Society).

A.

Δ11(Y454-A464 S)   R533A

125◤◢ 40 40 ◼◣ 1 μM

B.
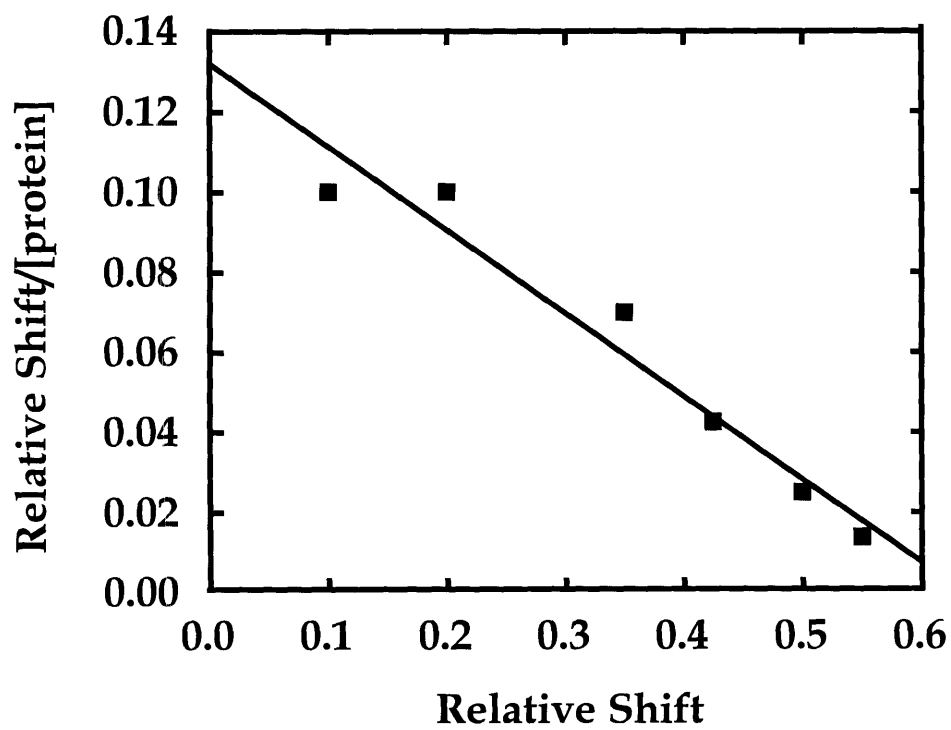
Figure 5-3

Chapter 6

Evidence that Specificity of Microhelix Charging by a Class I tRNA Synthetase Occurs in Transition State of Catalysis

INTRODUCTION

Synthetase-tRNA complexes are relatively loose, having dissociation constants (at pH 7.5) on the order of one micromolar (see Chapter 2) (Helene et al., 1971; Blanquet et al., 1973a; Lam and Schimmel, 1975; Schimmel and Söll, 1979; Meinnel et al., 1991b). The loose association of synthetases with their cognate tRNAs enables the enzymes to turn over rapidly during protein synthesis. The relative weakness of binding interactions associated with highly specific aminoacylation reactions suggests that additional interactions are required to achieve high specificity. This expectation has been demonstrated for the class II E. coli alanyl-tRNA synthetase, which discriminates tRNA substrates in large part on the basis of an acceptor stem G3·U70 base pair. This discrimination occurs at both the binding step and, additionally, during the transition state of catalysis, with the relative contribution of each part being dependent on pH (Park et al., 1989).

In this work, we focused on the class I E. coli methionyl-tRNA synthetase and the nature of the contribution of acceptor helix interactions to aminoacylation specificity and efficiency. Unlike alanyl-tRNA synthetase which makes no contact with the anticodon, the methionine enzyme has a strong interaction with the CAU anticodon of tRNA^{Met}. This interaction is a major determinant of the identity of methionine tRNAs (Schulman and Pelka, 1983; Schulman and Pelka, 1988).

At least ten different synthetases specifically aminoacylate small RNA substrates that recapitulate the acceptor stem (microhelix) or the acceptor and TΨC stems (minihelix) of their cognate tRNAs (Frugier et al., 1994; Hamann and Hou, 1995; Martinis and Schimmel, 1995). These include several that are known to interact with the anticodons of their cognate tRNAs. Notably the class I methionyl- (Martinis and Schimmel, 1992; Martinis and Schimmel,

1993; Martinis and Schimmel, 1995), valyl- (Frugier *et al.*, 1992) and isoleucyl-tRNA synthetases (Nureki *et al.*, 1993) specifically aminoacylate minihelix substrates, even though the anticodon is a major identity determinant for all of these enzymes (Stern and Schulman, 1977; Schulman and Pelka, 1983; Schulman and Pelka, 1988).

Although MetRS specifically aminoacylates microhelix^{Met} substrates, the rate of charging of these substrates is so low that k_{cat} and K_m can not be reliably determined. Nonetheless, consistent with the observed sensitivity of aminoacylation of tRNA^{fMet} to acceptor helix sequence alterations (Lee *et al.*, 1992; Meinnel *et al.*, 1993), the aminoacylation of microhelix^{Met} is sequence-specific (Martinis and Schimmel, 1992; Martinis and Schimmel, 1993). To investigate further the question of whether this specificity derived from the binding step or, additionally or alternatively, from the transition state of catalysis, we sought to obtain an independent measure of the association of wild-type and mutant microhelices with MetRS.

For these studies, RNA microhelix substrates were synthesized having sequences which reconstruct the acceptor stem of tRNA^{Met} and which gave variants of that stem. An adaption of the conventional aminoacylation assay was used to achieve a more sensitive detection of the charging of these substrates (The aminoacylation assays were done by Dr. J.-P. Shi). To study microhelix binding to methionyl-tRNA synthetase in isolation from kinetic phenomena, we utilized the affinity coelectrophoresis (ACE) procedure (see Chapter 2). In Chapter 4, I described the use of this method to investigate the interaction of the methionine enzyme with RNA hairpins which reconstructed the anticodon stem-loop of tRNA^{fMet} (Gale and Schimmel, 1995b). Thus, in addition to providing an approach to investigating the basis for specificity of microhelix aminoacylation by methionyl-tRNA synthetase,

these affinity coelectrophoresis studies enabled us to assess separately the relative contribution of binding interactions to each of the major subdomains of each of the two domains of the tRNA structure. The interaction free energies for the individual domains calculated from these data can be compared with the free energy of interaction of whole tRNA[fMet] with MetRS. This comparison, in turn, enabled us to estimate the free energy of distortion of the complex that occurs as a result of linking the two domains together.

MATERIALS AND METHODS

Synthesis and Radioactive Labeling of RNA Oligonucleotides. RNA oligonucleotides were chemically synthesized on a Gene Assembler Plus synthesizer (Pharmacia LKB Biotechnology Inc., Piscataway, NJ) as previously described (Usman *et al.*, 1987; Scaringe *et al.*, 1990; Musier-Forsyth *et al.*, 1991). The RNA substrate was 5'-[^{32}P]-labelled according to (Silberklang *et al.*, 1977; Park and Schimmel, 1988).

Aminoacylation of tRNA[fMet] and Microhelix RNA Substrates. All aminoacylation assays were carried out at 37 °C, in 50 mM HEPES pH 7.5, 0.1 mM EDTA, 150 mM NH$_4$Cl, 4 mM MgCl$_2$ and 100 μg/mL BSA. These assays (by Dr. J.-P. Shi) were carried out using a modification of described methods (Francklyn and Schimmel, 1989; Francklyn and Schimmel, 1990; Musier-Forsyth *et al.*, 1991). This modification was necessary to study the charging of inefficient substrates and is described in Franklyn *et al.* (Francklyn *et al.*, 1992). Briefly, aminoacylation reaction products were digested with RNase A (Boehringer Mannheim, Indianapolis, IN) until quenched with 0.7 M HOAc. After centrifugation to remove protein, the hydrolysate was fractionated on a Vydac 401 TP HPLC column to isolate radioactive aminoacyl-adenosine. This product was then quantitatively measured by placing a sample in Hydrofluor

(National Diagnostics, Manville, NJ) to measure radioactivity on an LKB Wallac model 1211 liquid scintillation counter (Gaithersburg, MD). Because of the low rates of aminoacylation, it was not practical to exploit a wide concentration range. For that reason, reported k_{cat}/K_m values should be viewed as "operational" or "apparent" kinetic parameters. However, in all cases the measured velocities were directly proportional either to total substrate or to total enzyme, depending on which was varied in the analysis of a particular microhelix. Either three different enzyme or three different (at least) substrate concentrations were investigated in each instance. These concentrations varied from two-fold to more than eight-fold, depending on the microhelix being investigated.

Protein Purifications. MetRS$_{1-547}$ and MetRS$_{1-676}$ were expressed from plasmid pAG112 (Gale and Schimmel, 1995b) and plasmid pJB103 (Burbaum and Schimmel, 1991a), respectively. The purification was performed as described earlier (Chapter 3) (Gale and Schimmel, 1995b). Protein concentration was determined by absorbance at 280 nm (Cassio and Waller, 1971). For the aminoacylation assays, MetRS$_{1-676}$ was purified as described previously (Burbaum and Schimmel, 1991a) and subsequently was stored at 4 °C in 25 mM Tris pH 7.5, 200 mM NaCl and 1 mM ß-ME. Samples were removed from time to time and enzyme concentrations were determined by active site titrations as described by Fersht *et al.* (1975).

AlaRS$_{1-461}$ was expressed from the plasmid pQE-461 cotransformed with plasmid pREP4 (which carries the *lacI* gene (Farabaugh, 1978)) into strain TG1 to express high levels of the *lac* repressor. Plasmid pQE-461 contains the gene for AlaRS$_{1-461}$-6H which encodes residues 1-461 of AlaRS joined to a C-terminal extension of 6 His codons (courtesy of L. Ribas, unpublished results) to facilitate purification of the expressed protein by affinity chromatography

on a Ni^{2+}-nitrilo-tri-acetic acid (Ni-NTA) resin column (Hochuli, 1989; Janknecht *et al.*, 1991) (Qiagen, Chatsworth, CA). Expression of $AlaRS_{1-461}$-6H was induced with 1 mM IPTG and the cells were harvested in late log phase. The cells were resuspended in 50 mM Na-phosphate (pH 7.8), 300 mM NaCl, and 0.5 mM phenylmethanesulfonyl fluoride and lysed in a French press at 15,000 lbs/in^2. The lysate was centrifuged at 30,000 rpm for 1 hr in a Beckman ultracentrifuge (Palo Alto, CA). $AlaRS_{1-461}$-6H was then purified on a 4 mL Ni-NTA resin column according to the manufacturer's instructions (Qiagen, Chatsworth, CA), except that none of the buffers used contained glycerol. Protein concentration was determined by the Bio-Rad Protein Assay (Bio-Rad Laboratories, Hercules, CA).

Affinity Coelectrophoresis. Affinity coelectrophoresis (Lee and Lander, 1991) was used to investigate the binding of the proteins to the RNA substrates, and was performed as described in Materials and Methods of Chapter 2 (see Figures 2-1 and 2-2). The standard buffer was 50 mM HEPES (pH 7.5), 0.1 mM EDTA, 4 mM $MgCl_2$, 1 mM ß-mercaptoethanol, and 100 μg/mL BSA. This buffer was used in all ACE gel experiments except where specifically indicated. All experiments were done in a thermostated circulating gel box (Hoefer Super Sub Model HE100, Hoefer Scientific, San Fransisco, CA) at 25 °C. Although the aminoacylation assays were performed at 37 °C, which provided a basis for comparison with related work (Lee *et al.*, 1992), affinity coelectrophoresis was not practical at 37 °C because low-melting point agarose was used to prevent excessive heating of the protein when it was mixed with liquid agarose to pour the gel.

For the affinity coelectrophoresis competition experiments, an ACE gel was prepared as described previously except that an unlabeled competitor tRNA (either $tRNA^{fMet}$ or $tRNA^{Val}$) was added to the gel along with the

protein (MetRS$_{1-676}$) in one lane. MetRS$_{1-676}$ was added to the gel in two lanes at a final concentration of 10 µM. The competitor tRNA sample was also added to one of these lanes at a final concentration of 12 µM. The [5'-^{32}P] microhelix RNA substrate was then electrophoresed through these lanes and the shift of [5'-^{32}P] RNA was compared between the lane with and the one without competitor tRNA.

RESULTS

Aminoacylation of tRNA^{fMet} and microhelix RNA substrates. Mutations in the acceptor stem of tRNA^{fMet} can substantially decrease V_{max}/K_m for aminoacylation. For example, for the 'discriminator base' G73 mutant, V_{max}/K_m for aminoacylation was decreased 30-fold relative to wild type tRNA^{fMet}. While the G72 mutant was reduced only 2.3-fold in its rate of aminoacylation, a double G72, G73 mutant had V_{max}/K_m reduced 475-fold, apparently due to a strong synergistic coupling of the two mutations in the double mutant. This double mutant was also demonstrated to be defective *in vivo*. Interestingly, the apparent K_m for aminoacylation was only decreased by 2.3-fold, showing that the acceptor helix interactions in the full tRNA have a strong influence on V_{max} (Lee *et al.*, 1992). Other acceptor stem mutations also strongly affect the kinetic parameters (Meinnel *et al.*, 1993).

We were interested to see whether the effects of mutations in the acceptor stem of full length tRNA^{fMet} would be reproduced in microhelices based on the acceptor stem alone, or whether the effects of these mutations in the whole tRNA were influenced by the part of the structure which is missing from microhelices. In particular, we wanted to determine if much of the discrimination of microhelix^{fMet} was due to interactions in the transition state of catalysis, as suggested for acceptor stem interactions of tRNA^{fMet}. In

previous work, Martinis *et al.* (1992) used a gel electrophoresis assay to detect directly the charging of microhelix^{fMet} with [^{35}S]-methionine. This assay was not sensitive enough for measuring k_{cat}/K_m. Alternatively, the sensitive HPLC assay developed by Francklyn *et al.* (1992) was adopted and used to determine the rate of aminoacylation under conditions where the rate is linear with respect to total enzyme or total substrate concentration.

The k_{cat}/K_m for the aminoacylation of tRNA^{fMet} is 2.8 X 10^6 M^{-1} s^{-1}, at pH 7.5, 37 °C (Table 6-1). (This value is comparable to a value of 1.43 X 10^6 (M^{-1} s^{-1}) (at pH 7.6, 25 °C) determined by Meinnel *et al.* (1993).) In contrast, k_{cat}/K_m for the aminoacylation of microhelix^{fMet} (Figure 6-1) is 9.4 X 10^{-1} M^{-1} s^{-1}. Thus, k_{cat}/K_m is decreased by 3.0 X 10^6-fold relative to the k_{cat}/K_m for the aminoacylation of tRNA^{fMet} (Table 6-1). Because of the large reduction in rate, we could not accurately measure individual k_{cat} and K_m parameters.

Two mutant microhelix^{fMet} substrates were also characterized. Mutation of the discriminator base from A73 to G73 decreases the k_{cat}/K_m for aminoacylation 7-fold below that of wildtype microhelix^{fMet}. The k_{cat}/K_m for the aminoacylation of the double mutant G72, G73 (Figure 6-1) is 13-fold less than that of wildtype microhelix^{fMet} (Table 6-1). Thus, the single and double mutants are defective for aminoacylation, but less so relative to the wild type counterpart than are the same mutations when placed in the full tRNA (see above).

In the acid gel techniques used by Martinis *et al.* (1992) , trace levels of charging of microhelix^{Ala} by MetRS were detectable. The k_{cat}/K_m of the noncognate substrate microhelix^{Ala} (Figure 1) was measured in this work and found to be 8.3 X 10^{-2} M^{-1} s^{-1} (Table 1), which is a decrease of about 11-fold relative to that of wild type microhelix^{fMet}. Earlier work showed that no aminoacylation was detected in the cases of microhelix^{His}, microhelix^{Gly},

microhelix^{Glu}, or microhelix^{Phe}, or in the cases of several mutant variants based on the tRNA^{Met} or tRNA^{fMet} acceptor stem (Martinis & Schimmel, 1992; Martinis & Schimmel, 1993). Therefore, with the exception of a weak aminoacylation of microhelix^{Ala}, microhelix^{fMet} charging is highly specific.

Binding of MetRS to Microhelix^{fMet} Investigated by Affinity Coelectrophoresis. To determine whether the effect of mutations on k_{cat}/K_m was due to a change in binding affinity, we chose to investigate the association of these microhelix substrates to native MetRS$_{1-676}$, using the technique of affinity coelectrophoresis. Affinity coelectrophoresis is a gel retardation method in which the protein of interest is imbedded directly in an agarose gel at defined concentrations. The labeled RNA substrate is then electrophoresed through the protein in the gel, allowing the measurement of binding affinities under equilibrium conditions (Lee and Lander, 1991; Lim *et al.*, 1991; Kim *et al.*, 1993b). Using this technique, we determined that MetRS and the C-terminal domain of MetRS bind specifically to an RNA substrate that recapitulates the anticodon stem-loop of tRNA^{fMet}. For both proteins, binding was not detectable when a single base of the anticodon was substituted within the anticodon stem-loop substrate (see Chapter 4) (Gale and Schimmel, 1995b).

As measured by affinity coelectrophoresis, full length *E. coli* MetRS$_{1-676}$ binds to tRNA^{fMet} with a K_d of 0.51 ± 0.14 μM (Table 6-2) (Gale and Schimmel, 1995a). We then found that MetRS$_{1-676}$ binds to the wildtype microhelix^{fMet} substrate with a K_d of 12 ± 3 μM. A K_d of 12 μM suggests a significant amount of binding energy for acceptor stem interactions with MetRS$_{1-676}$.

To further analyze binding of MetRS to the acceptor stem of tRNA^{fMet}, we investigated binding to G72, G73 microhelix^{fMet}. We also tested binding

of the noncognate microhelix^{Ala} to MetRS$_{1-676}$. In contrast to the aminoacylation results (Table 6-1), we found that the double mutation G72, G73 had little or no effect on binding to MetRS$_{1-676}$. MetRS$_{1-676}$ bound to both the wildtype microhelix^{fMet} and the G72, G73 microhelix^{fMet} with a K_d of 12 µM (Table 6-2, Figure 6-2A, B). In addition, microhelix^{Ala} binds tighter to MetRS$_{1-676}$ than to either of the microhelix^{fMet} substrates, with a K_d of 5.6 µM (Table 6-2, Figure 6-2C). Finally, a mutant C70 microhelix^{Ala} also bound to MetRS$_{1-676}$ (with a K_d of 4.6 µM) (Table 6-2).

The affinity coelectrophoresis experiments are carried out in the absence of added monovalent salt. In order to confirm that our results could be directly related to the aminoacylation experiments, NH$_4$Cl (150 mM) was added to the standard affinity coelectrophoresis buffer and the experiments were repeated. The resulting composition is identical to the buffer conditions used in the aminoacylation assays. Under these conditions, the binding of MetRS$_{1-676}$ to microhelix substrates was weakened 5-10-fold, but for all three substrates the relative decrease was about the same. Therefore, the relative binding constants for the three microhelix substrates were unchanged (data not shown).

These experiments collectively suggest that synthetase-microhelix interactions in the transition state rather than at the binding step are the major contributor to the specificity of microhelix aminoacylation.

Binding of AlaRS to Microhelix^{Ala} is Sensitive to 3·70 Base Pair. In Chapter 4, we showed that the affinity coelectrophoresis method could easily demonstrate the marked difference in affinity for methionyl-tRNA synthetase of a wild-type and mutant RNA hairpin mimicking the anticodon stem-loop of tRNA^{Met}. In particular, a hairpin with a CAU anticodon bound with a dissociation constant of about 30 µM, while binding of a GAU-

containing hairpin could not be detected (Gale and Schimmel, 1995b). These and other experiments support the idea that highly specific interactions can be monitored by the gel electrophoresis method, and suggest that the lack of specificity of binding of microhelix^{fMet} substrates to methionyl-tRNA synthetase truly reflects a greater emphasis on transition state interactions.

To demonstrate further the detection of specific interactions, however, we turned to alanyl-tRNA synthetase, where acceptor helix interactions have been well studied by other methods. The main identity element of tRNA^{Ala} is a G3·U70 base pair in the acceptor stem (Hou and Schimmel, 1988; McClain and Foss, 1988). Mutation of this basepair to G·C or to A·U eliminates aminoacylation *in vivo* and *in vitro* (Hou and Schimmel, 1988). Furthermore, a tRNA^{Ala} with a substituted 3·70 base pair does not inhibit charging of wild type tRNA^{Ala} (at pH 7.5), suggesting that binding is weakened by a factor of at least 30 (Park *et al.*, 1989). Therefore, we would expect that the binding of AlaRS to microhelix^{Ala} substrates would be sensitive to substitutions of the G3·U70 base pair.

We used a fragment of AlaRS that contains residues 1-461 (AlaRS$_{1-461}$-6H), because a fragment of the N-terminal 461 amino acids aminoacylates microhelix^{Ala} with the same efficiency as full length AlaRS (Buechter and Schimmel, 1993b). We found by affinity coelectrophoresis that AlaRS$_{1-461}$-6H bound to microhelix^{Ala} with a K_d of 12 ± 5 μM. However, we could not detect binding to AlaRS$_{1-461}$-6H of either G3·C70 microhelix^{Ala} or microhelix^{fMet} (Table 6-2). These results confirm that interactions with acceptor helices which differ by a single base pair can be discriminated by the ACE method.

Competition Between Binding of Microhelix^{fMet} and tRNA^{fMet}. In order to prove that binding of microhelix substrates to MetRS was at part of the same site as that occupied by tRNA^{fMet}, we performed an affinity coelectrophoresis

gel competition assay. MetRS$_{1-676}$ and tRNA^{fMet} were placed together into the ACE gel at concentrations of 10 μM and 12 μM, respectively, in one lane. In a parallel lane, MetRS$_{1-676}$ was added alone at a concentration of 10 μM. The three [5'-^{32}P]-microhelix substrates of interest were then separately electrophoresed through these lanes (Figure 6-3). Presumably, tRNA^{fMet} should compete for the binding sites on MetRS$_{1-676}$ and inhibit the binding of the microhelix substrates. Therefore, in the lane containing tRNA^{fMet}, the microhelix substrate should have a decreased shift relative to the lane without tRNA^{fMet}. This expectation was fulfilled for all three microhelix substrates (Figure 6-3). (The inhibition of shift was most pronounced for wild-type microhelix^{fMet}). As a negative control, tRNA^{Val} was used as the competitor RNA for microhelix^{fMet}. In this case, the shift of microhelix^{fMet} was only slightly inhibited (Figure 6-3). We conclude that wild-type and G72, G73 microhelix^{fMet}, and noncognate microhelix^{Ala}, each bind to the same site as the one occupied by tRNA^{Met}.

Influence of C-terminus on Microhelix^{fMet} Binding to N-terminal Domain. The dissociation constant for the complex of MetRS$_{1-676}$ with tRNA^{fMet} is 7-fold smaller than that for the complex between the truncated MetRS$_{1-547}$ and tRNA^{fMet} (Table 6-3 and Chapter 4) (Gale and Schimmel, 1995b). The relative difference in affinity for tRNA^{fMet} is comparable to that seen by Blanquet *et al.* (1973a), as measured by fluorescence quenching. We speculated that the difference in affinity (for tRNA^{fMet}) between the native and truncated forms of methionyl-tRNA synthetase was related to the role in acceptor helix binding of the peptide appendix located at the C-terminal end of MetRS$_{1-547}$. This peptide appendix is critical for the stability of the truncated synthetase (Mellot *et al.*, 1989), and mutations within a conserved portion of the appendix (Y531-D535) have a marked affect on binding of

125

tRNA^{fMet} or of microhelix^{fMet} (Mellot *et al.*, 1989; Kim *et al.*, 1993b). In particular, an Arg533Ala substitution abolished detectable binding of microhelix^{fMet} (Table 6-3 and Chapter 5) (Kim *et al.*, 1993b).

We reasoned that the conformational stability of this appendix might be weakened in MetRS$_{1-547}$ compared with MetRS$_{1-676}$ and, additionally or alternatively, that the C-terminal side of residue 547 might also contribute to acceptor helix interactions. In either case, weakened interactions with the acceptor stem could explain why MetRS$_{1-547}$ has a reduced affinity for tRNA^{fMet}. Alternatively, the strength of anticodon interactions could be different with the two forms of MetRS, especially because the C-terminal domain contains all of the determinants for binding to the anticodon of tRNA^{fMet}.

We found that MetRS$_{1-676}$ binds to an RNA hairpin that recreates the anticodon stem-loop (of tRNA^{fMet}) with a dissociation constant of 22 µM (Table 6-2). This value is similar to that observed for the complex of the RNA hairpin with MetRS$_{1-547}$ (31 µM) (Table 6-3 and Chapter 4) (Gale and Schimmel, 1995b). Therefore, the difference in affinity (for tRNA^{fMet}) between MeRS$_{1-676}$ and MetRS$_{1-547}$ is not due to a difference in binding to the anticodon stem-loop of tRNA^{fMet}. This result is consistent with anticodon interactions occurring entirely within the domain from Ile367-Lys547 (see Chapter 4) (Gale and Schimmel, 1995b) and suggests that the integrity of this structural unit for anticodon binding is not influenced by the region from residues 548-676.

In contrast, we found a large difference in binding of microhelix^{fMet} to MetRS$_{1-547}$ compared to MetRS$_{1-676}$. MetRS$_{1-676}$ binds to microhelix^{fMet} with an apparent K_d of 12 µM, while MetRS$_{1-547}$ binds with an apparent K_d of 330 µM (Table 6-2 and Table 6-3). A lack of binding discrimination between wild

type, mutant and the noncognate microhelix substrates was also seen with
MetRS$_{1-547}$ (Table 6-3). Therefore, the difference in binding affinity for
tRNA^{fMet} of native and truncated MetRS is mirrored in the affinity for
microhelix^{fMet}. This result suggests that, within the portion of MetRS that is
unique to the full length synthetase (residues 548-676), there are residues that
directly or indirectly influence the interaction of MetRS with the acceptor
stem of tRNA^{fMet}.

DISCUSSION

The structure of the co-crystal of class I GlnRS with tRNA^{Gln} shows
that, in order for the site of aminoacylation to fit into the active site, a large
conformational change in the tRNA is required. Some of these changes are at
the end of the acceptor stem where, for example, the U1·A70 base pair of
tRNA^{Gln} is disrupted. Also, the 2-amino group of G73 is hydrogen bonded to
the phosphate group of A72, thereby stabilizing a hairpin loop conformation
for bound tRNA^{Gln} (Rould et al., 1989). The sensitivity of aminoacylation of
tRNA^{Gln} and microhelix^{Gln} to specific sequences in the acceptor stem has
been investigated (Jahn et al., 1991; Wright et al., 1993). Mutation of G73, or of
the G2·C71 and G3·C70 base pairs of tRNA^{Gln} has effects on both k_{cat} and K_m,
possibly through effects on the conformational change at the acceptor end of
tRNA^{Gln}.

Comparison of the structure of MetRS$_{1-547}$ with the structure of the
GlnRS:tRNA^{Gln} co-crystal led to a model for binding of tRNA^{Met} to MetRS
which suggested binding-induced distortion of tRNA^{fMet} similar to that seen
with tRNA^{Gln} (Perona et al., 1991). If this distortion is required, then
substitution of the first base pair (C1-A72) and of the discriminator base (A73)

of tRNA^{fMet} would be expected to have a significant effect on this conformational change.

The effect of acceptor stem mutations on k_{cat}/K_m was qualitatively the same for tRNA^{fMet} and microhelix^{fMet}. However, our results show that the dissociation constant for microhelix^{fMet} is not affected by the G72, G73 substitution (Table 6-2). This observation is in parallel with that reported by Meinnel et al. (1993) for the whole tRNA substrate. These authors showed that acceptor stem substitutions in tRNA^{fMet} had little affect on binding interactions, even in cases where the K_m for aminoacylation was affected. Thus, the K_m for aminoacylation of tRNA^{fMet} is not measuring just a binding phenomenon.

The results obtained here suggest that the N73 and 1·72 determinants for aminoacylation of microhelix^{fMet} are responsible for correct orientation of the substrate in the transition state of the aminoacylation reaction. In the full length tRNA^{fMet}, the identity of N73 affects the stability of the end of the acceptor stem, as well as the conformation of the CCA end. In a tRNA^{fMet} variant with a C1·G72 bp, substitution of A73 with U or C destabilizes the C1·G72 bp, possibly due to a loss of the stacking interaction of A73 with G72 (Lee et al., 1993) . NMR analysis of microhelix^{fMet} substrates containing a mutant G1·C72 bp and either the wildtype A73 or mutant U73 discriminator base, showed a large effect of the U73 substitution on the conformation of the CCA end of the microhelix. In the A73 microhelix, the CCA end remains stacked on the acceptor stem. In the U73 microhelix, the CCA end folds back such that the 3'-terminal A76 is close to G1 (Puglisi et al., 1994). In related work, NMR studies of a tRNA^{Ala} acceptor stem duplex RNA substrates showed that the G1·C72 bp and A73 both contribute significantly to the stability of the acceptor stem helix. Substrates with a C73 substitution or a

U1·A72 bp were significantly less stable (Limmer *et al.*, 1993). Thus, in light of the studies by Lee *et al.* (1993), Limmer *et al.* (1993), and Puglisi *et al.* (1994), there is a sound structural basis for proposing that N73 and 1·72 determinants for aminoacylation affect the orientation of the acceptor stem in the transition state of catalysis.

The absence of a Watson-Crick base base pair at the end of the acceptor stem is a critical feature in prokaryotic initiator tRNAs that prevents them from being used as elongator tRNAs. This C-A mismatch at the end of the acceptor stem is critical for binding of Met-tRNA transformylase and in preventing the binding of elongation factor EF-Tu. Mutation of A72 to G72 creates a C·G base pair at the end of the acceptor stem, which enables tRNA^{fMet} to be utilized as an elongator tRNA. The tRNA^{fMet} variant with a weak U1·A72 bp has an intermediate level of activity as an elongator tRNA, whereas the U1-G72 species is inactive as an elongator tRNA (Seong and RajBhandary, 1987; Lee *et al.*, 1992). Therefore, a determining factor in EF-Tu binding is the stength of the base pair at the end of the acceptor stem. In contrast, MetRS shows little sensitivity of binding to substitutions of the first base pair (Tables 6-2 and 6-3), consistent with its needing to be active on both initiator and elongator methionine tRNAs.

The results reported here on binding of microhelix^{fMet} to MetRS, combined with the earlier results on the binding of the anticodon stem-loop, provide sufficient information to estimate the free energy cost of distorting the enzyme-tRNA complex when the two domains are linked together and bound simultaneously to the protein. This estimate can be achieved by adding the free energy of binding of each of the two stem-loop structures and comparing this sum with that obtained from an independent measure of the dissociation constant for the MetRS-tRNA^{fMet} interaction. This estimate

does not include all distortion energies such as, for example, that part of the free energy of distortion of the acceptor stem which is common to both microhelix^{fMet} and tRNA^{fMet}.

Calculating the free energy of binding ($\Delta G°$) as $RT\ln K_d$, and given the values for binding of the RNA substrates to MetRS$_{1-676}$ (Table 6-1), $\Delta G°$ for tRNA^{fMet} = -11 kcal mole^{-1}, $\Delta G°$ for the anticodon stem-loop = -8.7 kcal mole^{-1}, and $\Delta G°$ for microhelix^{fMet} = -9.1 kcal mole^{-1}. (These values have been corrected for the cratic entropy contribution ($-RT\ln 55$ = -2.4 kcal mole^{-1}) associated with a bimolecular reaction (Cantor and Schimmel, 1980b).) The sum of free energies for the anticodon stem-loop and microhelix^{fMet} is -17.8 kcal mole^{-1}, thus suggesting an estimate of about 7 kcal mole^{-1} for the free energy of strain associated with binding the linked domains of the whole tRNA. Because there may be additional favorable synthetase-tRNA contacts outside of the acceptor stem and anticodon, the actual free energy of distortion may be greater than 7 kcal mole^{-1}.

Our analysis of the higher affinity of MetRS$_{1-676}$ (compared to MetRS$_{1-547}$) for tRNA^{fMet} suggests that the incremental binding energy is due to contacts with the acceptor helix and not with the anticodon stem-loop. By comparison of the data in Tables 6-2 and 6-3, we estimate that this incremental contribution amounts to -1.2 (tRNA^{fMet}) and -2.0 (microhelix^{fMet}) kcal mole^{-1}. The smaller value for tRNA^{fMet}, (by 0.8 kcal mole^{-1}) may reflect a coupling of binding-dependent distortion of the acceptor helix to the rest of the tRNA structure.

Table 6-1: Kinetic parameters for aminoacylation of RNA substrates by *E. coli* MetRS at pH 7.5, 37 °C

RNA	k_{cat}/K_m (M^{-1} s^{-1})	Relative k_{cat}/K_m X 10^{6}[a]
tRNA[fMet]	2.8 X 10^6	1.0 X 10^6
Microhelix[fMet]	9.4 X 10^{-1}	0.34 (1)[b]
G73 Microhelix[fMet]	1.3 X 10^{-1}	0.046 (0.14)
G72, G73 Microhelix[fMet]	7.0 X 10^{-2}	0.025 (0.074)
Microhelix[Ala]	8.3 X 10^{-2}	0.030 (0.088)

[a]Relative k_{cat}/K_m is the ratio of k_{cat}/K_m of each RNA substrate to the k_{cat}/K_m of tRNA[fMet]. [b]The values in parenthesis are relative k_{cat}/K_m values for the microhelices relative to wild type microhelix[fMet]..

Table 6-2: Dissociation constants of $MetRS_{1-676}$ and $AlaRS_{1-461}$-6H for $tRNA^{fMet}$ and small RNA substrates at pH 7.5 and 25 °C[a]

	Dissociation constants (K_d, μM)	
	$MetRS_{1-676}$	$AlaRS_{1-461}$-6H
$tRNA^{fMet}$	0.51 ± 0.14[b]	Not tested
Anticodon S-L	22 ± 6	Not tested
Microhelix^{fMet}	12 ± 3	Not detectable
G72, G73 Microhelix^{fMet}	12 ± 1	Not tested
Microhelix^{Ala}	5.6 ± 1.6	12 ± 5
C70 Microhelix^{Ala}	4.6	Not detectable

[a]The K_d values were determined from Scatchard plots of the data obtained from affinity coelectrophoresis. [b]Result previously reported in Chapter 2 and (Gale and Schimmel, 1995a).

Table 6-3: Dissociation constants of MetRS$_{1-547}$ wild type and the R533A mutant for tRNA^{fMet} and small RNA substrates at pH 7.5 and 25 °C[a]

	Dissociation constants (K_d, μM)	
	MetRS$_{1-547}$	MetRS$_{1-547}$(R533A)[b]
tRNA^{fMet}	3.6[c,] (0.51)[d]	Not tested
Anticodon S-L	31[c,] (22)	5.4 ± 1.0
Microhelix^{fMet}	330 (12)	Not detectable
G72, G73 Microhelix^{fMet}	520 (12)	Not tested
Microhelix^{Ala}	210 (5.6)	Not tested

[a]The K_d values were determined from Scatchard plots of the data obtained from affinity coelectrophoresis. The values given had errors ranging from 16-28%. [b]Results for this protein previously reported in Chapter 5 and (Kim *et al.*, 1993b). [c]Results previously reported in Chapter 4 and (Gale and Schimmel, 1995b). [d]The numbers in parenthesis are the equivalent values for MetRS$_{1-676}$ shown in Table 2.

Legend to Figure 6-1

Sequence and cloverleaf structure of *E. coli* tRNA^{fMet} and microhelix variants

Sequence and cloverleaf structure of *E. coli* tRNA^{fMet} (left) (Sprinzl *et al.*, 1989). The acceptor stem and TΨC loop are highlighted to indicate portions of the tRNA recapitulated in microhelix RNA substrates shown on the right. From left to right are wild type microhelix^{fMet}, the double mutant G72, G73 microhelix^{fMet} and wild type microhelix^{Ala}.

Figure 6-1

Legend to Figure 6-2

ACE gel analysis of the binding of MetRS$_{1-676}$ to microhelix RNA substrates

Affinity coelectrophoresis analysis of the binding of MetRS$_{1-676}$ to microhelix RNA substrates. A: ACE gel of MetRS$_{1-676}$ with microhelix^{fMet}. MetRS$_{1-676}$ concentration ranged from 2 to 80 μM. B: ACE gel of MetRS$_{1-676}$ with G72, G73 microhelix^{fMet}. MetRS$_{1-676}$ concentration ranged from 2 to 80 μM. C: ACE gel of MetRS$_{1-676}$ with microhelix^{Ala}. MetRS$_{1-676}$ concentration ranged from 0.5 to 25 μM.

A. Microhelix ^{fMet}, WT

80 ◄▬▬▬▬▬ 2 µM
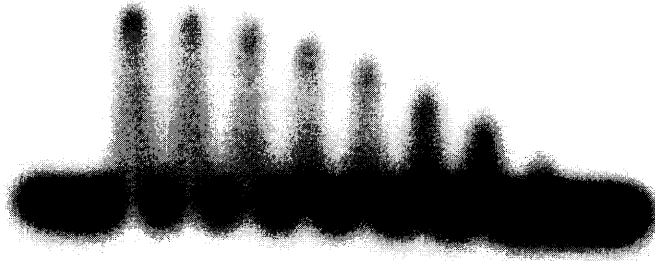
B. Microhelix ^{fMet}, G72G73

80 ◄▬▬▬▬▬ 2 µM
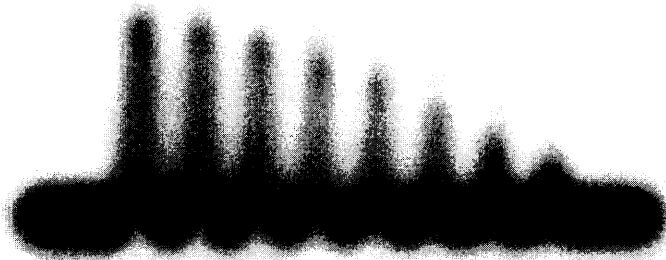
C. Microhelix ^{Ala}

25 ◄▬▬▬▬▬ 0.5 µM

Figure 6-2

137
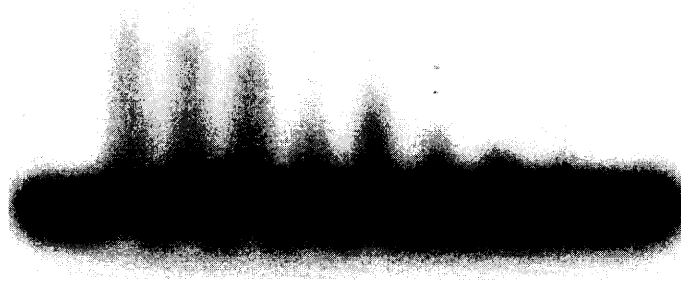
Legend to Figure 6-3

ACE gel competition assay

For each [5'-^{32}P] labeled microhelix RNA substrate, MetRS$_{1-676}$ at a concentration of 10 μM was placed in each of two lanes. Transfer RNA^{fMet} or tRNA^{Val} at a concentration of 12 μM was added to the left lane of each pair. The [5'-^{32}P] labeled microhelices were electrophoresed through the paired lanes (+ -) and unlabeled tRNA inhibited the shift of the labeled microhelix substrate, if the two RNA molecules competed for the same binding site on MetRS$_{1-676}$.

ACE Gel Competition Assay

	Microhelix			
	fMet WT	fMet WT	fMet G72G73	Ala WT
tRNA^{fMet}	+ -		+ -	+ -
tRNA^{Val}		+ -		
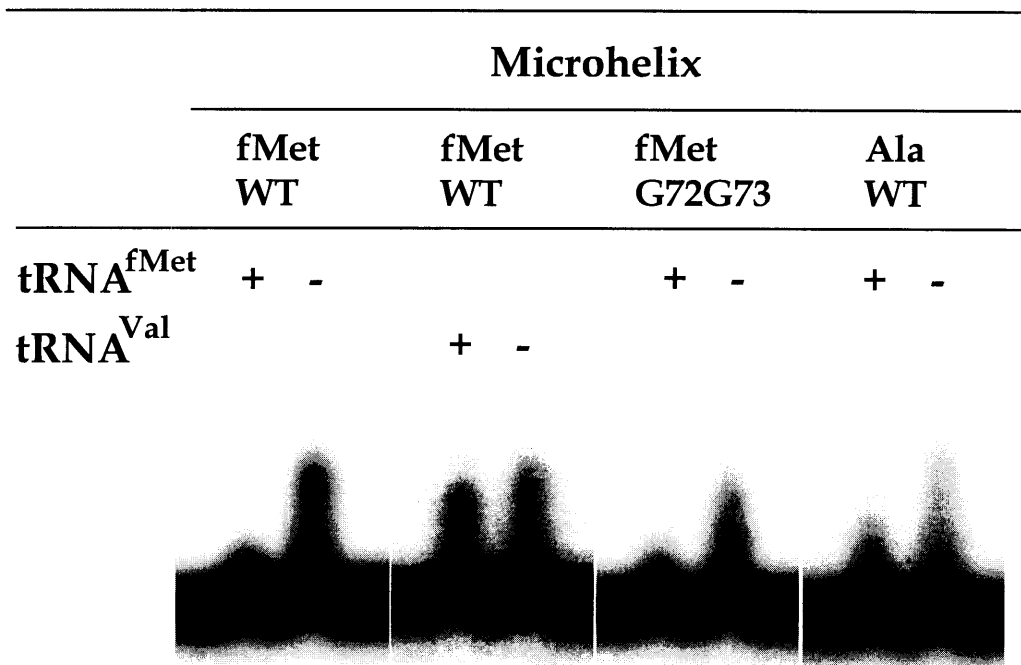
Figure 6-3

Appendix A

Analysis of the Fusion Protein MBP-C$_{1-676}$

INTRODUCTION

In addition to the fusion proteins analyzed in Chapters 3 and 4, we constructed another fusion protein that joined the C-terminal domain of full length $MetRS_{1-676}$ to MBP ($MBP-C_{367-676}$). This protein contains the dimerization domain of native *E. coli* MetRS, as well as the anticodon binding domain. Given that this protein includes the dimerization domain of MetRS, physical characterization focused on charactarization of the oligomeric state of the protein as well as determination of whether or not it maintained a native-like structure. Physical characterization utilized circular dichroism spectroscopy as described in Chapter 3 as well as analytical ultracentrifugation. Functional analysis was also performed as in Chapter 4 using the technique of affinity coelectrophoresis to measure specific binding to the anticodon stem-loop RNA substrate.

MATERIALS AND METHODS

Construction of Fusion Protein. The phagemid pJB103 (Burbaum and Schimmel, 1991a) contains the gene for the full length $MetRS_{1-676}$. The phagemid pAG117 was cleaved with *Pst* I and *Hind* III to produce a fragment of 592 bp. The phagemid pJB103 was also cut with *Pst* I and *Hind* III and the 592 bp fragment from phagemid pAG117 was inserted into The *Pst* I-*Hind* III site in pJB103 to create a phagemid encoding $MetRS_{1-676}$ with a *Bam* HI site directly before the codon for I367 (at bp 1620). This phagemid was designated as pAG118.A. Site-directed mutagenesis with the Sculptor *in vitro* mutagenesis system (Amersham, Arlington Heights, IL) was used to remove a *Bam* HI site at bp 856 of phagemid pAG118.A to create phagemid pAG118.B. The mutagenic primer 5'-CAGTGCCTGCGGAGCCGGGTAAGCAG-3' was used for this purpose. Site-directed mutagenesis was used again with the

mutagenic primer 5'-GCAGCGCCTTGAAGCTTGATTATTTCACCTG-3' and

phagemid pAG118.B to add a *Hind* III site at bp 682 of pAG118.B to create

pAG118.C. This *Hind* III site starts 2 bp beyond the stop codon of the coding

sequence of the gene for the full length MetRS.

Phagemid pAG118.C was cleaved with *Bam* HI and *Hind* III to create a

941 bp fragment. Plasmid pMal-c2 was also cleaved with *Bam* HI and *Hind* III

and the 941 bp fragment from phagemid pAG118.C was inserted into plasmid

pMal-c2 to produce a gene fusion between the MalE gene (encoding maltose

binding protein) and codons 367 to 676 of MetRS. This fusion included a

linker between the two genes that encodes 10 amino acids, including a Factor

Xa cleavage site. This plasmid was designated as pAG122.

Purification and Cleavage of Fusion Protein. MBP-C$_{367-676}$ was purified as

described in Chapter 3 for MBP-C$_{367-547}$. Factor Xa cleavage was also

performed as described in Chapter 3.

Affinity Coelectrophoresis. Affinity coelectrophoresis was performed as

described in Materials and Methods of Chapter 2 (see Figures 2-1 and 2-2).

MBP-C$_{367-676}$ was at a concentration range of 8-150 μM.

Circular Dichroism Spectroscopy. CD experiments were performed as

described in Chapter 3 with the following modifications. Two different buffer

compositions were used. The first composition was 20 mM sodium

phosphate (pH 7.3), 100 mM NaCl and 1 mM ß-ME (as in Chapter 3). The

second buffer was 50 mM sodium phosphate (pH 7.3), 0.1 mM EDTA, 4 mM

MgCl$_2$ and 1 mM ß-ME. The second buffer composition was used to more

closely duplicate the conditions under which the affinity coelectrophoresis

was done. In the first buffer, both spectroscopic and thermal denaturation

experiments were done as described in Chapter 3. In the second buffer,

spectroscopic and thermal denaturation experiments were done as described

in Chapter 3 except for the following details. Experiments were done at 50 µg/mL (0.65 µM), 1 mg/mL (13 µM) and 5 mg/mL (65 µM) protein with a 5 mm pathlength, 0.5 mm pathlength, and 0.1 mm pathlength, respectively. Thermal melts were also done with 5 mg/mL MBP-C$_{367-676}$ (65 µM) in admixture with 65 µM anticodon stem-loop RNA substrate.

Analytical Ultracentrifuge. Analytical ultracentrifugation was carried out with a Beckman analytical ultracentrifuge, model XL-A (Beckman Instruments, Inc., Palo Alto, CA). MBP-C$_{367-676}$ was dialyzed into 50 mM sodium phosphate (pH 7.3), 0.1 mM EDTA, 4 mM MgCl$_2$ and 1 mM ß-ME. Protein was loaded into a six-channel analytical cell at concentrations ranging from 50 µg/mL (0.65 µM) to 3 mg/mL (39 µM). The cell was centrifuged at 8000-10,000 rpm until the protein reached sedimentation equilibrium (14-20 hours). Absorbance scans were done with a 0.001 cm step size with 10 scans averaged together. Molecular weight values were calculated by fitting the data to the one-species function, $C(r) = C(a)\exp[\omega^2 M(1-v\rho)(r^2-a^2)/2RT]$ using the program NonLin *for Macintosh* (Version 0.9.8b4, Robelko Software, Carbondale, IL, courtesy of Alan Davidson, MIT), where $C(r)$ is the solute concentration at radius r, $C(a)$ is the solute concentration at a reference distance a, ω is the angular velocity, R is the gas constant, T is the temperature, M is the molecular weight of the protein species, v is the partial specific volume of the protein, and ρ is the density of the buffer (Cantor and Schimmel, 1980a; Johnson and Frazier, 1985). The partial specific volume was calculated from the standard formula (Laue *et al.*, 1992).

RESULTS AND DISCUSSION

Purification and Cleavage of MBP-C$_{367-676}$. The fusion protein MBP-C$_{367-676}$ was expressed at high levels in *E. coli* strain TG1, typically yielding 40 mg/L

of culture. The expressed fusion protein was soluble and stable and therefore amenable to purification (data not shown). Purification by ion exchange chromatography on a Mono Q HR 10/10 column yielded MBP-$C_{367-676}$ of about 90% purity.

Factor Xa at a 1:200 (wt:wt) ratio cleaved 100% of the fusion protein. However, $C_{367-676}$ precipitated out of solution during cleavage by Factor Xa. Therefore, it was not practical to isolate and characterize $C_{367-676}$ separate from maltose binding protein.

Affinity Coelectrophoresis. In the ACE assay, MBP-$C_{367-676}$ bound specifically to the wildtype anticodon stem-loop RNA substrate (Figure A-1). As was the case for MBP-$C_{367-547}$, binding was not detectable when a single base of the anticodon was substituted within the anticodon stem-loop substrate. Scatchard analysis suggested that MBP-$C_{367-676}$ was binding to the anticodon stem-loop in a partially cooperative manner. It was estimated that 50 % of the anticodon stem-loop RNA was bound at a concentration of 53 μM MBP-$C_{367-676}$. A Hill plot of the ACE data (Figure A-1) ($\log(R/1-R) = \log K_a + n\log[\text{protein}]$, where R is the relative shift as defined in Chapter 2 and K_a is the association constant), gave a Hill coefficient, n of 1.5-1.6, indicating significant apparent cooperativity in the binding of the anticodon stem-loop RNA. In contrast, binding of native MetRS$_{1-676}$ to the anticodon stem-loop (see Chapter 6) gave a Hill coefficient of 1.1 (data not shown).

One possible explanation for this observed cooperativity is that MBP-$C_{367-676}$ is less stable than MetRS$_{1-676}$ and only dimerizes at concentrations in the range of protein concentration studied here. In this case dimerization would stabilize the anticodon binding site.

Circular Dichroism and Analytical Ultrcentrifuge Analysis. In order to characterize the tertiary and quaternary structure of MBP-$C_{367-676}$ in solution,

we performed biophysical analysis using the techniques of circular dichroism spectroscopy and analytical ultracentrifugation. Initially, circular dichroism spectral analysis and thermal denaturations were performed with the same conditions utilized for the fusion proteins studied previously (see Chapter 3). In these conditions (including 100 mM NaCl), MBP-$C_{367-676}$ showed a high level of α-helical character similar to that seen in MetRS$_{1-547}$ and MBP-$C_{367-547}$. However, at a concentration of 1 mg/mL, MBP-$C_{367-676}$ was significantly less thermostabile than MBP-$C_{367-547}$, having an apparent T_m of 55.5 °C compared to an apparent T_m of 63 °C for MBP-$C_{367-547}$. As was the case for MBP-$C_{367-547}$, the denaturation of MBP-$C_{367-676}$ was not reversible. Denaturation of MBP-$C_{367-676}$ was somewhat concentration-dependent, with an apparent T_m of 53.5 °C at 50 µg/mL.

Thermal denaturation analysis was also done in Na-phosphate buffer without added NaCl in order to more closely duplicate the conditions under which the affinity coelectrophoresis experiments were done. The buffer used contained 50 mM Na-phosphate (pH 7.3), 4 mM MgCl$_2$, 0.1 mM EDTA and 1 mM ß-ME. Thermal denaturations were done at 50 µg/mL (0.65 µM), 1 mg/mL (13 µM) and 5 mg/mL (65 µM), as well as at 5 mg/mL with 65 µM added anticodon stem-loop RNA. The thermal denaturation curve of MBP-$C_{367-676}$ (at 1 mg/mL) with 4 mM MgCl$_2$ had two denaturation transitions. This behavior is in contrast to the thermal denaturation curve seen in phosphate buffer with 100 mM NaCl added instead of MgCl$_2$ (Figure A-2,A). The first denaturation transition (with 4 mM MgCl$_2$) had an apparent T_m of 55 °C and the second transition had an apparent T_m of 76 °C.

The denaturation curves of MBP-$C_{367-676}$ at 50 µg/mL and 5 mg/mL both differed significantly from the denaturation at 1 mg/mL (Figure A-2,B). Both curves only had one denaturation transition. The apparent T_m for MBP-

$C_{367-676}$ at 50 μg/mL was 55.5 °C. The apparent T_m for MBP-$C_{367-676}$ at 5 mg/mL was 60 °C. This denaturation curve also had an increase in -θ_{222} directly before the melting transition began. The thermal denaturation curve of MBP-$C_{367-676}$ at 5 mg/mL with 65 μM anticodon stem-loop present did not differ significantly from MBP-$C_{367-676}$ alone (data not shown). The shapes of the CD spectra curves (200-260 nm) were invariant over the concentration range of 50 μg/mL (0.65 μM) to 5 mg/mL (65 μM) (data not shown).

To determine the oligomeric state of MBP-$C_{367-676}$ we analyzed the protein by sedimentation equilibrium with an analytical ultracentrifuge. MBP-$C_{367-676}$ was centrifuged in 4 mM MgCl$_2$ at 4 different concentrations ranging from 50 μg/mL to 3 mg/mL (0.65 μM to 39 μM). At all concentrations, the calculated M_r from analysis of the sedimentation equilibrium was consistent with MBP-$C_{367-676}$ being primarily in a dimeric form. Figure A-3 shows analysis of MBP-$C_{367-676}$ at 3 mg/ml. Single-species best fit analysis gave an average Mr of 139,000 ± 4% for the four concentrations tested. The calculated molecular weight of dimeric MBP-$C_{367-676}$ is 154,000 daltons. However, at all concentrations the experimental data deviate somewhat from the theoretical single-species function. At the lower concentrations, this deviation is characteristic of aggregation (1993). Nonetheless, n-$2n$ species analysis (Van Holde, 1975) does not significantly improve the fit. At 3 mg/mL, the deviation from ideality is not clearly due to aggregation. The deviation may be due to impurities in the protein preparation or to a small amount of dissociation. Shown also in Figure A-3 is the hypothetical sedimentation equilibrium curve for monomeric MBP-$C_{367-676}$ (M_r = 77,000 daltons). That curve does not fit the experimental data.

Because MBP-$C_{367-676}$ is primarily dimeric at and significantly below the concentration range used in the ACE gel analysis (analytical

ultracentrifuge at 0.65-39 μM, ACE gel at 8-150 μM MBP-C$_{367-676}$), we conclude that the observed cooperativity of anticodon stem-loop binding is not due to dissociation of the MBP-C$_{367-676}$ dimer in the concentration range studied. However, the thermal denaturation data clearly show a concentration dependent change in the structural characteristics of MBP-C$_{367-676}$ (at 0.65-65 μM MBP-C$_{367-676}$). These changes may reflect aggregation of the thermally denatured species and not aggregation of the native dimer. For instance (at least up to 39 μM of fusion protein), the sedimentation equilibrium analysis does not demonstrate higher order aggregation, which would tend to give significantly higher experimental M_r values. Possibly the observed cooperativity of binding is due to a genuine effect of binding an RNA molecule to one subunit on the structure of the binding site on the other subunit. Because the MetRS$_{1-676}$ dimer does not elicit this behaviour, we suggest that the replacement of the N-terminal domain of MetRS may have artificially generated a novel dimer where new subunit interactions give rise to cooperativity.

MBP-C$_{367-676}$, Anticodon S-L

150 ◢ 8 μM

Figure A-1

ACE gel analysis of the binding of MBP-C$_{367-676}$ to the tRNA^{fMet}

anticodon stem-loop RNA hairpin

ACE gel of MBP-C$_{367-676}$ with the wildtype anticodon stem-loop RNA hairpin (MBP-C$_{367-676}$ concentration range from 8 to 150 μM).

148

Circular dichroism analysis of MBP-C$_{367-676}$.

A: Thermal denaturation curves of MBP-C$_{367-676}$ at a concentration of 1 mg/mL. The "100 mM NaCl buffer" is 20 mM sodium phosphate (pH 7.3), 100 mM NaCl and 1 mM ß-ME. The "4 mM MgCl$_2$" buffer is 50 mM sodium phosphate (pH 7.3), 4 mM MgCl$_2$, 0.1 mM EDTA and 1 mM ß-ME. B. Thermal denaturation curves of MBP-C367-676 at concentrations of 50 µg/mL (0.65 µM), 1 mg/mL (13 µM) and 5 mg/mL (65 µM) in 50 mM sodium phosphate (pH 7.3), 4 mM MgCl$_2$, 0.1 mM EDTA and 1 mM ß-ME.

A.
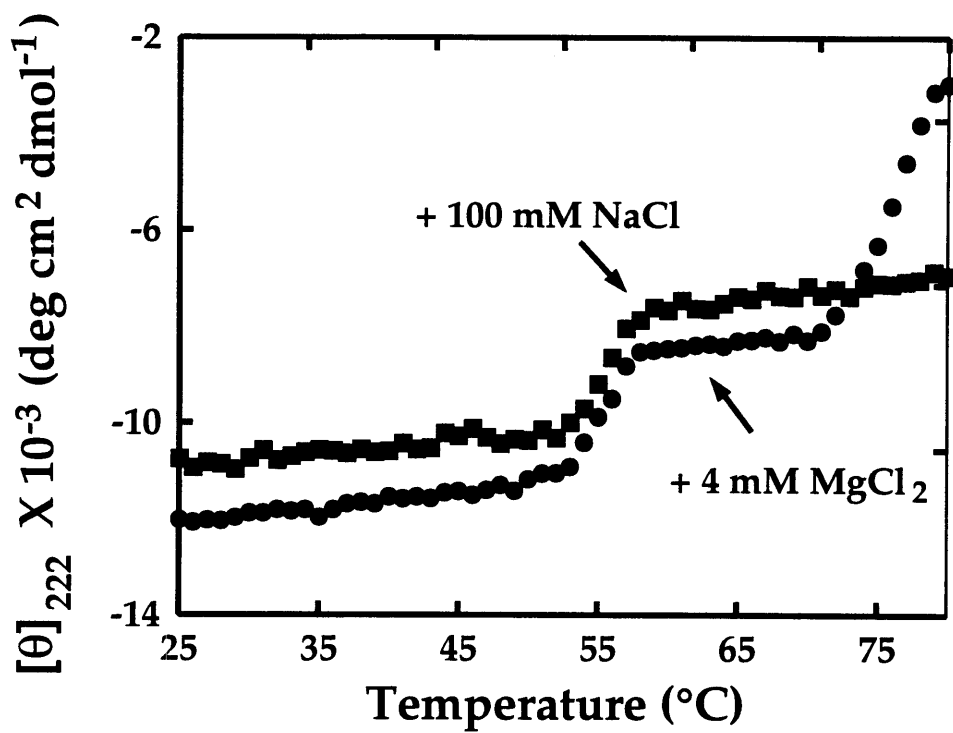
B.
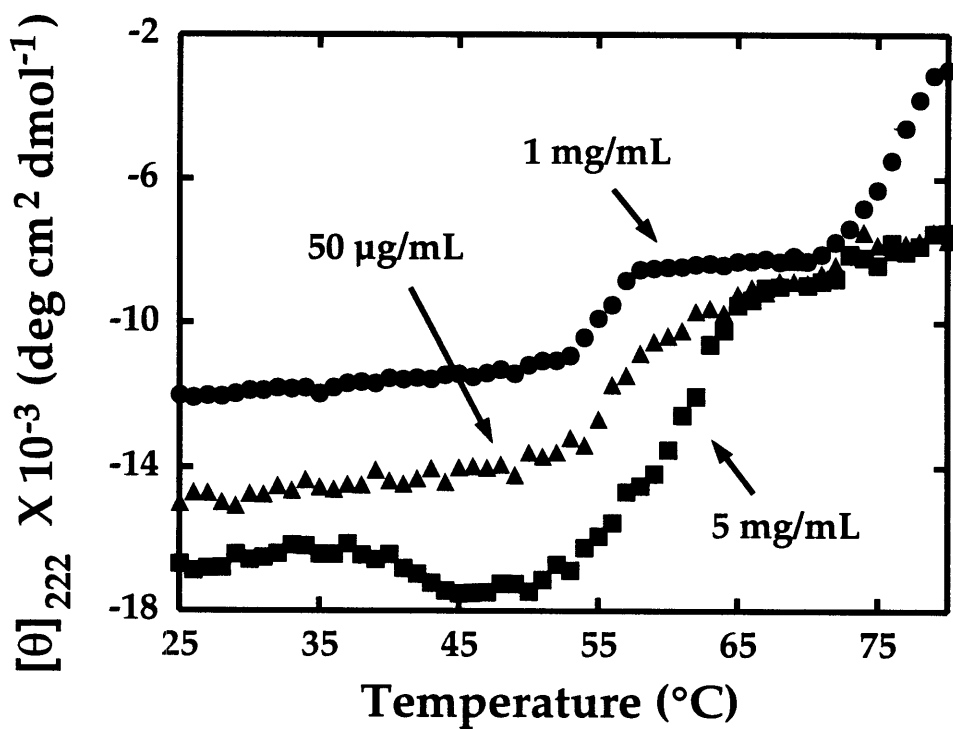
Figure A-2

Legend to Figure A-3

Analytical ultracentrifuge analysis of MBP-C$_{367-676}$.

Mass distribution of MBP-C$_{367-676}$ at 3 mg/mL (39 µM) following centrifugation to equilibrium at 10,000 rpm. The best-fit theoretical curve is superimposed over the data points. The theoretical curve for monomeric MBP-C$_{367-676}$ (M_r = 77,000 daltons) is also shown. The M_r is the average M_r determined at four protein concentrations from 50 µg/mL to 3 mg/mL (0.65 to 39 µM). Experiments were performed in 50 mM sodium phosphate (pH 7.3), 4 mM MgCl$_2$, 0.1 mM EDTA and 1 mM ß-ME at 25 °C.
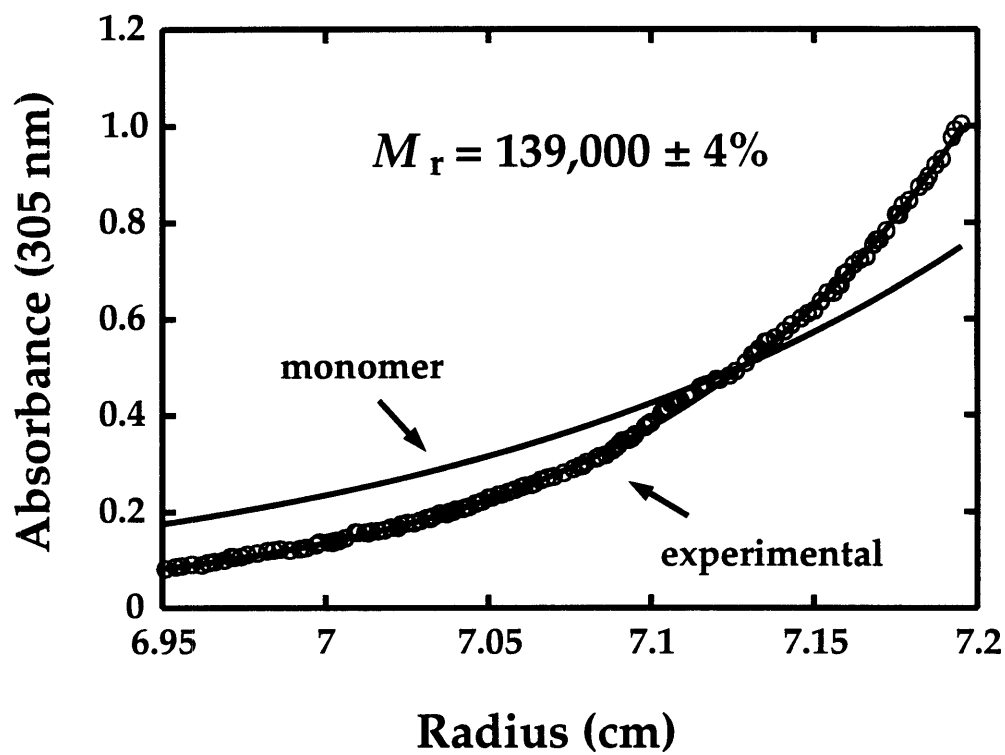
Figure A-3

Appendix B

Plasmids

Plasmid	Description	Source
pBluescript (KS+)	phagemid vector for mutagenesis and protein expression	Stratagene
pJB103	pBluescript (KS+) containing the full-length *metG* gene inserted between the *Kpn* I and *Sac* I sites (Burbaum and Schimmel, 1991a)	J. Burbaum (MIT)
pJB104	pBluescript (KS+) containing the truncated *metG* gene encoding residues 1 to 547; created by replacing the *Pst* I-*Eco* RI DNA fragment of pJB103 with the corresponding fragment of pRS735 that contains the MetRS gene encoding tandem stop codons after K547 (R.Starzyk and P. Schimmel, unpublished data) (Kim and Schimmel, 1992)	J. Burbaum (MIT)
pKK223-3	vector for protein expression and having the pBR322 backbone and a *tac* promoter	Pharmacia
pMal-c2	vector for construction and expression of fusion proteins with maltose binding protein; contains a *tac* promoter	New England Biolabs
pAG112	vector pKK223-3 with the gene for MetRS$_{1-547}$ inserted after the *tac* promoter; phagemid pJB104 was cleaved with *Eco* RI and *Sal* I, plasmid pKK223-3 was cleaved with *Eco* RI and both fragments were digested with mung bean nuclease to remove single-stranded ends. The MetRS$_{1-547}$ gene was then blunt-end-ligated into pKK223-3.	Chapter 3
pAG117	phagemid pJB104 with a *Bam* HI site introduced at codon 365 of the gene for MetRS$_{1-547}$	Chapter 3
pAG118.C	pJB103 with the *Bam* HI site at codon 365 of the pAG117 gene for Met$_{1-547}$	Chapter 3

154

transferred into the *metG* gene of pJB103;
The *Bam* HI site at codon 621 of the *metG*
gene was also removed, a *Hind* III site
was introduced 2 basepairs after the stop
codon of the *metG* gene.

pAG120   pMal-c2 with the *Bam* HI fragment from   Chapter 3
           pAG117 with the gene for MetRS$_{367-547}$
           inserted into the *Bam* HI site; encodes the
           protein MBP-C$_{367-547}$

pAG122   pMal-c2 with the *Bam* HI-*Hind* III fragment   Appendix A
           from pAG118.C with the gene for
           MetRS$_{367-676}$ inserted into the *Bam* HI-
           Hind III site; encodes the protein
           MBP-C$_{367-676}$

pAG123   pJB104 with the codon for Trp461   Chapter 3
           mutated to Ala

pAG124   pAG120 with a *Cla* I fragment of pAG123   Chapter 3
           inserted into the place of the *Cla* I fragment
           of pAG120 to encode the protein
           MBP-C$_{367-547}$(W461A)

pQE-461   pQE-70 from Qiagen with the gene for   L. Ribas (MIT)
           codons 1-461 of AlaRS inserted into the
           multiple cloning site to encode the protein ·
           AlaRS$_{1-461}$-6H

pREP4   A plasmid encoding the *lac* repressor from   Qiagen
           the *lacI* gene .

155

Oligonucleotides

Name	Sequence/Description
Bam365	CGATATCATCAATGGATCCAGAGAGTTTCGC used to introduce a *Bam* HI site at codon 365 of the gene for MetRS$_{1-547}$ in pJB104
RBam118.B	CAGTGCCTGCGGAGCCGGGTAAGCAG used to remove *Bam* HI site at codon 621 in the *metG* gene in pAG118 (basepair 856)
Hind118.C	GCAGCGCCTTGAAGCTTGATTATTTCACCTG used to add *Hind* III site at basepair 682 in pAG118, 2 basepairs after the stop codon of the *metG* gene in pAG118
W461A	TGTTTCGCCACCACCGCCGGAGCCTGTTCATC used to mutate Trp461 to Ala in the gene for MetRS$_{1-547}$ in pJB104
PNR7	TACGGGAGGCCAGGT used for sequencing of anticoding strand of the gene for MetRS starting at codon 391
AG2(PNR9)	TCAGGTAAGTCATCAGCACGCG used for sequencing of anticoding strand of the gene for MetRS starting at codon 484
495-500	CTGCCGAAACTGACCGAG used for sequencing of coding strand of the gene for MetRS starting at codon 500
515-520	ATCCAGCAACCGCTGCTG used for sequencing of coding strand of the gene for MetRS starting at codon 520
PRM12	CAAACTGCTGCGCCTG used for sequencing of coding strand of the gene for MetRS starting at codon 600
PRM13	TGCCGGTCCTGGCGGG used for sequencing of coding strand of the gene for MetRS starting at codon 657

Abbreviations

ACE	affinity coelectrophoresis
AMP	adenosine 5'-monophosphate
ATP	adenosine 5'-triphosphate
ß-ME	ß-mercaptoethanol
bp	base pair(s)
BSA	bovine serum albumin
CD	circular dichroism
CP1, CP2	connective polypeptides 1 and 2
$C(r)$	solute concentration at radius r
DEAE-TSK	diethylaminoethyl-TSK
DHU	dihydrouridine
EDTA	(ethylenedinitrilo)tetraacetic acid
FPLC	fast protein liquid chromatography
g	gravitational force
HEPES	N-(2-hydroxyethyl)-piperazine-N'-(2-ethanesulfonic acid)
IPTG	isopropylthio-ß-D-galactopyranoside
K_a	association constant
k_{cat}	catalytic rate constant
K_d	dissociation constant
K_m	Michaelis constant
LMP agarose	low melting point agarose
MBP	maltose binding protein
$MgCl_2$	magnesium chloride
M_r	relative molecular weight
NaCl	sodium chloride
ρ	density
PEI	poly(ethyleneimine)
PMSF	phenylmethylsulfonyl fluoride
R	gas constant
rpm	revolutions per minute
SDS-PAGE	sodium-dodecyl-sulfate polyacrylamide gel electrophoresis
T	temperature
Tris	tris(hydroxymethyl)aminomethane
tRNA	transfer RNA
v	partial specific volume
V_{max}	maximum velocity
ω	angular velocity
XxxRS	aminoacyl-tRNA synthetase specific for amino acid Xxx (three letter code)

References

158

(1993). *Model XL-A analytical ultracentrifuge optima series training guide.* (Palo Alto, CA, Spinco Business Unit of Beckman Instruments, Inc.).

Arnez, J. G., Harris, D. C., Mitschler, A., Rees, B., Francklyn, C. S., and Moras, D. (1995). Crystal structure of histidyl-tRNA synthetase from *Escherichia coli* complexed with histidyl-adenlylate. *EMBO J.* in press.

Auld, D. S., and Schimmel, P. (1995). Switching recognition of two tRNA synthetases with an amino acid swap in a designed peptide. *Science 267*: 1994-1996.

Belrhali, H., Yaremchuk, A., Tukalo, M., Larsen, K., Berthet-Colominas, C., Leberman, R., Beijer, B., Sproat, B., Als-Nielson, J., Grübel, G., Legrand, J.-F., Lehmann, M., and Cusack, S. (1994). Crystal structures at 2.5 angstrom resolution of seryl-tRNA synthetase complexed with two analogs of seryl adenylate. *Science 263*: 1432-1436.

Berg, P. (1961). Specificity in protein synthesis. *Ann. Rev. Biochem. 30*: 292-324.

Biou, V., Yaremchuk, A., Tukalo, M., and Cusack, S. (1994). The 2.9 Å crystal structure of *T. thermophilus* seryl-tRNA synthetase complexed with tRNA^{Ser}. *Science 263*: 1404-1410.

Blanquet, S., Iwatsubo, M., and Waller, J.-P. (1973a). The mechanism of action of methionyl-tRNA synthetase from *Escherichia coli* 1. Fluorescence studies on tRNA^{Met} binding as a function of ligands, ions and pH. *Eur. J. Biochem. 36*: 213-226.

Blanquet, S., Petrissant, G., and Waller, J.-P. (1973b). The mechanism of action of methionyl-tRNA synthetase 2. Interaction of the enzyme with specific and unspecific tRNAs. *Eur. J. Biochem 36*: 227-233.

Borel, F., Vincent, C., Leberman, R., and Härtlein, M. (1994). Seryl-tRNA synthetase from *Escherichia coli*: Implication of its N-terminal domain in aminoacylation activity and specificity. *Nucleic Acids Res. 22*: 2963-2969.

Brick, P., Bhat, T. N., and Blow, D. M. (1988). Structure of tyrosyl-tRNA synthetase refined at 2.3 Å resolution: Interaction of the enzyme with the tyrosyl adenylate intermediate. *J. Mol. Biol. 208*: 83-98.

Brunie, S., Zelwer, C., and Risler, J.-L. (1990). Crystallographic Study at 2.5 Å Resolution of the Interaction of Methionyl-tRNA Synthetase from *Escherichia coli* with ATP. *J. Mol. Biol. 216*: 411-424.

159

Buechter, D. D., and Schimmel, P. (1993a). Aminoacylation of RNA minihelices: Implications for tRNA synthetase structural design and evolution. *Crit. Rev. Biochem. Mol. Biol. 28*: 309-322.

Buechter, D. D., and Schimmel, P. (1993b). Dissection of a class II tRNA synthetase: determinants for minihelix recognition are tightly associated with domain for amino acid activation. *Biochemistry 32*: 5267-5272.

Burbaum, J. J., and Schimmel, P. (1991a). Assembly of a class I tRNA synthetase from products of an artificially split gene. *Biochemistry 30*: 319-324.

Burbaum, J. J., and Schimmel, P. (1991b). Structural relationships and the classification of aminoacyl-tRNA synthetases. *J. Biol. Chem. 266*: 16965-16968.

Burbaum, J. J., Starzyk, R. M., and Schimmel, P. (1990). Understanding structure relationships in proteins of unsolved three-dimensional structure. *Proteins: Struc. Funct. Gen. 7*: 99-111.

Cantor, C. R., and Schimmel, P. R. (1980a). *Biophysical Chemistry Part II: Techniques for the study of biological structure and function.* (San Francisco, W. H. Freeman and Company).

Cantor, C. R., and Schimmel, P. R. (1980b). *Biophysical Chemistry Part III: The behavior of biological macromolecules.* (San Francisco, W. H. Freeman and Company).

Cassio, D., and Waller, J.-P. (1971). Modification of methionyl-tRNA synthetase by proteolytic cleavage and properties of the trypsin-modified enzyme. *Eur. J. Biochem. 20*: 283-300.

Cavarelli, J., Eriani, G., Rees, B., Ruff, M., Boeglin, M., Mitschler, A., Martin, F., Gangloff, J., Thierry, J.-C., and Moras, D. (1994). The active site of yeast aspartyl-tRNA synthetase: Structural and functional aspects of the aminoacylation reaction. *EMBO J. 13*: 327-337.

Cavarelli, J., Rees, B., Ruff, M., Thierry, J.-C., and Moras, D. (1993). Yeast tRNA^{Asp} recognition by its cognate class II aminoacyl-tRNA synthetase. *Nature 362*: 181-184.

Crothers, D. M., Seno, T., and Soll, D. G. (1972). Is there a discriminator site in transfer RNA? *Proc. Natl. Acad. Sci. U.S.A. 69*: 3063-3067.

Cusack, S., Berthet-Colominas, C., Biou, V., Borel, F., Fujinaga, M., Härtlein, M., Krikliviy, I., Nassar, N., Price, S., Tukalo, M. A., Yaremchuk, A. D., and Leberman, R. (1993). "The crystal structure of seryl-tRNA synthetase and its complexes with ATP and tRNA^{Ser}" in *The Translation Apparatus* . K. H. Nierhaus, F. Franceschi, A. R. Subramanian, V. Erdmann, A. and B. Wittmann-Liebold Eds. (New York, Plenum Press). 1-12.

Cusack, S., Berthet-Colominas, C., Härtlein, M., Nassar, N., and Leberman, R. (1990). A second class of synthetase structure revealed by X-ray analysis of *Escherichia coli* seryl-tRNA synthetase at 2.5 A. *Nature 347*: 249-255.

Dardel, F., Fayat, G., and Blanquet, S. (1984). Molecular cloning and primary structure of the *Escherichia coli* methionyl-tRNA synthetase gene. *J. Bacteriol. 160*: 1115-1122.

de Duve, C. (1988). The second genetic code. *Nature 333*: 117-118.

Doublié, S., Bricogne, G., Gilmore, C., and Carter, C. W., Jr. (1995). Tryptophanyl-tRNA synthetase crystal structure reveals an unexpected homology to tyrosyl-tRNA synthetase. *Structure 3*: 17-31.

Edelhoch, H. (1967). Spectroscopic determination of tryptophan and tyrosine in proteins. *Biochemistry 6*: 1948-1954.

Eriani, G., Delarue, M., Poch, O., Gangloff, J., and Moras, D. (1990). Partition of tRNA synthetases into two classes based on mutually exclusive sets of sequence motifs. *Nature 347*: 203-206.

Eriani, G., Dirheimer, G., and Gangloff, J. (1991). Cysteinyl-tRNA synthetase: determination of the last *E. coli* aminoacyl-tRNA synthetase primary structure. *Nucleic Acids Res. 19*: 265-269.

Farabaugh, P. J. (1978). Sequence of the *lacI* gene. *Nature 274*: 765-769.

Fersht, A. R. (1987). Dissection of the structure and activity of the tyrosyl-tRNA synthetase by site-directed mutagenesis. *Biochemistry 26*: 8031-8037.

Fersht, A. R., Ashford, J. S., Bruton, C. J., Jakes, R., Koch, G. L. E., and Hartley, B. S. (1975). Active site titration and aminoacyl adenylate binding stoichiometry of aminoacyl-tRNA synthetases. *Biochemistry 14*: 1-4.

Fourmy, D., Dardel, F., and Blanquet, S. (1993a). Methionyl-tRNA synthetase zinc binding domain: Three-dimensional structure and homology with rebredoxin and gag retroviral proteins. *J. Mol. Biol. 231*: 1078-1089.

161

Fourmy, D., Meinnel, T., Mechulam, Y., and Blanquet, S. (1993b). Mapping of the zinc binding domain of *Escherichia coli* methionyl-tRNA synthetase. *J. Mol. Biol. 231*: 1068-1077.

Francklyn, C., and Schimmel, P. (1989). Aminoacylation of RNA minihelices with alanine. *Nature 337*: 478-481.

Francklyn, C., and Schimmel, P. (1990). Enzymatic aminoacylation of an eight-base-pair microhelix with histidine. *Proc. Natl. Acad. Sci. U.S.A. 87*: 8655-8659.

Francklyn, C., Shi, J.-P., and Schimmel, P. (1992). Overlapping nucleotide determinants for specific aminoacylation of RNA microhelices. *Science 255*: 1121-1125.

Frugier, M., Florentz, C., and Giegé, R. (1992). Anticodon-independent aminoacylation of an RNA minihelix with valine. *Proc. Natl. Acad. Sci. U.S.A. 89*: 3990-3994.

Frugier, M., Florentz, C., and Giegé, R. (1994). Efficient aminoacylation of resected RNA helices by class II aspartyl-tRNA synthetase dependent on a single nucleotide. *EMBO J. 13*: 2218-2226.

Gale, A. J., and Schimmel, P. (1995a). Affinity coelectrophoresis for dissecting protein-RNA domain-domain interactions in a tRNA synthetase system. *Pharmaceutica Acta Helvetiae.* in press.

Gale, A. J., and Schimmel, P. (1995b). Isolated RNA binding domain of a class I tRNA synthetase. *Biochemistry 34*: 8896-8903.

Ghosh, G., Kim, H. Y., Demaret, J.-P., Brunie, S., and Schulman, L. H. (1991). Arginine-395 is required for efficient in vivo and in vitro aminoacylation of tRNAs by *Escherichia coli* methionyl-tRNA synthetase. *Biochemistry 30*: 11767-11774.

Ghosh, G., Pelka, H., and Schulman, L. H. (1990). Identification of the tRNA anticodon recognition site of *Escherichia coli* methionyl-tRNA synthetase. *Biochemistry 29*: 2220-2225.

Giegé, R., Puglisi, J. D., and Florentz, C. (1993). tRNA structure and aminoacylation efficiency. *Prog Nucleic Acids. Res. Mol. Biol. 45*: 129-206.

Guan, C., Li, P., Riggs, P. D., and Inouye, H. (1987). Vectors that facilitate the expression and purification of foreign peptides in *Escherichia coli* by fusion to maltose-binding-protein. *Gene 67*: 21-30.

Hamann, C. S., and Hou, Y.-M. (1995). Enzymatic aminoacylation of tRNA acceptor stem helices with cysteine is dependent on a single nucleotide. *Biochemistry 34*: 6527-6532.

Hélène, C., Brun, F., and Yaniv, M. (1971). Fluorescence studies of interactions between *E. coli* valyl-tRNA synthetase and its substrate. *J. Mol. Biol. 58*: 349-365.

Hochuli, E. (1989). Aufarbeitung von Bioproteinen: Elegant und wirtschaftlich. *Chemische Industrie 12*: 69-70.

Hou, Y.-M., and Schimmel, P. (1988). A simple structural feature is a major determinant of the identity of a transfer RNA. *Nature 333*: 140-145.

Hou, Y.-M., Shiba, K., Mottes, C., and Schimmel, P. (1991). Sequence determination and modeling of structural motifs for the smallest monomeric aminoacyl-tRNA synthetase. *Proc. Natl. Acad. Sci. U.S.A. 88*: 976-980.

Hountondji, C., and Blanquet, S. (1985). Methionyl-tRNA synthetase from *Escherichia coli*: primary structure at the binding site for the 3'-end of tRNA^{fMet}. *Biochemistry 24*: 1175-1180.

Hountondji, C., Dessen, P., and Blanquet, S. (1986). Sequence similarities among the family of aminoacyl-tRNA synthetases. *Biochimie 68*: 1071-1078.

Jahn, M., Rogers, M. J., and Söll, D. (1991). Anticodon and acceptor stem nucleotides in tRNA^{Gln} are major recognition elements for *E. coli* glutaminyl-tRNA synthetase. *Nature 352*: 258-260.

Janknecht, R., de Martynoff, G., Lou, J., Hipskind, R. A., Nordheim, A., and Stüber, D. (1991). Rapid and efficient purification of native histidine-tagged protein expressed by recombinant vaccinia virus. *Proc. Natl. Acad. Sci. U.S.A. 88*: 8972-8976.

Jasin, M., Regan, L., and Schimmel, P. (1983). Modular arrangement of functional domains along the sequence of an aminoacyl tRNA synthetase. *Nature 306*: 441-447.

Johnson, M. L., and Frazier, S. G. (1985). Nonlinear least-squares analysis. *Methods Enzymol. 117*: 301-342.

Kim, H. Y., Pelka, H., Brunie, S., and Schulman, L. H. (1993a). Two separate peptides in *Escherichia coli* methionyl-tRNA synthetase form the anticodon binding site for methionine tRNA. *Biochemistry 32*: 10506-10511.

Kim, S., Landro, J. A., Gale, A. J., and Schimmel, P. (1993b). C-terminal peptide appendix in a class I tRNA synthetase needed for acceptor-helix contacts and microhelix aminoacylation. *Biochemistry 32*: 13026-13031.

Kim, S., Ribas de Pouplana, L., and Schimmel, P. (1993c). Diversified sequences of peptide epitope for same-RNA recognition. *Proc. Natl. Acad. Sci. U.S.A. 90*: 10046-10050.

Kim, S., Ribas de Pot plana, L., and Schimmel, P. (1994). An RNA binding site in a tRNA synthetase with a reduced set of amino acids. *Biochemistry 33*: 11040-11045.

Kim, S., and Schimmel, P. (1992). Functional independence of microhelix aminoacylation from anticodon binding in a class I tRNA synthetase. *J. Biol. Chem. 267*: 15563-15567.

Kim, S. H., Suddath, F. L., Quigley, G. J., McPherson, A., Sussman, J. L., Wang, A. H. J., Seeman, N. C., and Rich, A. (1974). Three-dimensional tertiary structure of yeast phenylalanine transfer RNA. *Science 185*: 435-440.

Kisselev, L. L., and Favorova, O. g. O. (1974). Aminoacyl-tRNA synthetases: Some recent results and achievements. *Adv. Enzymol. 40*: 141-238.

Kohda, D., Yokoyama, S., and Miyazawa, T. (1987). Functions of isolated domains of methionyl-tRNA synthetase from an extreme thermophile, *Thermus thermophilus* HB8. *J. Biol. Chem. 262*: 558-563.

Lam, S. S. M., and Schimmel, P. R. (1975). Equilibrium measurements of cognate and noncognate interactions between aminoacyl transfer RNA synthetase and transfer RNA. *Biochemistry 14*: 2775-2780.

Landès, C., Perona, J. J., Brunie, S., Rould, M. A., Zelwer, C., Steitz, T. A., and Risler, J. L. (1995). A structure-based multiple sequence alignment of all class I aminoacyl-tRNA synthetases. *Biochimie 77*: 194-203.

Landro, J. A., and Schimmel, P. (1993). Metal-binding site in a class I tRNA synthetase localized to a cysteine cluster inserted into a nucleotide-binding fold. *Proc. Natl. Acad. Sci. U.S.A. 90*: 2261-2265.

Laue, T. M., Shah, B. D., Ridgeway, T. M., and Pelletier, S. M. (1992). "Computer-aided interpretation of analytical sedimentation data for

proteins" in *Analytical Ultracentrifugation in Biochemistry and Polymer Science* . S. Harding, A. Rowe and J. Horton Eds. (Cambridge, U.K., Royal Soc. Chem.). 90-125.

Lee, C.-P., Dyson, M. R., Mandal, N., Varshney, U., Bahramian, B., and RajBhandary, U. L. (1992). Striking effects of coupling mutations in the acceptor stem on recognition of tRNAs by *E. coli* methionyl-tRNA synthetase and methionyl-tRNA transformylase. *Proc. Natl. Acad. Sci. U.S.A. 89*: 9262-9266.

Lee, C. P., Mandal, N., Dyson, M., R., and RajBhandary, U. L. (1993). The discriminator base influences tRNA structure at the end of the acceptor stem and possibly its interaction with proteins. *Proc. Natl. Acad. Sci. U.S.A. 90*: 7149-7152.

Lee, M. K., and Lander, A. D. (1991). Analysis of affinity and structural selectivity in the binding of proteins to glycosaminoglycans: Development of a sensitive electrophoretic approach. *Proc. Natl. Acad. Sci. USA 88*: 2768-2772.

Leon, O., and Schulman, L. H. (1987a). Covalent coupling of 4-thiouridine in the initiator methionine tRNA to specific lysine residues in *Escherichia coli* methionyl-tRNA synthetase. *Biochemistry 26*: 7113-7121.

Leon, O., and Schulman, L. H. (1987b). tRNA recognition site of *Escherichia coli* methionyl-tRNA synthetase. *Biochemistry 26*: 5416-5422.

Lim, W. A., Sauer, R. T., and Lander, A. D. (1991). Analysis of DNA-protein interactions by affinity coelectrophoresis. *Methods Enzymol. 208*: 196-210.

Limmer, S., Hofmann, H.-P., Ott, G., and Sprinzl, M. (1993). The 3-terminal end (NCCA) of tRNA determines the structure and stability of the aminoacyl acceptor stem. *Proc. Natl. Acad. Sci. U.S.A. 90*: 6199-6202.

Logan, D. T., Mazauric, M.-H., Kern, D., and Moras, D. (1995). Crystal structure of glycyl-tRNA synthetase from *Thermus thermophilus*: New functional domains and substrate specificity. *EMBO J.* in press.

Maina, C. V., Riggs, P. D., Grandea, A. G. I., Slatko, B. E., Moran, L. S., Tagliamonte, J. A., McReynolds, L. A., and Guan, C. (1988). A vector to express and purify foreign proteins in *Escherichia coli* by fusion to, and separation from, maltose binding protein. *Gene 74*: 365-373.

Maizels, N., and Weiner, A. M. (1993). "The genomic tag Hypothesis: Modern viruses as molecular fossils of ancient strategies for genomic

replication" in *The RNA World* . R. F. Gesteland and J. F. Atkins Eds. (Plainview, NY, Cold Spring Harbor Laboratory Press). 577-602.

Martinis, S., and Schimmel, P. (1993). Microhelix aminoacylation by a class I tRNA synthetase: Non-conserved base pairs required for specifity. *J. Biol. Chem. 268*: 6069-6072.

Martinis, S. A., and Schimmel, P. (1992). Enzymatic aminoacylation of sequence-specific RNA minihelices and hybrid duplexes with methionine. *Proc. Natl. Acad. Sci. U.S.A. 89*: 65-69.

Martinis, S. A., and Schimmel, P. (1995). "Small RNA oligonucleotide substrates for specific aminoacylations" in *tRNA: Structure, Biosynthesis, and Function* . D. Söll and U. RajBhandary Eds. (Washington, D.C., American Society for Microbiology Press). 349-370.

McClain, W. H. (1993). Rules that govern tRNA identity in protein synthesis. *J. Mol. Biol. 234*: 257-280.

McClain, W. H. (1995). "The tRNA identity problem: Past, present, and future" in *tRNA: Structure Function and Biosynthesis* . D. Söll and U. L. RajBhandary Eds. (Washington, D.C., American Society for Microbiology Press). 335-347.

McClain, W. H., and Foss, K. (1988). Changing the identity of a tRNA by introducing a G-U wobble pair near the 3' acceptor end. *Science 240*: 793-796.

Mechulam, Y., Dardel, F., Le Corre, D., Blanquet, S., and Fayat, G. (1991). Lysine 335, part of the KMSKS signature sequence, plays a crucial role in the amino acid activation reaction catalysed by the *E. coli* methionyl-tRNA synthetase. *J. Mol. Biol. 217*: 465-475.

Meinnel, T., Mechulam, Y., Blanquet, S., and Fayat, G. (1991a). Binding of the anticodon domain of tRNA[fMet] to *Escherichia coli* methionyl-tRNA synthetase. *J. Mol. Biol. 220*: 205-208.

Meinnel, T., Mechulam, Y., Dardel, F., Schmitter, J.-M., Hountondji, C., Brunie, S., Dessen, P., Fayat, G., and Blanquet, S. (1990). Methionyl-tRNA synthetase from *E. coli* - A review. *Biochimie 72*: 625-632.

Meinnel, T., Mechulam, Y., Lazennec, C., Blanquet, S., and Fayat, G. (1993). Critical role of the acceptor stem of tRNA[Met] in their aminoacylation by *Escherichia coli* methionyl-tRNA synthetase. *J. Mol. Biol. 229*: 26-36.

166

Meinnel, T., Mechulam, Y., Le Corre, D., Panvert, M., Blanquet, S., and Fayat, G. (1991b). Selection of suppressor methionyl-tRNA synthetase: Mapping the tRNA anticodon binding site. *Proc. Natl. Acad. Sci. U.S.A.* *88*: 291-295.

Mellot, P., Mechulam, Y., Corre, D. L., Blanquet, S., and Fayat, G. (1989). Identification of an amino acid region supporting specific methionyl-tRNA synthetase:tRNA recognition. *J. Mol. Biol. 208*: 429-443.

Möller, W., and Janssen, G. M. (1990). Transfer RNAs for primordial amino acids contain remnants of a primitive code at position 3 to 5. *Biochimie 72*: 361-368.

Moras, D. (1992). Structural and functional relationships between aminoacyl-tRNA synthetases. *Trends in Biochem. Sci. 17*: 159-164.

Moras, D., Comarmond, M. B., Fischer, J., Weiss, R., Thierry, J. C., Ebel, J. P., and Giegé, R. (1980). Crystal structure of yeast $tRNA^{Asp}$. *Nature 288*: 669-674.

Mosyak, L., Reshetnikova, L., Goldgur, Y., and Delarue, M. (1995). Structure of phenylalanyl-tRNA synthetase from *Thermus thermophilus*. *Nature Structural Biology 2*: 537-547.

Musier-Forsyth, K., Scaringe, S., Usman, N., and Schimmel, P. (1991). Enzymatic aminoacylation of single-stranded RNA with an RNA cofactor. *Proc. Natl. Acad. Sci. U.S.A. 88*: 209-213.

Musier-Forsyth, K., and Schimmel, P. (1992). Functional contacts of a transfer RNA synthetase with 2'-hydroxyl groups in the RNA minor groove. *Nature 357*: 513-515.

Musier-Forsyth, K., Usman, N., Scaringe, S., Doudna, J., Green, R., and Schimmel, P. (1992). Specificity for aminoacylation of an RNA helix:unpaired exocyclic amino group in the minor groove. *Science 253*: 784-786.

Nagel, G. M., and Doolittle, R. F. (1991). Evolution and relatedness in two aminoacyl-tRNA synthetase families. *Proc. Natl. Acad. Sci. U.S.A. 88*: 8121-8125.

Noller, H. F. (1993). "On the origin of the ribosome: Coevolution of subdomains of tRNA and rRNA" in *The RNA World* . R. F. Gesteland and J. F. Atkins Eds. (Plainview, NY, Cold Spring Harbor Laboratory Press). 137-156.

Nureki, O., Niimi, T., Muto, Y., Kanno, H., Kohno, T., Muramatsu, T., Kawai, G., Miyazawa, T., Giegé, R., Florentz, C., and Yokoyama, S. (1993). "Conformational change of tRNA upon interaction of the identity-determinant set with aminoacyl-tRNA synthetase" in *The Translational Apparatus* . K. H. Nierhaus, F. Franceschi, A. R. Subramanian, V. A. Erdmann and B. Wittmann-Liebold Eds. (New York, Plenum Press). 59-66.

Nureki, O., Vassylyev, D. G., Katayanagi, K., Shimizu, T., Sekine, S.-i., Kigawa, T., Miyazawa, T., Yokoyama, S., and Morikawa, K. (1995). Architectures of class-defining and specific domains of glutamyl-tRNA synthetase. *Science 267*: 1958-1965.

Onesti, S., Miller, A. D., and Brick, P. (1995). The crystal structure of lysyl-tRNA synthetase (LysU) from *Escherichia coli*. *Structure 3*: 163-176.

Park, S. J., Hou, Y.-M., and Schimmel, P. (1989). A single base pair affects binding and catalytic parameters in the molecular recognition of a transfer RNA. *Biochemistry 28*: 2740-1746.

Park, S. J., and Schimmel, P. (1988). Evidence for interaction of an aminoacyl transfer RNA synthetase with a region important for the identity of its cognate transfer RNA. *J. Biol. Chem. 263*: 16527-16530.

Perona, J. J., Rould, M. A., Steitz, T. A., Risler, J.-L., Zelwer, C., and Brunie, S. (1991). Structural similarities in glutaminyl- and methionyl-tRNA synthetases suggest a common overall orientation of tRNA binding. *Proc. Natl. Acad. Sci. U.S.A. 88*: 2903-2907.

Puglisi, E. V., Puglisi, J. D., Williamson, J. R., and RajBhandary, U. L. (1994). NMR analysis of tRNA acceptor stem microhelices: Discriminator base change affects tRNA conformation at the 3' end. *Proc. Natl. Acad. Sci. U.S.A. 91*: 11467-11471.

Putney, S. D., Royal, N. J., Neuman de Vegvar, H., Herlihy, W. C., Biemann, K., and Schimmel, P. (1981a). Primary structure of a large aminoacyl-tRNA synthetase. *Science 213*: 1497-1500.

Putney, S. D., Sauer, R. T., and Schimmel, P. R. (1981b). Purification and properties of alanine tRNA synthetase from *Escherichia coli*. *J. Biol. Chem. 256*: 198-204.

Quinn, C. L., Tao, N., and Schimmel, P. (1995). Species-specific microhelix aminoacylation by a eukaryotic pathogen tRNA synthetase dependent on a single base pair. *Biochemistry* submitted.

Regan, L., Bowie, J., and Schimmel, P. (1987). Polypeptide sequences essential for RNA recognition by an enzyme. *Science 235*: 1651-1653.

Rich, A., and Kim, S. H. (1978). The three-dimensional structure of transfer RNA. *Scientific American 238*: 53-62.

Rich, A., and RajBhandary, U. L. (1976). Transfer RNA: molecular structure, sequence, and properties. *Ann. Rev. Biochem. 45*: 805-860.

Robertus, J. D., Ladner, J. E., Finch, J. T., Rhodes, D., Brown, R. S., Clark, B. F. C., and Klug, A. (1974). Structure of yeast phenylalanine tRNA at 3 Å resolution. *Nature 250*: 546-551.

Rossmann, M. G., Moras, D., and Olsen, K. W. (1974). Chemical and biological evolution of a nucleotide-binding protein. *Nature 250*: 194-199.

Rould, M. A., Perona, J. J., Söll, D., and Steitz, T. A. (1989). Structure of *E. coli* glutaminyl-tRNA synthetase complexed with tRNA[Gln] and ATP at 2.8 Å resolution. *Science 246*: 1135-1142.

Rould, M. A., Perona, J. J., Söll, D., and Steitz, T. A. (1991). Structural basis of anticodon loop recognition by glutaminyl-tRNA synthetase. *Nature 352*: 213-218.

Rudinger, J., Florentz, C., Dreher, T., and Giegé, R. (1992). Efficient mischarging of a viral tRNA-like structure and aminoacylation of a minihelix containing a pseudoknot: Histidinylation of turnip yellow mosaic virus RNA. *Nucleic Acids Res. 20*: 1865-1870.

Ruff, M., Krishnaswamy, S., Boeglin, M., Poterszman, A., Mitschler, A., Podjarny, A., Rees, B., Thierry, J. C., and Moras, D. (1991). Class II aminoacyl transfer RNA synthetase: Crystal structure of yeast aspartyl-tRNA synthetase complexed with tRNA[Asp]. *Science 252*: 1682-1689.

Saks, M. E., Sampson, J., R., and Abelson, J. N. (1994). The transfer RNA identity problem: A search for rules. *Science 263*: 191-197.

Sambrook, J., Fritsch, E. F., and Maniatis, T. (1989). *Molecular Cloning: A Laboratory Manual.* (2nd ed.). Cold Spring Harbor Laboratory, Cold Spring Harbor, NY).

Sampson, J., and Saks, M. (1993). Contributions of discrete tRNA[Ser] domains to aminoacylation by E. coli seryl-tRNA synthetase: A kinetic analysis using model RNA substrates. *Nucleic Acids Res. 21*: 4467-4475.

Scaringe, S. A., Francklyn, C., and Usman, N. (1990). Chemical synthesis of biologically active oligoribonucleotides using β-cyanoethyl protected ribonucleoside phosphoramidites. *Nucleic Acids Res. 18*: 5433-5441.

Schimmel, P. (1991). Classes of aminoacyl-tRNA synthetases and the establishment of the genetic code. *Trends in Biochem. Sci. 16*: 1-3.

Schimmel, P., Giegé, R., Moras, D., and Yokoyama, S. (1993). An operational RNA code for amino acids and possible relationship to genetic code. *Proc. Natl. Acad. Sci. U.S.A. 90*: 8763-8768.

Schimmel, P., and Ribas de Pouplana, L. (1995). Transfer RNA: From minihelix to genetic code. *Cell 81*: 983-986.

Schimmel, P. R., and Söll, D. (1979). Aminoacyl-tRNA synthetases: general features and recognition of transfer RNAs. *Ann. Rev. Biochem. 48*: 601-648.

Schmitt, E., Meinnel, T., Panvert, M., Mechulam, Y., and Blanquet, S. (1993). Two acidic residues of *Escherichia coli* methionyl-tRNA synthetase are negative discriminants towards the binding of non-cognate tRNA anticodons. *J. Mol. Biol. 233*: 615-628.

Schulman, L. H., and Pelka, H. (1983). Anticodon loop size and sequence requirements for recognition of formylmethionine tRNA by methionyl-tRNA synthetase. *Proc. Natl. Acad. Sci. U.S.A. 80*: 6755-6759.

Schulman, L. H., and Pelka, H. (1988). Anticodon switching changes the identity of methionine and valine transfer RNAs. *Science 242*: 765-768.

Schulman, L. H., Pelka, H., and Susani, M. (1983). Base substitutions in the wobble position of the anticodon inhibit aminoacylation of *E. coli* tRNA^{fMet} by E. coli Met-tRNA synthetase. *Nucleic Acids Res. 11*: 1439-1455.

Senger, B., Despons, L., Walter, P., and Fasiolo, F. (1992). The anticodon triplet is not sufficient to confer methionine acceptance to a transfer RNA. *Proc. Natl. Acad. Sci. U.S.A. 89*: 10768-10771.

Seong, B. L., and RajBhandary, U. L. (1987). Mutants of *Escherichia coli* formylmethionine tRNA: A single base change enables initiator tRNA to act as an elongator *in vitro*. *Proc. Natl. Acad. Sci. U.S.A. 84*: 8859-8863.

Shepard, A., Shiba, K., and Schimmel, P. (1992). RNA binding determinant in some class I tRNA synthetases identified by alignment-guided mutagenesis. *Proc. Natl. Acad. Sci. U.S.A. 89*: 9964-9968.

Shiba, K., and Schimmel, P. (1992a). Functional assembly of a randomly cleaved protein. *Proc. Natl. Acad. Sci. U.S.A.* **89**: 1880-1884.

Shiba, K., and Schimmel, P. (1992b). Tripartite functional assembly of a large class I aminoacyl tRNA synthetase. *J. Biol. Chem.* **267**: 22703-22706.

Shiba, K., Suzuki, N., Shigesada, K., Namba, Y., Schimmel, P., and Noda, T. (1994). Human cytoplasmic isoleucyl-tRNA synthetase: Selective divergence of the anticodon-binding domain and acquisition of a new structural unit. *Proc. Natl. Acad. Sci. U.S.A.* **91**: 7435-7439.

Silberklang, M., Gillum, A. M., and RajBhandary, U. L. (1977). The use of nuclease P1 in sequence analysis of end group labeled RNA. *Nucleic Acids Res.* **4**: 4091-4108.

Sprinzl, M., Hartmann, T., Weber, J., Blank, J., and Zeidles, R. (1989). Compilation of tRNA sequences and sequences of tRNA genes. *Nucleic Acids Res.* **17**: r1-r172.

Starzyk, R. M., Webster, T. A., and Schimmel, P. (1987). Evidence for dispensable sequences inserted into a nucleotide fold. *Science* **237**: 1614-1618.

Stern, L., and Schulman, L. H. (1977). Role of anticodon bases in aminoacylation of *Escherichia coli* methionine transfer RNAs. *J. Biol. Chem.* **252**: 6403-6408.

Usman, N., Ogilvie, K. K., Jiang, M.-Y., and Cedergren, R. J. (1987). Automated chemical synthesis of long oligoribonucleotides using 2'-O-silylated ribonucleoside 3'-O-phosphoramidites on a controlled-pore glass support: Synthesis of a 43-nucleotide sequence similar to the 3'-half molecule of an *Escherichia coli* formylmethionine tRNA. *J. of the Am. Chem. Soc.* **109**: 7845-7854.

Valenzuela, D., and Schulman, L. H. (1986). Identification of peptide sequences at the tRNA binding site of *Escherichia coli* methionyl-tRNA synthetase. *Biochemistry* **25**: 4555-4561.

Van Holde, K. E. (1975). "Sedimentation analysis of proteins" in *The Proteins* . Academic Press).

Webster, T. A., Tsai, H., Kula, M., Mackie, G. A., and Schimmel, P. (1984). Specific sequence homology and three-dimensional structure of an aminoacyl transfer RNA synthetase. *Science* **226**: 1315-1317.

Weiner, A. M., and Maizels, N. (1987). tRNA-like structures tag the 3' ends of genomic RNA molecules for replication: Implications for the origin of protein synthesis. *Proc. Natl. Acad. Sci. U.S.A. 84*: 7383-7387.

Wright, D. R., Martinis, S. A., Jahn, M., Söll, D., and Schimmel, P. (1993). Acceptor stem and anticodon RNA hairpin helix interactions with glutamine tRNA synthetase. *Biochimie 75*: 1041-1049.

Yarus, M., and Berg, P. (1967). Recognition of tRNA by aminoacyl tRNA synthetases. *J. Mol. Biol. 28*: 479-490.

Yarus, M., and Berg, P. (1970). On the properties and utility of a membrane filter assay in the study of isoleucyl-tRNA synthetase. *Anal. Biochem. 35*: 450-465.

Zelwer, C., Risler, J. L., and Brunie, S. (1982). Crystal structure of *Escherichia coli* methionyl-tRNA synthetase at 2.5 Å resolution. *J. Mol. Biol. 155*: 63-81.